PEOPLE'S DEMOCRATIC REPUBLIC OF ALGERIA
MINISTRY OF HIGHER EDUCATION AND SCIENTIFIC RESEARCH
University of Abou Bakr Belkaïd – Tlemcen
Faculty of TECHNOLOGY
Department of Electrical and Electronic Engineering

Master's Thesis

Presented for obtaining a Master's **degree**
Filière: Electrotechnique
Specialité: Commandes Electriques

By: **Eric RANGA** & **Macdonald PHIRI**

Title:

STUDY AND SIMULATION OF A PHOTOVOLTAIC WATER PUMPING SYSTEM

Defended, on 30 / 06 / 2021, before the jury composed of:

Mr Mourad LOUCIF	**MCB**	**Univ. Tlemcen**	**President**
Mr Mohammed Amine BRIKCI NIGASSA	**MAA**	**Univ. Tlemcen**	**Examiner**
Mr Mohamed Choukri BENHABIB	**MCA**	**Univ. Tlemcen**	**Supervisor**
Mr Sidi Mohammed MELIANI	**Professor**	**Univ. Tlemcen**	**Co- Supervisor**

Year 2020/2021

Dedication

This study is wholeheartedly dedicated to my beloved parents Mike PHIRI and Winnie TAMBALA who have been my source of inspiration when I thought of giving up, who continually provide their moral, spiritual, emotional and financial support,
To my sisters Vivian, Millicent and Aggie, to my friend Immaculate, to all my relatives and friends who have provided their unwavering support.

To my colleague Eric RANGA.

And above all I give thanks to Almighty God for his protection, healthy and sound mind.

Macdonald PHIRI

I wholeheartedly dedicate this work to Almighty God who gave me strength, courage and protection, and who kept me health during the research process, for that, I'm sincerely and truly grateful.

To our beloved parents as you have been my pillars of strength and inspirational through your continuous moral and emotional support throughout the process.

To my precious brothers, sisters, relatives, as you have been a source of motivation and encouragement till the completion of this work.

To my colleague Macdonald PHIRI, my professors and supervisors.

Eric RANGA

Acknowledgement

First and foremost, we would to like express our sincere gratitude to Almighty God, for his grace and mercy that has sustained during this challenging yet exciting process.

We would like express also our special thanks to our supervisor Mr Mohamed Choukri BENHABIB and our co-supervisor Mr Sidi Mohammed MELIANI for their unwavering support, guidance, encouragement, and their tireless efforts which without, we could not have completed this work in time.

Our special thanks go to all the members of the jury who agreed to examine and evaluate this work: Mr Mourad LOUCIF, lecturer at the University of Tlemcen for having honored us by his presence as president of the jury and also to Mr Mohammed Amine BRIKCI NIGASSA as our examiner.

We do appreciate our committed and dedicated professors and all other members of the Electrical Engineering department, with their direct or indirect contribution up to the completion of this Master's thesis.

Abstract

The unavailability of water for domestic and agricultural use is becoming one of the major challenges faced in different countries in Africa. Most of the pumps which being used in remote areas which are isolated from the grid are diesel water pumps and these pumps lead to environmental pollution which has short- or long-term consequences. However, water pumping systems based on solar energy is a better alternative since, it is pollution free and abundant in Africa. This Master's thesis is aimed at designing and simulate ng solar water pumping systems for two cases studies using Simulink/ MATLAB. These pumping systems consisting of a BLDC motor driving a multistage; submersible centrifugal pump for a vertical uplift of water from a deep well. In order to extract maximum power from the PV array, a Fuzzy Logic Controller MPPT technique has been used, as it is effective in nonlinear condition and in presence of uncertainties. A directly coupled configuration (PV – pump) without batteries has been used incorporating a DC –DC boost converter which serves a dual purpose, that is stepping up the DC voltage and acting as a dynamic optimizer in tracking the maximum power point. A trapezoidal control for the BLDC motor has used and a classic PI regulator for speed control as it affects the flow rate. Finally, two area studies were chosen to introduce the solar water pumps with their dimensioning.

Keywords:
Solar Water Pumping System, Brushless DC motor, Boost converter, MPPT, Fuzzy Logic controller, PI regulator, Photovoltaic Generator, Centrifugal Pump.

Résumé

L'indisponibilité de l'eau pour l'usage domestique et agricole est en train de devenir l'un des principaux défis auxquels sont confrontés différents pays d'Afrique. La plupart des pompes utilisées dans les régions éloignées et isolées du réseau sont des pompes à eau diesel et ces pompes entraînent une pollution de l'environnement qui a des conséquences à court ou à long terme. Cependant, les systèmes de pompage de l'eau basés sur l'énergie solaire sont une meilleure alternative car ils ne sont pas polluants et sont abondants en Afrique. Ce mémoire de maîtrise vise à concevoir et à simuler des systèmes de pompage d'eau solaire pour deux études de cas en utilisant Simulink/ MATLAB. Ces systèmes de pompage sont constitués d'un moteur BLDC entraînant une pompe centrifuge submersible multi-étage pour une remontée verticale de l'eau d'un puits profond. Afin d'extraire une puissance maximale du réseau PV, une technique MPPT de contrôleur à logique floue a été utilisée, car elle est efficace dans des conditions non linéaires et en présence d'incertitudes. Une configuration directement couplée (PV - pompe) sans batteries a été utilisée en incorporant un convertisseur élévateur DC-DC qui sert un double objectif, c'est à dire augmenter la tension DC et agir comme un optimiseur dynamique dans le suivi du point de puissance maximale, un contrôle trapézoïdal pour le moteur BLDC a été utilisé et un régulateur PI classique pour le contrôle de la vitesse car il affecte le débit. Pour terminer, deux études de site ont été choisies pour introduire les pompes à eau solaire avec leurs dimensionnements.

Mots-clés :
Système de pompage d'eau solaire, moteur CC sans balais, convertisseur survolteur, MPPT, contrôleur logique floue, régulateur PI, irradiation, générateur photovoltaïque, pompe centrifuge.

ملخص

تعد أنظمة ضخ المياه القائمة على الطاقة الشمسية بديلاً أفضل لأنها خالية من التلوث ومتوفرة في إفريقيا. تهدف أطروحة الماجستير هذه إلى تصميم ومحاكاة أنظمة ضخ المياه بالطاقة الشمسية لدراستي حالة باستخدام Simulink / MATLAB . تتكون أنظمة الضخ هذه من محرك BLDC بدون بطاريات PV ، مضخة طرد مركزي غاطسة لرفع المياه من بئر عميق. تم استخدام تقنية MPPT Fuzzy Logic Controller من أجل استخلاص الطاقة القصوى من المصفوفة الكهروضوئية ، تم استخدام تقنية (مضخة الذي يخدم غرضًا مزدوجًا ، وهو زيادة جهد التيار المستمر والعمل كمحسِّن ديناميكي في DC- DC يتضمن محول تعزيز كلاسيكي للتحكم في السرعة لأنه PI ومنظم BLDC تتبع أقصى نقطة طاقة. تم استخدام عنصر تحكم شبه منحرف لمحرك يؤثر على معدل التدفق. أخيرًا ، تم اختيار دراستين للمناطق لتقديم مضخات المياه بالطاقة الشمسية بأبعادها.

الكلمات المفتاحية:

PI جهاز تحكم منطقي ضبابي ، منظم ، MPPT ، بدون فرشات ، محول دفعة DC نظام ضخ المياه بالطاقة الشمسية ، محرك تشعيع ، مولد ضوئي ، مضخة طرد مركزي ،.

Nomenclature

NREL	National Renewable Energy Laboratory
PR	Standard performance ratio
Ppv	Total PV power produced (W)
Nps	Number of panels in series
Npp	Number of panels in parallel
TDH	Total dynamic head
SWPS	Solar water pumping system
CSI	Current source Inverter
VSI	Voltage source inverter
SVPWM	Space vector pulse width modulation
PWM	Pulse width modulation
INC	Incremental conductance
SO	Self-oscillation method
IGBT	Integrated bipolar transistor
MOSFET	Metal oxide semiconductor field effect transistor
AC	Alternating current
DC	Direct current
PV	Photovoltaic
BLDC	Brushless direct current
EMF	Electromotive force
MPPT	Maximum Power Point Tracking
AM	Air Mass
UV	Ultraviolet light
IR	Infra-red light
STC	Standard test conditions
GHI	Global Horizontal Irradiation
DNI	Direct Normal Irradiance
MW	Megawatts
Mono-Si	Monocrystalline Silicon
TFSC	Thin-film solar cells
A-Si	Amorphous silicon solar cells
p-Si	Polycrystalline solar cells
MPP	Maximum power point
FF	Fill factor
NASA	National Aeronautics and Space Administration
NB	Negative Big
NS	Negative Small
NM	Negative Medium
Z	Zero

PS	Positive Small
PM	Positive Medium
PB	Positive Big
M	Medium
B	Big
VB	Very Big

Symbols

$R_{a, b, c}$	Stator resistance per phase (Ω)
Q	Flow rate (m^3/s)
v	Velocity of the water in meters per second (m^2/s)
g	Gravity ($9.81 m^2/s$)
A	Area (m^2)
H_L	Friction loss (m)
C	Roughness coefficient variable of pipe material (m)
Q	Flow rate (m^3/s).
D	Pipe inside diameter (m)
L	Length of the pipe (m)
H	Total Dynamic Head (m)
ρ	Water density (1000 kg/m^3);
P_m	Pump power (kW)
P_m	Pump power in (kW)
$L_{a, b, c}$	Stator inductances per phase (H)
$V_{a, b, c}$	Stator phase voltages (V)
$I_{a, b, c}$	Stator phase currents (A)
$e_{a, b,c}$	Motor Back EMFs (V)
K	Back EMFs constant (V/rad/s)
θ	Electrical angle (°)
ω	Mechanical speed of the rotor (rad/s)
rpm	Revolution per minute
T	Torque (Nm.)
%	Percentage
W	Watt (W)
P (k)	Photovoltaic cells power output for a sampling time of k times (W)
U (K)	Photovoltaic cells voltage output for a sampling time of k times (V)
Vin	Supply voltage
V_L	Inductance voltage (V)
D	Duty cycle
Vout	Output voltage (V)
f	Frequency (Hz)
ΔI_L	Ripple current (A)
ΔV	Ripple voltage (V)
Io	Output current (A)
Vo	Output voltage (V)

Ro	Resistance of the load (Ω)
℃	Degree Celsius
C	Capacitor (μF)
d	Diode
L	Inductor (H)
R	Resistor (Ω)
$\boldsymbol{\mu}$F	Microfarad
Ω	Ohm
t	Time (s)
s	Second
V	Voltage
π	Pi
%	Percentage
V	Voltage
I	Current
L	Inductance
K	Kelvin
E	Energy
C	Capacitance
$\boldsymbol{\mu}$m	Micrometre
λ	Wavelength
c	Speed of light
h	Plank's constant
$\boldsymbol{\beta}$	Zenith angle (degree (◦))
H_2O	Water
CO_2	Carbon dioxide gas
nm	Nanometre
W/m^2	Watt per square metre
$KWh/m^2/day$	Kilowatt-hour per square meter per day
℉	Fahrenheit
Iph	Generated current due to sunlight irradiation
Id	Current through a diode
Rs	Resistor in series
Rp	Resistor in parallel
Ip	Parallel Resistor current
Vt	Thermal Voltage
Isc	Short circuit current
Voc	Open circuit voltage
P_{max}	Maximum Power
I_{max}	Maximum current

V_{mpp}	Voltage at maximum point
I_{mp}	Current at maximum point
I_s	Diode reverse saturation current (A)
q	Diode ideality factor
R_p	Shunt resistance (Ω)
K	Boltzman constant
q	Electron charge = ($1,602.10^{-19}$ C)
T	Temperature in Kelvin (K)
g	Gate terminal of the MOSFET
d	Grain terminal of the MOSFET
s	Source terminal of the MOSFET

Table of Contents

Chapter I: Generality on Photovoltaic Systems

Chapter II: An Overview of Solar water Pumping Systems

Chapter III: Designing and Simulation of the Solar Water Pumping System

List of Figures

List of Tables

General Introduction

General introduction

The conversion of the incident solar energy into electricity by photovoltaic panels is becoming one of the interesting and important energy source alternatives as the world is shifting towards the use of green energy from renewable resources so as to minimize the use of non-renewable resources. The use of nonrenewable energy sources has resulted in continuous emission of carbon dioxide and other greenhouse gases leading to global warming and climate change. The availability of solar energy in abundance in most of the countries of the world provides a better opportunity of reducing the emission of these gases as photovoltaic technology can be employed in several sectors to generate electric power to meet the challenges of the day.

The photovoltaic systems can either be tied to the grid or act as standalone systems powering homes, schools, clinics and other remote places or areas which are isolated from the grid (Off-grid PV systems). One of the most important application of photovoltaic energy is water pumping in remote rural areas in Africa which are isolated from the grid. The most common type of water pumps in these areas are diesel pumps. These pumps emit carbon dioxide while in operation and they can be costly in the long run as fuel has to be readily available for the operation of the pump. The source of water in such areas determines the type of solar pumping system to be used in order to provide safe and clean drinking water to such communities. These configurations include, direct coupling of a photovoltaic generator to a water pump which is the common configuration.

In order to improve the efficiency of photovoltaic systems in harnessing solar energy, several maximum power point tracking (MPPT) techniques have been proposed which are either direct or indirect as shall be discussed in chapter I. These techniques help in dynamically optimizing the photovoltaic generator hence improving the efficiency of the power extraction from the photovoltaic panels. Furthermore, electric motors are the key components of such solar water pumping system (SPWS) as they act as prime movers by providing mechanical energy needed to rotate the mechanical parts of the water pumps. These motors can either be AC or DC motors. DC motors can be coupled directly to photovoltaic generator through a controller, but the major challenge is on the wearing of brushes as it sorely relies on mechanical commutation. The invention of a brushless DC motor with electronic commutation provides a better alternative if the DC motor performances and characteristics are to be retained. AC motors are robust, relatively cheap and have got a longer life span as compared to DC counterparts.

The main aim of this research work:

- ✓ To propose a solar water pumping system design using MATLAB/Simulink for a rural set up powered by solar energy which is harnessed and converted into electricity by photovoltaic modules. This includes the use of power electronic converters such as boost converter and an inverter or drivers as required by the pumping system.

- ✓ The application of the Fuzzy Logic MPPT technique for the tracking of the maximum power point of the photovoltaic generator in relation to the present solar radiation and temperature.

- ✓ Simulation of a vertical, submersible, multistage centrifugal pump driven by a brushless DC motor for a vertical uplift of water from the deep well into a storage tank.

- ✓ Regulation of the speed of the BLDC using a classic PI controller since the speed of rotation and torque directly affects the maximum flow rate of the pump.

This research work is divided into three chapters:

Chapter I focuses on the photovoltaic systems including, the generality on photovoltaic generators and its characteristics. Moreover, this chapter contains a discussion on power electronic converters used in SWPS including a study and application of the Fuzzy Logic MPPT technique which helps in extracting the maximum power from the PV array.

Chapter II is dedicated on the generality on solar water pumping systems. This includes a discussion on the types of electric motors used in these systems, the types of SWPS, different configuration of solar water pumping systems, the types of pumps used, and different configuration of these pumping systems. Moreover, it contains the steps taken in theoretically designing a SPWS.

Chapter III is consecrated on the application of the concepts discussed in chapter I and II including a simulation and designing of the SWPS using MATLAB/Simulink then, an evaluation and discussion on the results of the simulation.

Problematic and motivation of study

The availability of clean, safe and running water is one of the challenges being faced in most of the developing countries in Africa and some other third world countries. Most of the communities isolated from electrical power grid have been depending on diesel water pumps which in turns contribute to the pollution of the atmosphere. As the world is slowly moving towards the use of green energy harnessed from renewable resources including solar energy, wind power for water pumping systems, it is of paramount importance that, a better, cleaner, reliable and effective alternative way of providing water to such communities has to be found so as to address these urgent issues.

It is estimated that, one in 10 people on this planet lack access to clean water [1]. In rural Africa, an average woman travels a considerable distance to fetch water from unprotected source like rivers and dams. This has led to the outbreak of diseases like diarrhea, cholera, typhoid. The COVID-19 pandemic has demonstrated the critical importance of sanitation, hygiene and adequate access to clean water for hand washing and cleaning [2]. Apart from diseases, most of the countries are experiencing serious drought witnessed by serious food shortages and higher food importation costs. The use of solar water pumping systems can help to provide water for irrigation from deep wells, dams and lakes thus minimizing the adverse effects of drought.

Some of the communities which are connected to the grid are also experiencing the same crisis due to prolonged power outages either due to the depletion of the raw materials like coal, lack of efficient technologies to exploit some of the raw materials. Moreover, poor rainfall patterns have crippled the hydropower generation capacity in some countries including Zimbabwe leading to prolonged and persistent load sheddings and power outages which has a negative effect on production and provision of essential goods and services. Photovoltaic power generation is an interesting alternative that can help in improving and addressing these issues through establishment of grid-tied photovoltaic power generation centers.

Therefore, an investment in this technology of generating power from solar energy can significantly improve and address some of the problems being faced by most countries in Africa. The desire to see an improvement of the lives of people by providing safe and clean drinking water for the communities isolated from the grid using the free and abundant solar energy in Africa is the motivation behind this project.

Chapter I

Generality on Photovoltaic Systems

I.1. Introduction

The basic unit of a photovoltaic generator is a solar cell or a photovoltaic cell which transforms incident solar energy into electricity through a process called photovoltaic effect. The photovoltaic (PV) cells are made from silicon semiconductors which are doped by introducing extrinsic elements to create a p-n junction. In this chapter, we will focus on the generality of PV systems, the power electronic devices that are utilized and the fuzzy MPPT technique used to extract maximum power from the photovoltaic generators.

I.2. History of solar cells

The history and evolution of the technological development of photovoltaic cells over quite a number of years is briefly described below [3]:

1839 – **Edmond Becquerel** discovered the photovoltaic effect which later became known as BECQUEREL effect:

1873– Willoughby Smith discovered that selenium could function as a photoconductor.

1876 – **Adams and Richard Evans Day** discovered that illuminating a junction between Selenium and platinum has a photovoltaic effect.

1883 – **C.E. Fritts** built a selenium solar cell whereby less than 1% of solar energy was being converted to electricity. Despite of this fact, the cell was responding to visible light spectrum which was big achievement that time.

1950 – Darryl **Chapin, Calvin Fuller and Gerald Pearson** from Bell Labs, New Jersey, United States constructed a cell from semiconductor devices such as Silicon.

1954 – **Bell Labs** invented first usable solar cell containing doped silicon slices which increased its efficiency up to 6%.

1958 – First PV cells in space which were used on the US space satellite, **Vanguard 1**

1962 – Solar cells were used to power **Telstar** communications satellite

1964 – NASA launched the Nimbus satellite, which ran entirely on its 470-watt photovoltaic solar panel array.

1978 – Casio introduced the first solar-powered calculator series.

And, today electricity from solar modules is being used to power homes, street lighting and other applications including solar water pumping in remote areas.

I.3. Solar radiation

The sun is the main energy source located about 149 million kilometers from earth. The energy arrives on earth as solar radiation. A huge collection of tiny packets known as photons, which travel in waves emitting electromagnetic radiation with a wavelength band varying from 0.22 to 10 µm. The energy possessed by photon is directly related to the wavelength λ as illustrated by the following relation [4].

$$E_p = \frac{hc}{\lambda} \quad \text{(I.1)}$$

Where:
h: is Planck's constant,
c: is the speed of light and λ its wavelength.

When the sunlight passes through the atmosphere, air molecules, water vapor, clouds, dust, pollutants, forest fires or volcanoes reflect some of it and this is referred to as diffuse solar radiation. On the other hand, direct beam solar radiation refers to the solar radiation that reaches the Earth's surface without being diffused. The combination of the diffuse and direct solar radiation is called global solar radiation. The atmosphere reduces the direct beam radiation by 10% on clear, dry days and by 100% during thick, cloudy days [5]. The amount of solar radiation that reaches any one spot on the Earth's surface depend on:

- ✓ Geographic location,
- ✓ Time of day,
- ✓ Season,
- ✓ Local landscape,
- ✓ Local weather.

The solar radiation that reaches the earth’s surface can be captured and turned into useful forms of energy, such as heat and electricity, using a variety of technologies. However, the available resources determine the technical feasibility and economical operation of these technologies at a specific location.
When the solar radiation crosses the atmosphere, it undergoes a modification of its spectrum. This is mainly due to the partial absorption of radiation by atmospheric gases and water vapor.

When the relative position of the sun which modifies the thickness of the atmosphere is taken into account; this introduces a coefficient called air mass (AM). The Air Mass constant calculates the depletion of light intensity as it passes through the atmosphere where some of it is absorbed [6].
The Air Mass is defined as:

$$AM = \frac{1}{\cos \beta} \quad (I.2)$$

where:

$\boldsymbol{\beta}$: The angle from the vertical (zenith angle).
When the sun is directly overhead, the Air Mass as shown on figure 1.1 below:

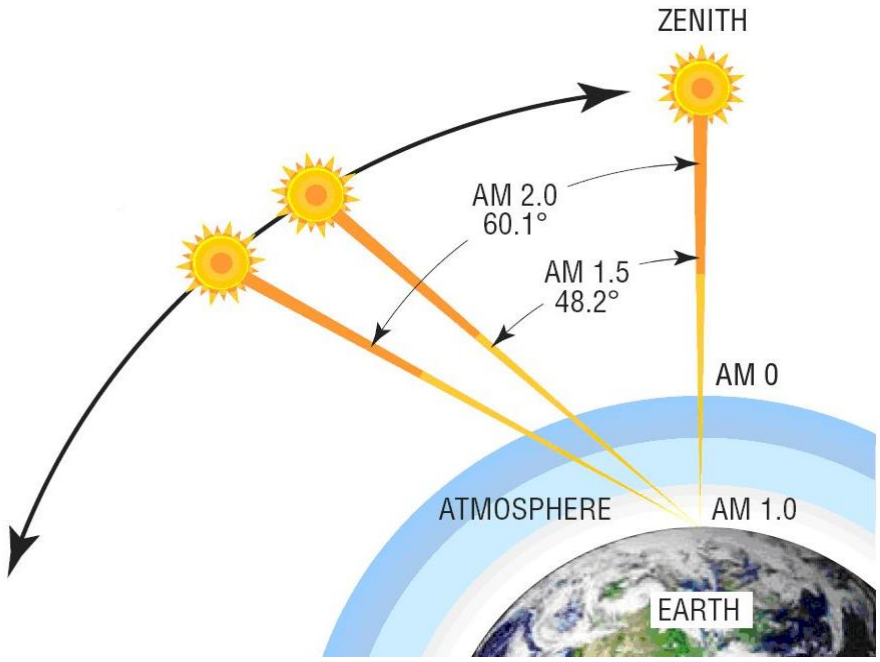

Figure 1.1 The AM concept [7]

The concept of air mass number characterises the power carried by the solar radiation, on the other hand, it is used to define a reference spectrum to calibrate the standard cells intended to qualify the performances of the photovoltaic devices. A portion of the electromagnetic radiation emitted from the sun is refers to as the sunlight, which is in particular infrared, visible, and ultraviolet light. It is scattered and filtered through Earth's atmosphere before it reaches the earth surface, as daylight when the sun is above the horizon. The sunlight is diffused as shown in figure 1.2.

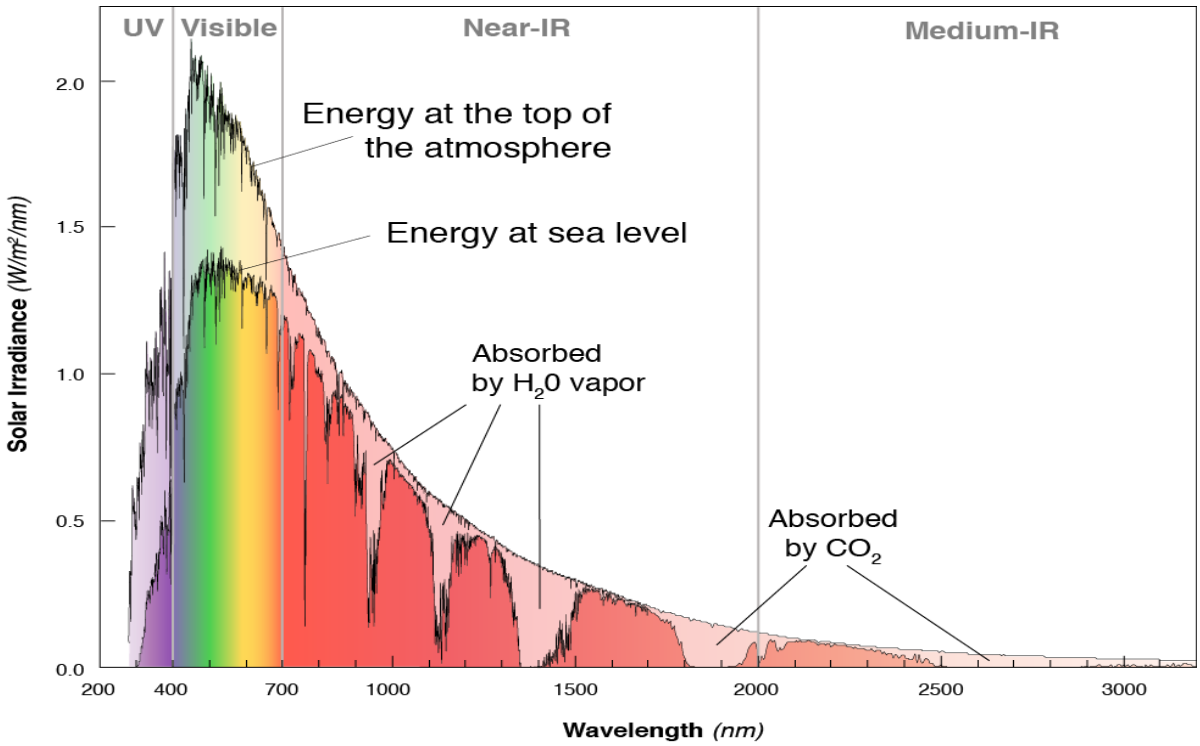

Figure 1.2. Solar spectrum. [8]

The standard conditions for cell qualification at sea level spectrum are, an incident solar radiation of 1000 W / m², temperature of 25 °C and an air mass of 1.5. These conditions are called STC (Standard Test Conditions). The STC is an industry-wide standard to indicate the performance of PV modules. These conditions create a uniform test conditions which make it possible to conduct uniform comparisons of photovoltaic modules by different manufacturers.

The solar irradiation can be expressed in terms of global horizontal irradiation (GHI) which refers to the total amount of radiation received by a surface considered to be horizontal to the ground from above. This value is crucial for photovoltaic installation due to the fact that, it include both direct normal irradiance and diffuse horizontal irradiance. The amount of incident irradiation received per unit area by a surface that is perpendicular to the sun rays is known as direct normal irradiance while diffuse horizontal irradiance refers to the irradiation received per unit area by a surface after the light has been scattered by molecules and particles in the atmosphere. Generally, it is the illumination that diffuses from clouds and the blue sky [9].

The amount solar energy received in Algeria and Zimbabwe are shown in

Figure 1.3 and figure 1.4 respectively.

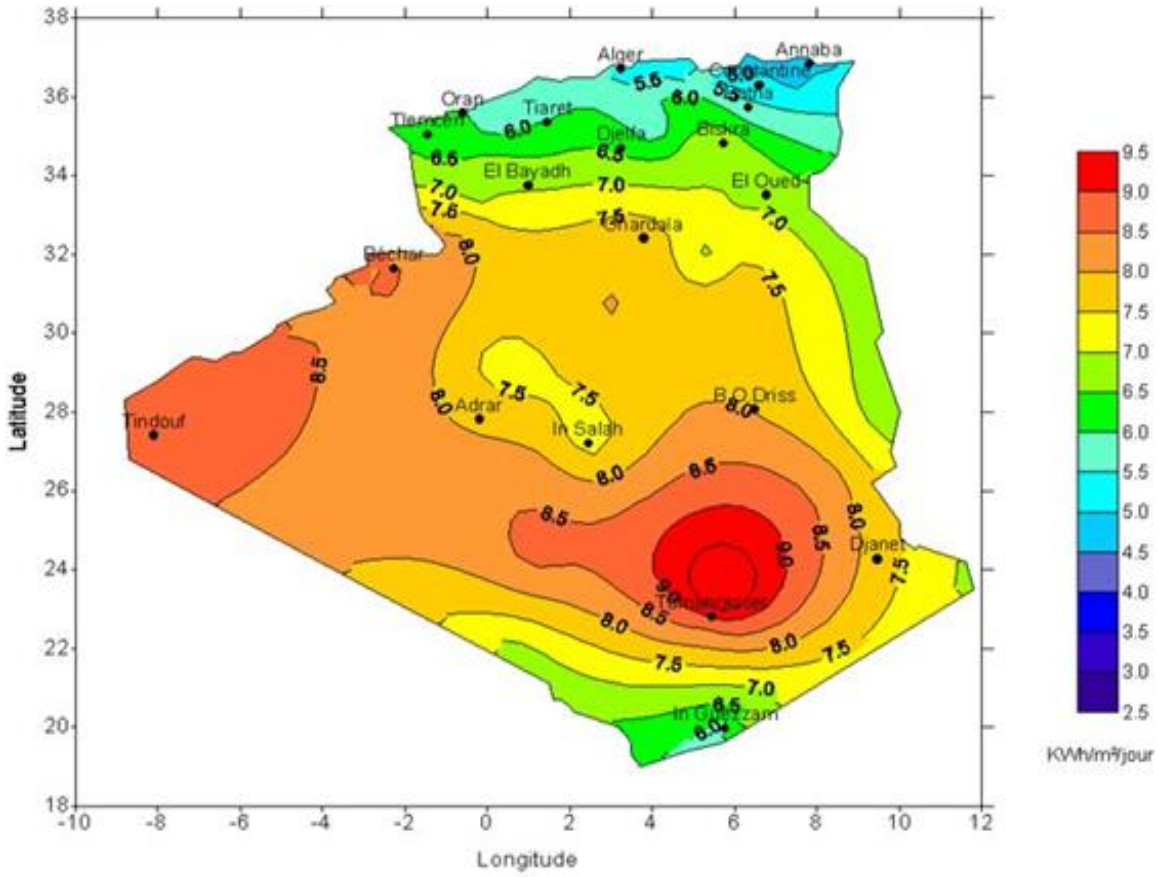

Figure 1.3. Monthly mean direct solar radiation in Algeria [10]

The map shown in Figure 1.3, shows that, the highest temperatures are experienced around Tamanrasset region with mean solar radiation of 9.5 KWh/m^2/day, while the coastal strip, around Annaba, Algiers, Oran and Tairet receives about 5 KW/h/m^2/day mean solar radiation

Algeria's capacity of generating PV energy is estimated at 13.9 TWh/year [11] and this energy can be applied in various contexts, such as attaching small panels to the roofs of houses, large panels on schools, hospitals and supermarkets, or installing a large-scale PV farm.

The isolated communities can also benefit from electricity generated from PV arrays which then support farming activities, e.g. pumping water from wells or by operating solar refrigerators to preserve food and medicine. Another industrial application of PV system is for desalination plants to produce drinking water.

The map below (Figure 1.4) shows the amount of solar radiation received in Zimbabwe

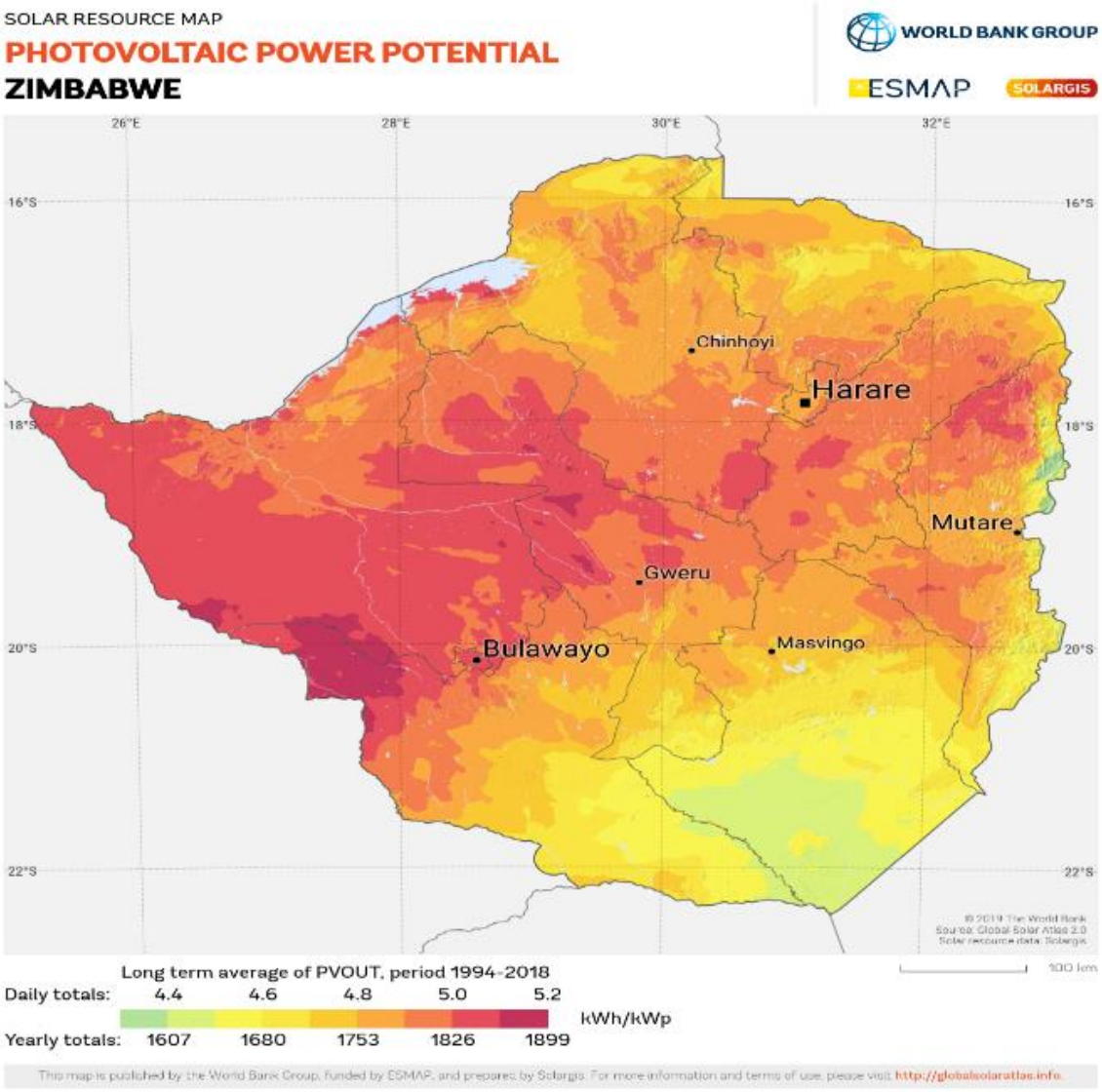

Figure 1.4. Map showing the daily sunshine hours in Zimbabwe [12]

The amount solar insolation is greatly influenced by the rainfall patterns experienced in the country and seasonal changes. The average solar irradiation is 5.7 kWh/m^2 /day with the north and west regions of the country having the highest irradiation and the country has a potential of generating over 300 MW of electricity from solar energy [12].

The abundant solar energy received in Zimbabwe provides an opportunity of adding electric power to the national grid, thus minimizing power cuts and load shedding which have got negative across several sectors of the economy.

I.4. Different types of photovoltaic cells

There are three generations of photovoltaic cells based on the technological developments that has happened over a number of years which are as follows:

I.4.1. First generation solar cells

These are the most commonly used solar panels made up of monocrystalline silicon or polycrystalline found in most of our surroundings. Monocrystalline solar panels (Mono-SI) are made up of pure silicon and they can easily be identified by a dark look and round edges. The purity of silicon used gives this solar panel highest efficiency rate reaching around 20%. Polycrystalline solar panels, can easily be identified by its blue, speckled color, consisting of squares with uncut angles. They made by fast and cheaper process of melting raw silicon as compared to monocrystalline panels. This gives it a shorter life span, lower efficiency around 15 percent and low space efficiency and they are affected by hot temperatures [13].

I.4.2. Second generation solar cells

These thin film solar cells are mainly used for photovoltaic power stations, integrated in buildings or smaller solar systems. Thin-film solar cells (TFSC) are manufactured by the process of depositing one or more films of photovoltaic material (such as silicon, cadmium or copper) into a substrate. They are a cheaper alternative due to less material being needed for their production and they are less affected by high temperatures despite having a shorter life span and taking up a lot of space. Amorphous silicon solar cells (A-Si) has got relatively low efficiency. These solar cells mainly used for pocket calculators having only about 7 percent efficiency rate despite having an advantage of being relatively low in cost[13].

I.4.3. Third generation solar cells

These are solar panels which are still in research and development phase. They use either organic or inorganic materials to generate electricity, such as hybrid solar cells, cadmium telluride solar cells and concentrated solar cells [13].

The following table below summarizes different solar cells technologies and their performances:

Table I.1. Summary of different solar cells technologies and their performances [13]

Solar Cell Type	**Efficiency Rate**	**Advantages**	**Disadvantages**
Monocrystalline Solar cells (Mono –Si)	~ 20%	• High Efficiency, • High time value, • Optimized for commercial use.	-Expensive
Polycrystalline Solar cells (p-Si)	~ 15 %	-Lower Price	• Sensitive to high temperatures • Lower lifespan • Slightly less efficient
Thin Film Amorphous Silicon Solar panels (A-SI)	5 – 9%	• Relatively low cost • Easy to produce • Flexible	• Shorter lifespan
Cadmium Telluride	7 – 11 %	• Absorbs 90% of the incident photons	• Cadmium is a pollutant and toxic

Since Algeria experiences temperatures range from –10° to 34° C, with extreme highs of around 49° C [14] in Sahara Desert, monocrystalline solar panels are better suited for this project. The same can be said about Zimbabwe which has a tropical climate having Matabeleland as the warmest region with temperatures reaching 31 °C [15]. Such a choice is motivated by the fact that:

- They are efficient
- Longer lifespan
- They are not affected by high temperatures.

These regions we have mentioned in Algeria and Zimbabwe experiences less annual rain fall, thereby limiting the humidity which greatly reduces the efficiency of a solar panels.

I.5. Photovoltaic effect

It is a process by which the direct incident solar radiation is converted into electricity by a photovoltaic cell. A photovoltaic cell is an electrical device that is made of a semiconductor material which is doped with other extrinsic elements to form a p-n junction as shown in figure 1.5.

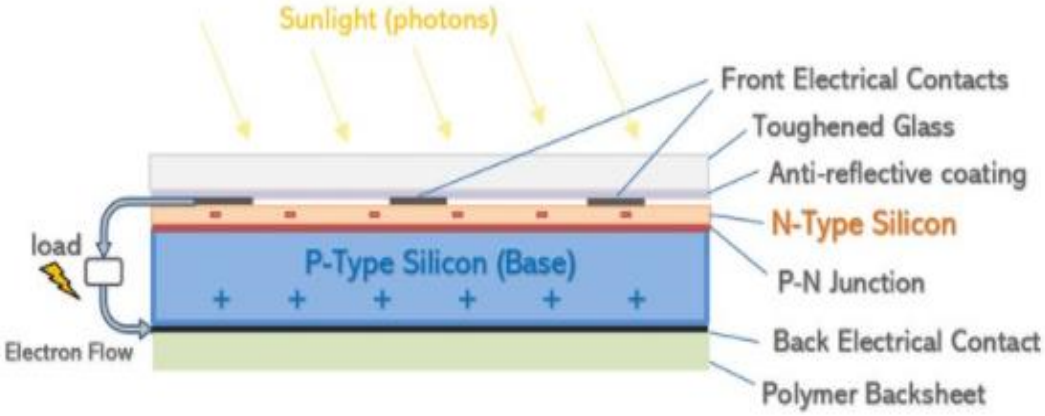

Figure 1.5. Structure of a solar cell [16]

I.5.1. Working principle

When light reaches the p-n junction, light energy, in the form of photons, supplies sufficient energy to the junction to create of electron-hole pairs. The incident light breaks the thermal equilibrium condition of the junction. The free electrons in the depletion region migrates to the n-type side of the junction. Similarly, the holes in the depletion migrates to the p-type side of the junction.[16]

The newly free electrons created migrates to the n-type side, the barrier potential of the junction created stops them from crossing and the same can be said for the holes created and this makes the concentration of electrons and holes to build up. As the concentration of electrons becomes higher on n-type side of the junction and concentration of holes becomes more on the p-type side of the junction, the p-n junction creates a potential difference called photo voltage causing the junction to behave like a small battery cell. When a load is connected across the junction, current flows through it. [16]

The performance of these solar cell depends mainly on the atmospheric condition (humidity, cloud cover etc.), solar irradiation, temperature, air mass and the material used to build up the solar cells.

I.5.2. Photovoltaic cell model

An equivalent circuit of a PV cell consist of a current source I_{ph}, a resistor in series (R_s) and a resistor in parallel (R_p). The resultant current is the difference between the photocurrent Iph, the series resistor current (I) and the parallel resistor current (I_p) as shown in figure 1.6.

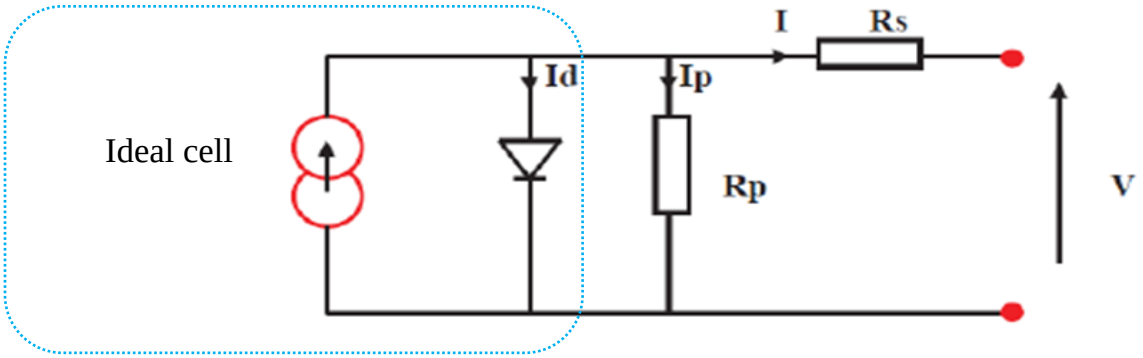

Figure 1.6. Equivalent circuit of an ideal photovoltaic cell [17]

The characteristics of the PV cell can be determined by the following equation after applying Kirchhoff's law.

$$I_{ph} = I_D + I_p + I \tag{I.3}$$

Since it's a single diode model, I_D can be modeled by Shockley equation:

$$I_D = I_s.\left[e^{\frac{V+R_S.I}{nV_t}} - 1\right] \tag{I.4}$$

Whereby V_t is the thermal voltage, with:

$$V_t = \frac{KT}{q} \tag{I.5}$$

And the saturation current is given by I_s:

$$I_s = KT^3 e^{\frac{Eg}{KT}} \tag{1.6}$$

The parallel resistor current I_p is given as follows:

$$I_p = \frac{V+IR}{R_p} \tag{1.7}$$

where:

V: Diode voltage

I_{ph}: Light current (A)

I_s: Diode reverse saturation current (A)

q : Diode ideality factor

R_p : Shunt resistance (Ω)

K : Boltzman constant

Q : Electron charge = ($1{,}602.10^{-19}$ C)

T: Temperature in Kelvin (K)

E_g : Gap energy (1.12 eV for Crystalline-Silicon)

Therefore, the output current of a PV cell is given by the following equation:

$$I = I_{ph} - I_s \left[e^{\frac{V+R_S.I}{nV_t}} - 1\right] - \frac{V+IR}{R_p} \qquad (1.8)$$

V: The potential difference across the cell

I: The output current

In this project we chose the single diode model as it is simple and easy to implement.

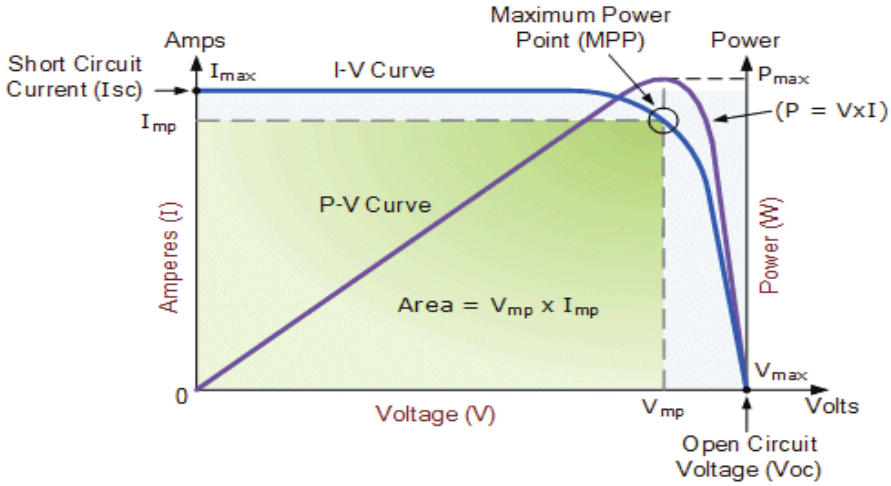

Figure 1.7. I-V and P-V characteristics of a photovoltaic module.[18]

The characteristics of a PV module are illustrated in figure 1.7 above where:
Voc: Open –Circuit Voltage is the maximum voltage that an array produces when the terminals are not connected to any load (an open circuit condition).

Isc: Short-circuit current is the maximum current provided by the PV array when the output connectors are shorted together (a short circuit condition).

MPP: Maximum power point is related to the point where the power supplied by the array that is connected to the load (batteries, inverters) is at its maximum value which is a product of V_{mp} and I_{mp}.

FF: Fill Factor indicates an important role when comparing the performance of different photovoltaic module. A high fill factor is equal to a high-quality module which has low internal losses.

1.6. Arrangement of photovoltaic cells

Photovoltaic (PV) generators are made of multiple interconnected PV cells linked together to form a PV module. When multiple modules are interconnected together, they form a PV array. The connection of these PV modules can either be, series, parallel or both, and the type of connection depends on the voltage and the current levels desired by the power processing system dedicated to the PV generator.

1.6.1. String connection of photovoltaic cells

The photovoltaic cells are arranged in series in photovoltaic panels. This type of configuration is applied because the operating voltage is few hundreds of millivolts as shown in figure 1.8 below:

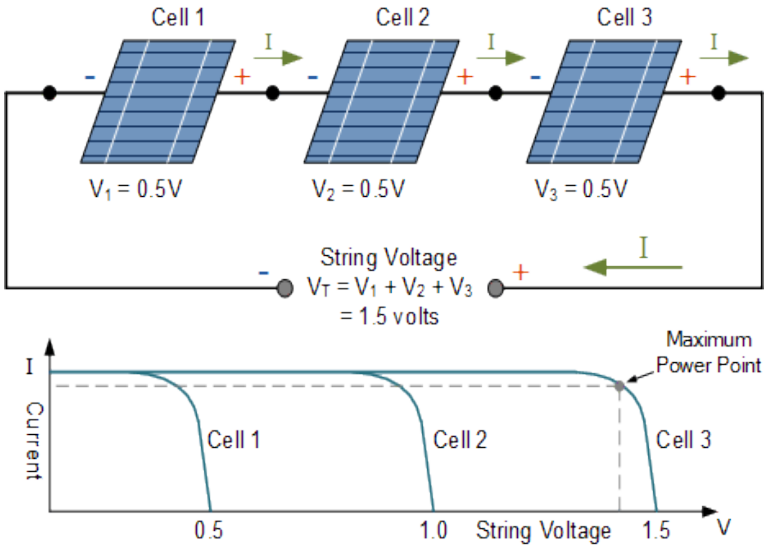

Figure 1.8. Series connection of solar cells [19]

So, the PV cells are connected in series to form strings in order to reach a voltage level that meets the input requirements of the power processing system.

1.6.2. Parallel arrangement of photovoltaic cells.

The figure 1.9 illustrated how the generated current can be increase through parallel connection of photovoltaic cells:

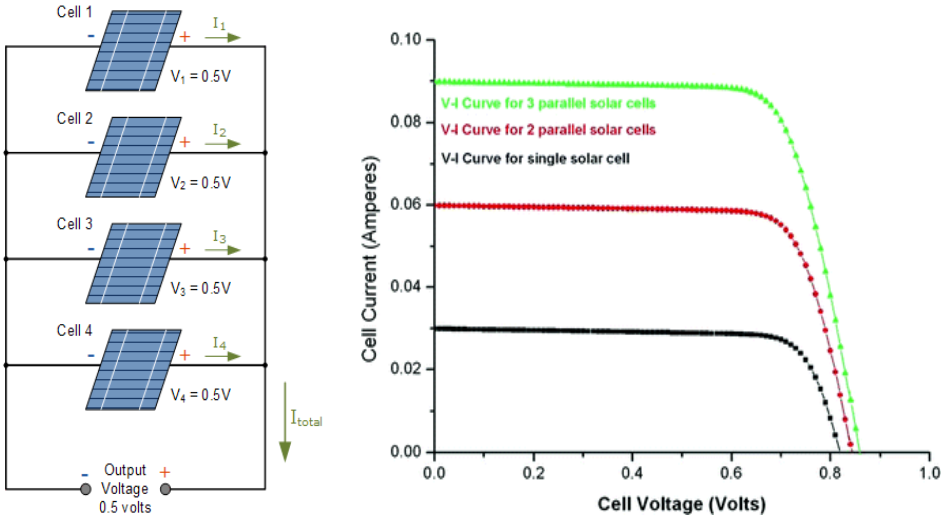

Figure 1.9. Parallel connection of photovoltaic cells [19]

Therefore, a parallel arrangement of photovoltaic cells increases the output current as The potential difference across the terminals is constant

1.6.3. Parallel and series connection of photovoltaic cells

The parallel and series connection of PV cells increases the output voltage and current. The output voltage is obtained by multiplying the voltage value of each cell by the number of cells in series of each panel. The resultant output current is obtained by multiplying the cell current values by the number of strings connected in parallel.

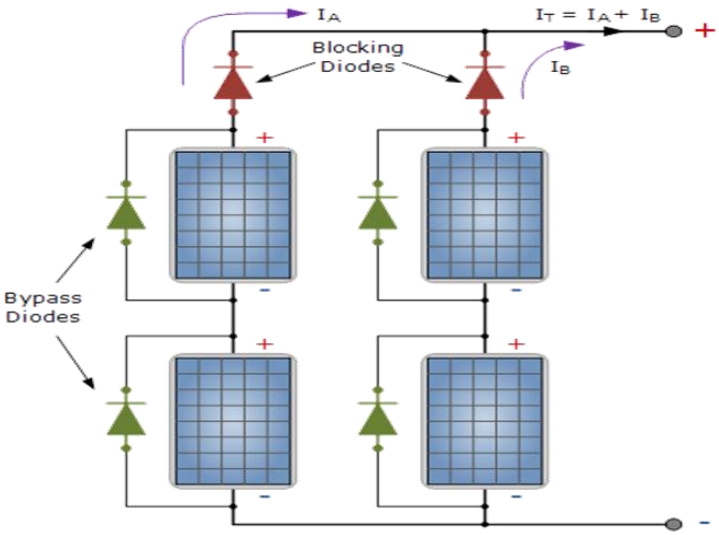

Figure 1.10. Parallel and series connection of photovoltaic cells [20]

In the event of an accident where one cell is broken or simply disconnected, the current of all the cells in series in the string is interrupted and the power contribution of the whole string is missed. The effect of such events is solved by PV panel manufacturers, whereby, they connect a bypass diode in parallel to the PV cell, usually two or three depending on the power rating of the PV panels.

1.7. Effect of temperature and irradiance on the performance of a PV module

In order to determine using MATLAB/Simulink the effects of temperature and irradiation on the performance of a PV panel, a **SUNTECH POWER STP250S -20-Wd** solar panel integrated in MATLAB library has been chosen with the following parameters:
Table I.2. Electrical Characteristics of the module (STC, 1000W/m^2, 25°C, AM = 1.5)

Parameters (STC)	**Values**
Maximum Power	250 W
Optimum operating voltage	30.7 V
Optimum Operating Current	8.15 A
Open Circuit voltage	37.4 V
Short Circuit current	8.63 A
Module Efficiency	15.4%
Operating temperature	-40° C to +85°C
Maximum Voltage	1000 V
Maximum Series Fuse rating	20 A
Power Tolerance	0/ +5%

1.7.1. Effect of temperature on the performance of a PV module

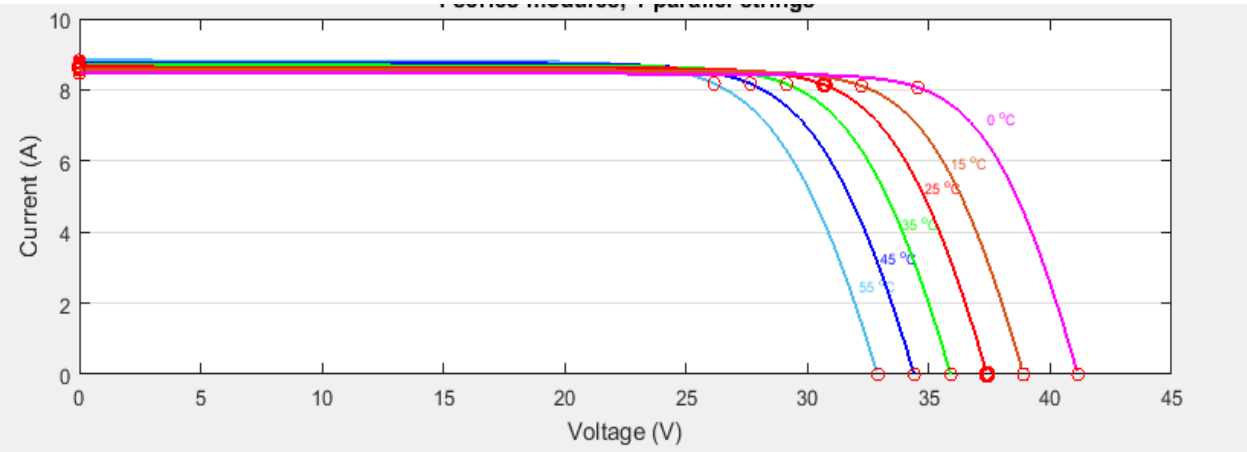

Figure 1.11. Effect of temperature on output voltage and current

When the irradiance is maintained at 1000W/m^2, the voltage and current of the PV panel is inversely proportional to the temperature as shown in figure1.11.

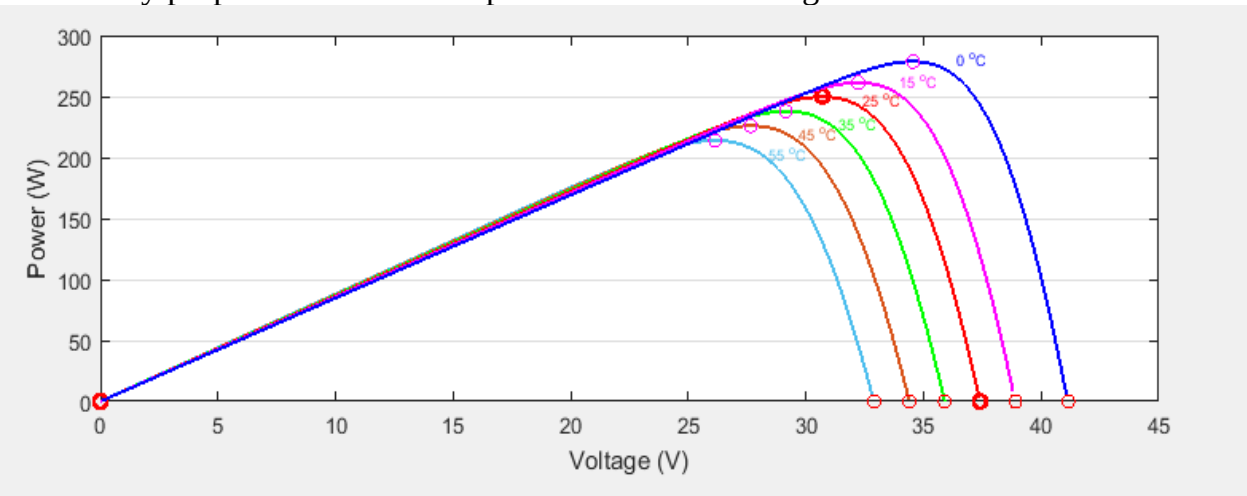

Figure 1.12. Effect of temperature on solar power output

The power produced by the photovoltaic modules decreases with an increase in temperature because; the band gap energy decreases and more photons have enough energy to create electron-hole pairs which eventually reduces the efficiency of the panel [21].

1.7.2. Effect of irradiance on the performance of a photovoltaic module

While the temperature is maintained at 25°C, the voltage and current output of a photovoltaic module is directly proportional to the solar radiation as shown in figure 1.13.

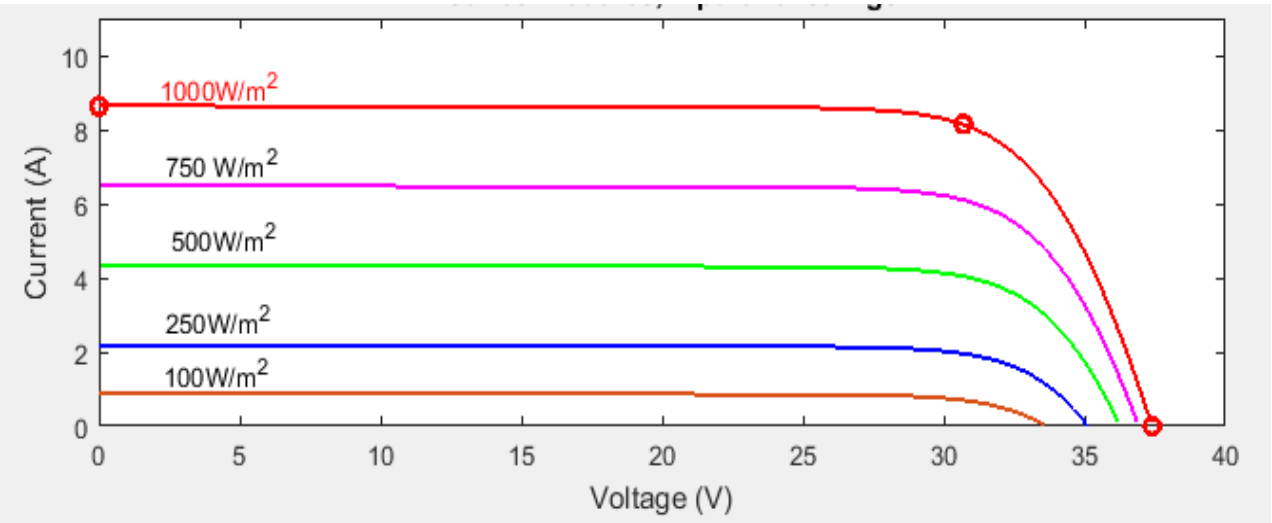

Figure 1.13. Effect of the irradiation on the PV voltage and current output

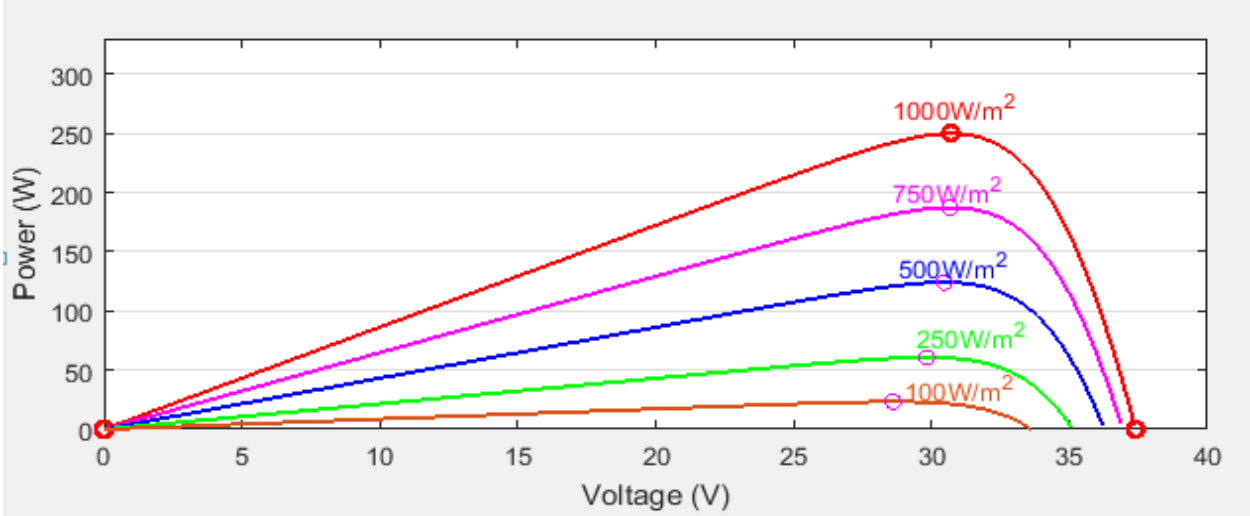

Figure 1.14. Effect of irradiation on PV power output

The curves shown in figure 1.14 shows that, the power produced by the solar panel is directly proportion to the solar radiation.

I.8. Power electronic converters

Power electronic devices plays a major in the functioning of photovoltaic system either in stepping up or stepping down DC the voltage generated by the solar panels and these are known as DC-DC converters or during the conversion of direct current to alternating current and these referred to as (DC-AC converters). The choice of these power electronic devices rests entirely on the types of load used, either AC or DC loads.

I.8.1. DC-DC converters

These are solid state power electronic devices which steps up of steps down DC voltage. The DC-DC converters are driven by PWM, whereby a high frequency pulse signal is used to turn on and off the electronic switches, thus controlling the converter voltage. These DC-DC converters include:

- ✓ Buck converters,
- ✓ Boost converters
- ✓ Buck – boost converters

In this project, we will focus mainly on the boost converter which play a key role in stepping up the DC voltage and also in tracking the maximum power point.

I.8.1.1. Boost converter

Generally, a boost converter as shown in Figure 1.15 is a DC-DC converter with an output voltage greater than the source voltage. It is sometimes called a step-up converter since it "steps up" the source voltage as it is designed to provide an efficient method of taking a given DC voltage supply and boost it to a desired value.

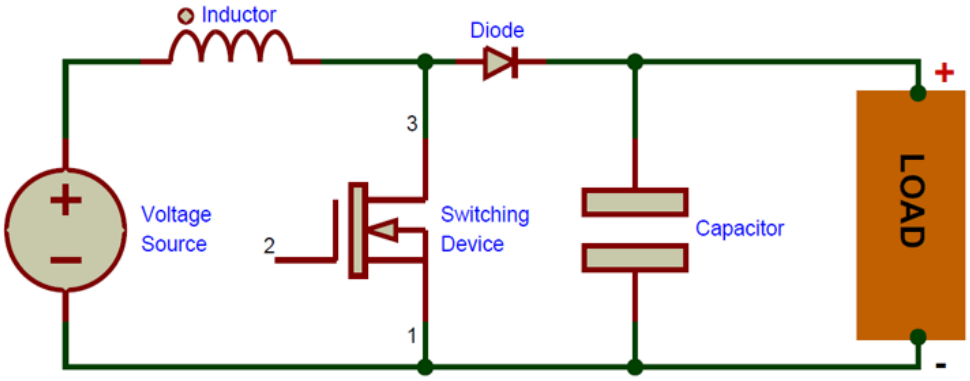

Figure 1.15. Schematic diagram of a boost converter [22]

The voltage source for the boost converter comes from any suitable DC sources, such as DC generators, batteries, solar panels, and rectifiers. The operation of the boost converter can be divided into three modes that is, mode 1 and mode 2 and mode 3 as shown in figure 1.16 and figure 1.17

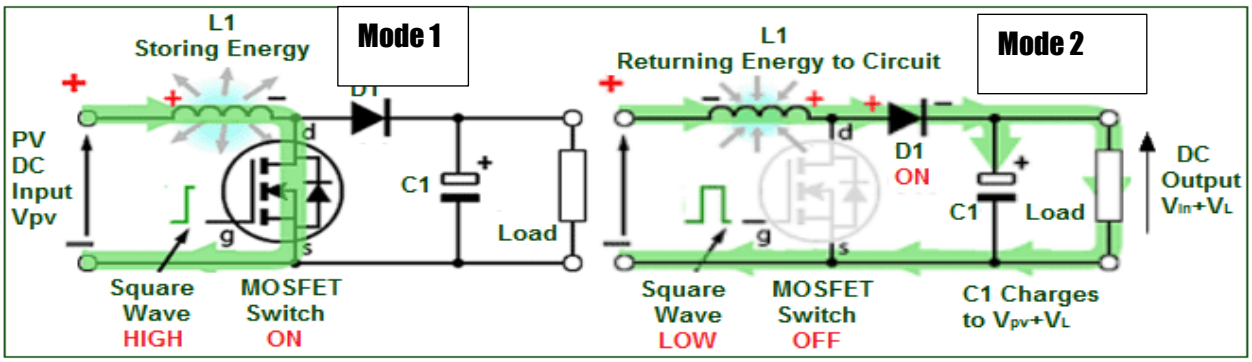

Figure 1.16. Working Principle of a boost converter [23]

I.8.1.1.1. Mode 1

When the boost converter circuit is energized by a DC voltage from a DC source and when the switching pulse signal applied to the transistor (IGBT or MOSFET) is on HIGH period, the MOSFET conducts, allowing current to flow between the positive and negative supply terminals of L1.

This allows energy to be stored in its magnetic field while part of circuit is short circuited as shown in figure 1.16 and, no current flowing in the remainder of the circuit.

I.8.1.1.2. Mode 2

During the LOW period of the switching pulse cycle, the MOSFET is rapidly turned off and a sudden drop in current occurs in the MOSFET causing L1 to generate a back e.m.f. in the opposite polarity to the voltage across L1 to keep the current flowing. This results in two voltages, the supply voltage (Vin) and the back e.m.f. (V_L) across L1 in series with each other. This produces a higher voltage (Vin +V_L) and there is no current flowing through the MOSFET, because of the forward biased diode on the MOSFET. [23] The resulting current through D1 charges up C1 and supply the load as shown in figure 1.16

I.8.1.1.3. Mode 3

When the MOSFET is conducting during the next cycle, the cathode of D1 is more positive than its anode, due to the charge on C1. D1 is therefore turned off so the output of the circuit is isolated from the input, however the load continues to be supplied by the stepped-up voltage (Vin +V_L) from the charged capacitor C1.

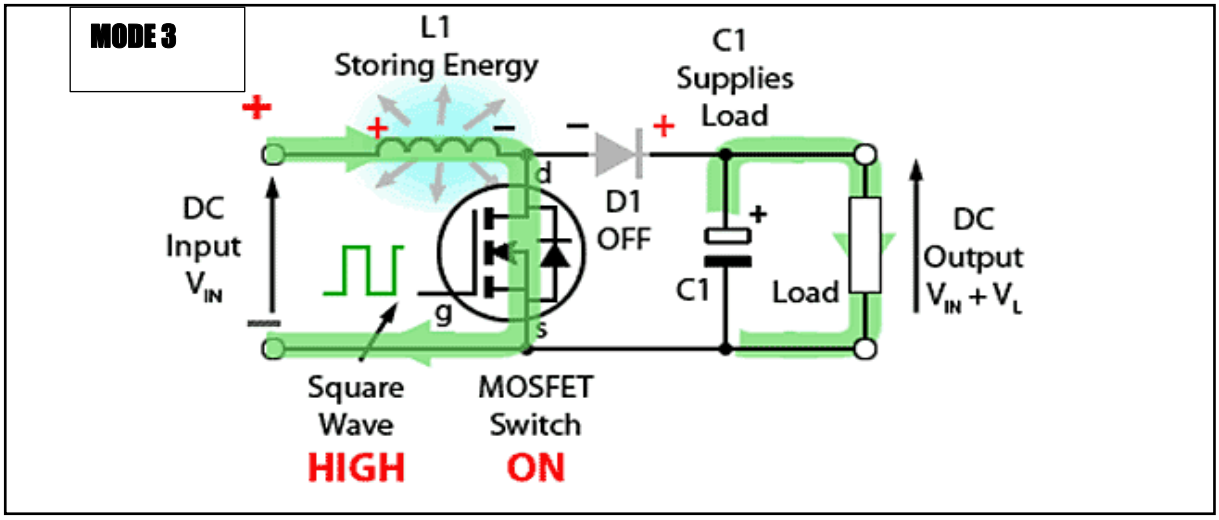

Figure 1.17. Third stage of the operation of the Boost Converter [23]

Although the charged C1 drains away through the load during this period, C1 is recharged each time the MOSFET switches off, so maintaining an almost steady output voltage across the load.

I.9. Determination of the size of the boost converter components

The parameters of the boost converter are calculated as follows

I.9.1. Duty Cycle

The duty cycle of the boost converter is calculated by the equation below:

$$V_{out} = \frac{V_{in}}{1-D} \quad \text{and this implies that} \quad D = \frac{V_{out}-V_{in}}{V_{out}} \tag{I.9}$$

where:

V_{in} : Input voltage (V)
V_{out} : Output voltage (V)
D: Duty cycle

I.9.2. The voltage and current ripples

The inductance voltage is calculated as follows:

$$V = L\frac{di}{dt} \quad \text{this implies that:} \quad V.\,Ton = L\Delta I_L \tag{I.10}$$

Therefore: $$\Delta I_L = \frac{V_{in}}{L\,f} D \tag{I.11}$$

And the voltage ripple (ΔV) is determined by the equation below:

$$\Delta V = \frac{1}{f\,C_2} D \tag{I.12}$$

where:
ΔI_L: The ripple current and ΔV: The ripple voltage

I.9.3. Determination of the size of the capacitor

The value of the capacitor is calculated by the equation below:

$$C_2 = \frac{D\ I_0}{f\,\Delta V_0} \tag{I.13}$$

where:

I_0: Output current
f: Switching frequency
ΔV_0: Voltage ripple is strictly constrained at 1% of V_0

I.9.4. Determination of the size of the inductor

The value of the inductor is given by the equation below:

$$L = D\frac{V_{in}}{f\,\Delta I_L} \tag{I.14}$$

where:

V_{in}: Input voltage

f: Switching frequency
ΔI_L: Current ripple is calculated as 10-30% of I_L

I.9.5. Load calculation

$$R_0 = \frac{V_0}{I_0} \quad \text{(I.15)}$$

where, R_0: Resistance of the load (Ohm), V_0: Output voltage (V), I_0: Output current (A)

I.10. Inverters

An inverter is solid state power electronic device which converts DC voltage to AC voltage. This type of a converter is used if the PV array is connect to AC loads like most of the home appliances ad AC motors. There are two main types of inverters namely, the current source inverters (CSI) and the voltage source inverter (VSI). In this project, we focus mainly on a three phase voltage source inverter.

I.10.1. Inverter model

The three-phase inverter is composed of six IGBT switches (k_{11}, k_{12}, k_{21}, k_{22}, k_{31}, k_{32}) each shunted in parallel by a fast-freewheeling diode, in order to return the negative current to the filter capacitor provided at the input of the converter as shown in figure 1.18:

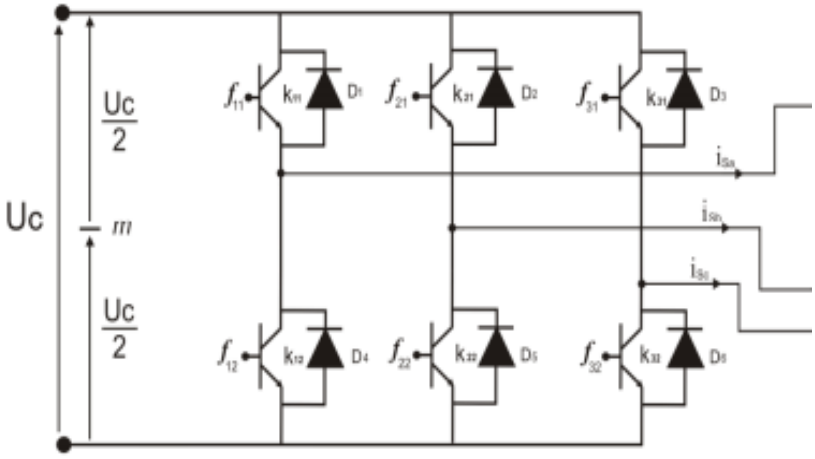

Figure 1.18. Schematic diagram of a three-phase inverter [21]

The inverter is controlled by commanding the opening and closing of the IGBT switches, with f_{ci} ($c \in \{1, 2, 3\}$, $i \in \{1, 2\}$) as the state of switches denoted as kci:

$$\begin{cases} f_{11} = 1 - f_{10} \\ f_{21} = 1 - f_{20} \\ f_{31} = 1 - f_{30} \end{cases} \quad \text{(I.16)}$$

where:

c: represents the branch
i: represents the switch number on the branch
$f_{ci} = 1$ if the switch is ON
$f_{ci} = 0$ if the switch is OFF

The input voltage and the control signal determine the output voltage as illustrated below.

$$\begin{cases} u_{sab} = U_c(f_{11} - f_{21}) \\ u_{sbc} = U_c(f_{21} - f_{31}) \\ u_{sca} = U_c(f_{31} - f_{11}) \end{cases} \quad \text{(I.17)}$$

This in turn ensures that the stator voltages are as follows:

$$v_{sa} + v_{sb} + v_{sc} = 0 \quad \text{(I.18)}$$

Therefore

$$\begin{bmatrix} v_{sa} \\ v_{sb} \\ v_{sc} \end{bmatrix} = \frac{U_c}{3} \begin{bmatrix} 2 & -1 & -1 \\ -1 & 2 & -1 \\ -1 & -1 & -2 \end{bmatrix} \begin{bmatrix} f_{11} \\ f_{21} \\ f_{31} \end{bmatrix} \quad \text{(I.19)}$$

I.10.2. Control of inverters

Several control techniques have been proposed since the invention of AC drives which helps in varying the frequency, hence speed of electric motors, and these techniques include Space Vector Pulse Width modulation (SPWM) and the basic (PWM) technique which is characterized by a comparison between a reference signal and a carrier wave signal with different frequencies [24]. The comparison of these two signals generates pulses which are then used in turning ON and OFF of the electronic switches like IGBTs.

For our project we chose a BLDC motor which requires a special driver, an electronic commutator which will be discussed in chapter II.

I.11. Maximum power point tracking

The relationship of PV systems with external grids, battery banks, or other electrical loads exist in a lot of different configurations. Regardless of the application of the solar power systems, the efficiency of power transfer from the PV module(s) depends on incident solar radiation on PV panels, the temperature and the electrical characteristics of the load.

These external conditions and the load characteristic vary and the problem is on delivering the maximum power with a given irradiation and temperature. This requires the efficiency of the system to be optimized when the load characteristic, temperature and solar irradiation, changes to keep the power transfer at the highest point which is then called the maximum power point (MPP) [25]

As a consequence, it is of paramount importance that an intermediate conversion stage, has to be adopted interfacing the PV array and the power system that processes or uses the electrical power produced by PV panel (s). In addition to that, this power system energized by the PV power must be capable of adapting its input voltage and current levels to the instantaneous PV source changes, while keeping its output voltage and current levels in line with the load requirements. Therefore, dynamical optimizer plays a crucial role in performing this adaptation in the presence of time-varying operating conditions affecting the PV generator.

In order to maximize the power extraction from the PV module(s), it is pivotal that an interface power converter must be capable of self-adjusting its own parameters during the operation time, thus changing its input voltage/current levels based on the PV source while operating at the MPP position. In this project a DC-DC converter has been chosen and the duty cycle D as the controlling the input. The duty cycle (D) value must be changed continuously by a controller to ensure that the PV generator always operates at its MPP with the current irradiance and temperature and that is why it is called a maximum power point tracking (MPPT) controller [25]. Based on the values of the current and voltage sensed at the PV module(s) terminals, the MPPT controller dynamically adjusts the converter duty cycle to follow the MPP. The following schematic diagram illustrated the basic components MPPT control system

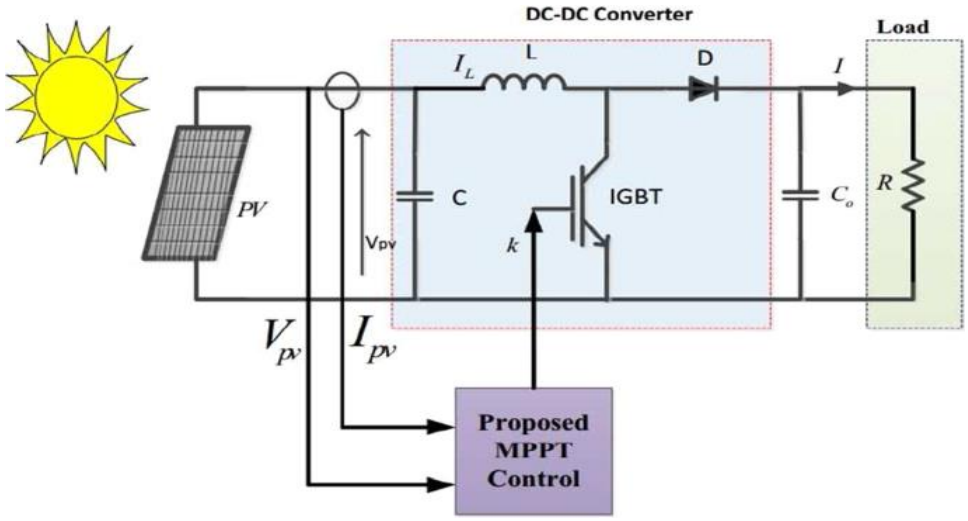

Figure 1.20. Maximum power point tracking implementation [26]

I.11.1. MPPT techniques

The MPPT techniques mostly used in commercial products usually measure both current and voltage values of the PV generator. The direct measurement of the temperature and irradiance values requires expensive devices that have to be placed throughout the PV generator that is why it is avoided. A lot of techniques have been proposed in order to track the maximum point which are either direct or indirect MPPT techniques.

I.11.1.1. Direct MPPT techniques

In the event that, the maximum power point tracking capability is required with high precision and in varying environmental conditions which the PV generator is operating in, then direct MPPT methods is the best choice [25). These techniques require a continuous measurement of the PV current and voltage, in order to realize a proper adjustment of the system operating conditions in order to track the MPP. These techniques include, Perturb and Observe Approach, Incremental conductance (INC), Self-Oscillation method (SO) and Extremum Seeking control.

I.11.1.2. Indirect MPPT techniques

Indirect methods track the MPP using empiric data or mathematical expressions with numerical corrections and approximations. The main drawback of such a technique is that when the real conditions deviate too much with respect to those supposed in the modeled adopted, the MPPT may not be properly tracked. These techniques include**, fuzzy Logic** and **Neural Network Methods.**

Fuzzy logic-based trackers have shown very good performances under varying irradiance conditions without any detailed knowledge of the PV source model [25]. On the other hand, deep knowledge of the system operation and experience is required to choose the relevant computation error and the rule base table.

I.11.1.2.1. MPPT by fuzzy logic

Fuzzy control is one of the new indirect control methods based on fuzzy set theory. It is suitable for the mathematical model of the unknown and complex nonlinear system. Since, a PV system is a strongly nonlinear system, the performance of the PV cells is difficult to describe with accurate mathematical model, and therefore, fuzzy control method for MPPT is very appropriate and this technique produce, rapid response to the external environment and weaken the power oscillation near the maximum power point. [27].

To realize the MPPT control method, the fuzzy control system samples the data to determine the positional relationship between the operation point and the MPP. The input variables are the slope value of the continuous sampling points of the error E and the change in unit time of the slope CE of the P-V curve. These parameters are calculated as shown in equation I.20 and I.21

I.11.2. Fuzzy logic controller

A fuzzy control system is a control system based on fuzzy logic, a mathematical system that analyzes analog input values in terms of logical variables that take on continuous values between 0 and 1. The structure of a fuzzy logic controller consist of three basic components, fuzzification module, inference engine and defuzzification module as shown in figure 1.21

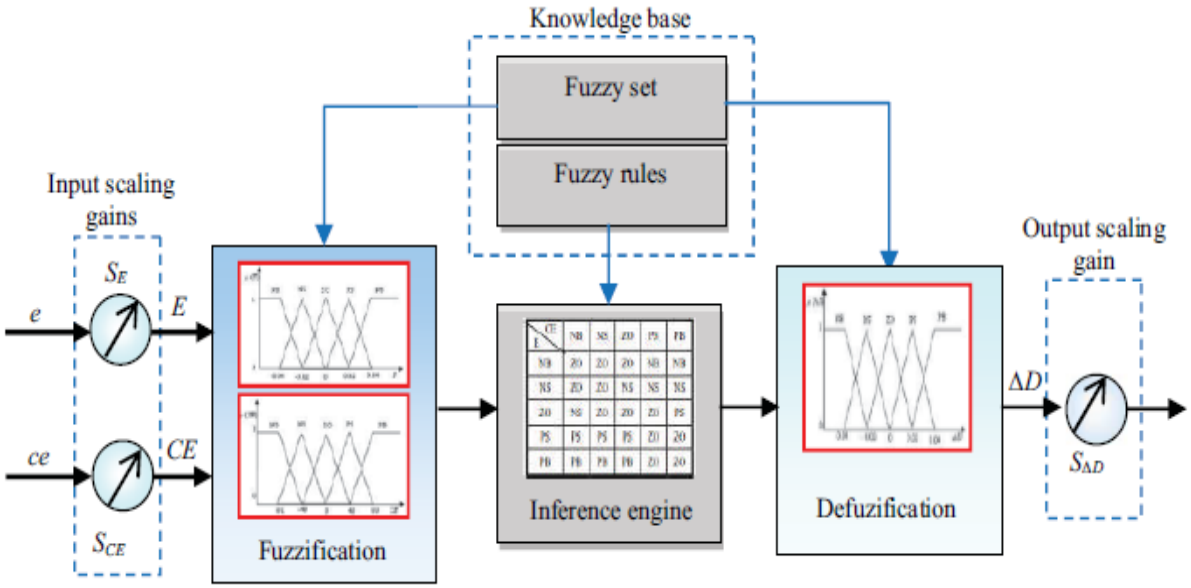

Figure 1.21. Structure of fuzzy logic controller [28]

I.11.2.1. Fuzzification

This technique requires the transformation of numerical values to fuzzy quantities which a controller can identify and this is called *fuzzification*. The linguistic terms which describe the variable characteristics are:

Inputs: PB: *Positive Big*, **PM**: *Positive Medium*, **PS**: *Positive Small*, **Z***: Zero*,

NS *Negative Small*, **NM**: *Negative Medium*, **NB**: *Negative Big*

Output: **Z**: *Zero*, **S**: *Small*, **M***: Medium*, **B**: *Big*, **VB**: *Very Big*

The fuzzification makes it possible to pass from the real variables to fuzzy variables. The actual voltage and current of PV generator can be measured continuously and the power can be calculated. The control is determined on the basis of satisfaction of two criteria relating to two input variables of proposed controller, namely error E (which represents the slope of P-V characteristic) and change of this error (CE), at a sampling instant *k*.

The variable *E* and *CE* are expressed as follows,

$$E(k) = \frac{dP(k)}{dU(k)} = \frac{P(k)-P(k-1)}{U(k)-U(k-1)} \quad \text{(I.20)}$$

$$CE(k) = E(k) - E(k-1) \quad \text{(I.21)}$$

Where P (k) and U (k) are the output power and the output voltage of PV cells for a sampling time of ***k*** times.

I.11.2.2. Tracking of the maximum power point

Therefore, the input *E*(*k*) shows if the operating point at the instant k is located on the left side or on the right side of the MPP on the *P-V* characteristic, while the input *CE*(k) expresses the displacement direction of this point. The change in duty ratio of the DC-DC converter is used as the output of the controller. Therefore, the control is done by changing this duty ratio according to the slope *E* (*k*) in order to bring back the operation point on the optimal point where the slope is zero. If the error E (k) =0, this shows that PV cells have been working at the maximum power output state as shown in figure 1.22.

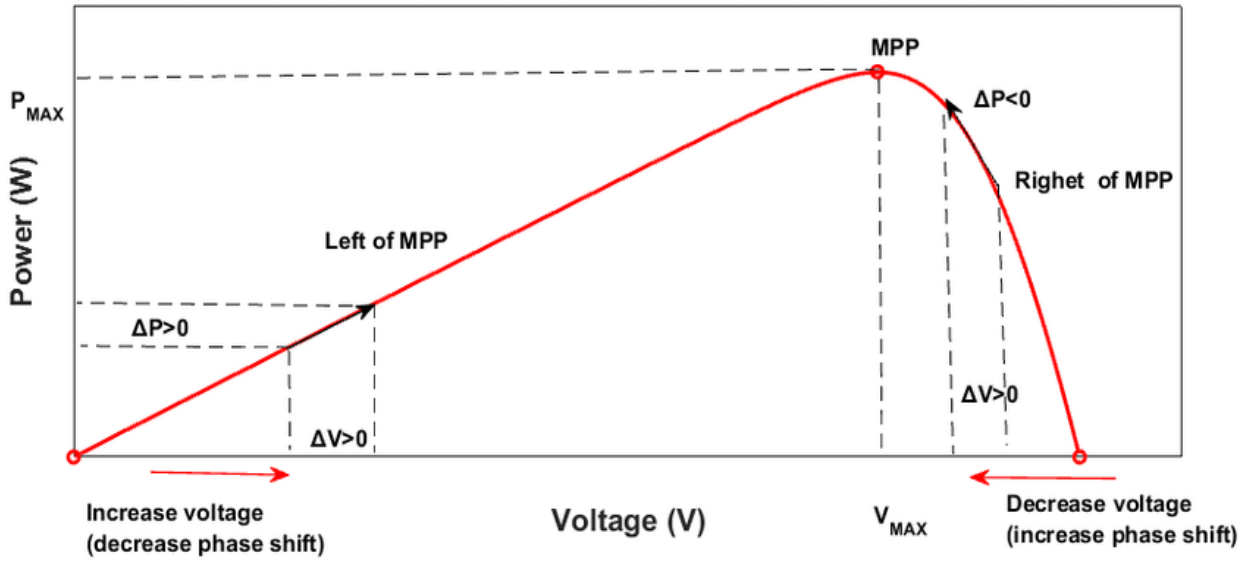

Figure 1.22. Tracking of the MPPT by fuzzy logic controller [29]

I.11.2.3. Rules of fuzzy logic controller

For the PV to produce the maximum power from the given irradiation and temperature, the following rules are put into play.

1. When **E(k) < 0** and **CE(k) < 0**, P from the left side of the MPP, **D** should be positive, to reach the MPP.

2. When **E (**k) < 0 and **CE (k) > 0**, P from the left side far away from the MPP**, D** should be positive, to reach the MPP.

3. When **E (k) > 0** and **CE (k) < 0**, P from the right side close to the MPP, **D** should be negative, in order to return to the MPP.

4. When **E (k) > 0** and **CE (k) > 0**, P from the right side far away from the MPP, **D** should be negative, in order to return to MPP.

I.11.2.4. Inference engine

Inference engine applies the rules in Table 1.3 of the fuzzy inputs (that were generated from the fuzzification process) to determine the fuzzy outputs. Therefore, before the rules can be evaluated, the crisp input value must be fuzzified to obtain the corresponding linguistic values and the degree to which each part of the antecedent has been satisfied for each rule. The memberships function for the fuzzy logic controller which are, error (E), change of error (CE) and the duty ratio are shown in figure 1.22.

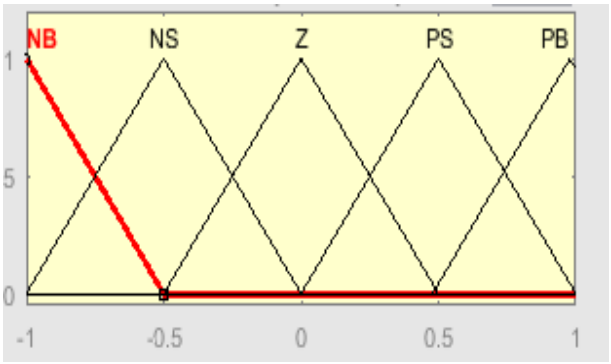

Figure 1.22(a). Error (C)

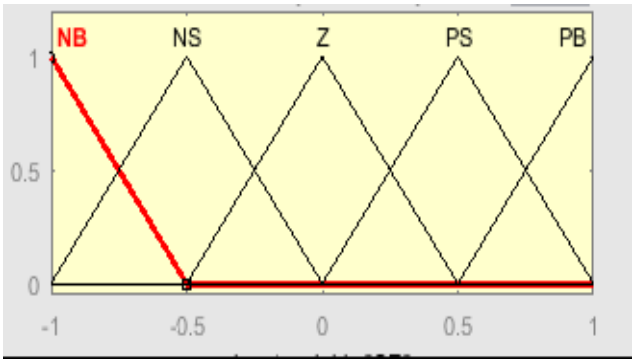

Figure 1.22 (b). Change of error (CE)

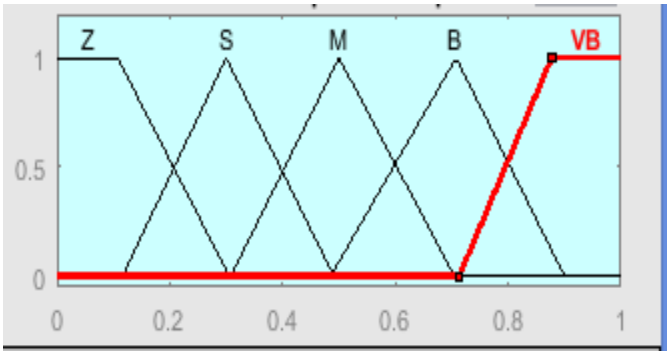

Figure 1.22(c). Duty cycle (D)

E	CE				
	NB	**NS**	**Z**	**PS**	**PB**
NB	Z	Z	Z	B	M
NS	Z	Z	S	M	B
Z	Z	S	M	B	VB
PS	S	M	B	VB	VB
PB	M	B	VB	VB	VB

Table I.3 Inference matrix

The membership function uses a uniform triangular membership function to determine the input (E and CE) and output variable (D) between the different values with corresponding linguistic variables of membership (D).

I.11.2.5. Defuzzification

Defuzzification refers to the conversion of fuzzy variables to a precise numerical value, which is calculated according to the output of fuzzy subset membership function. There are many methods used in the defuzzification process, which usually use maximum membership degree method and the area of the center of gravity method given by the following equation:

$$D = \frac{\sum_{i=1}^{n} \mu(D_i).D_i}{\sum_{i=1}^{n} \mu.(D_i)} \qquad (I.22)$$

Where D represents the duty cycle.

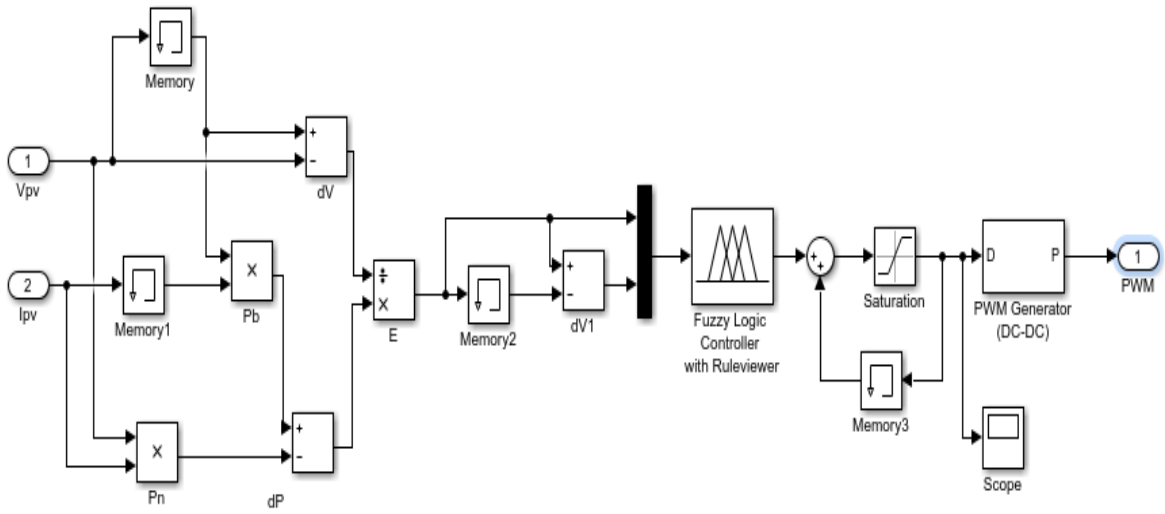

Figure 1.23. Simulink model of a fuzzy MPPT controller

The duty cycle calculated passes through the pulse with modulation (PWM) generator and the output square wave pulse signal is fed to the switching transistor of the boost converter to step up the DC voltage. The fuzzy logic controller with rule viewer shows the evolution of the crisp entries (error E, and change of error CE) and the calculated duty cycle as shown in figure 1.24. The evolution of these crisp entries is determined by 25 rules shown in the inference matrix, Table 1.3.

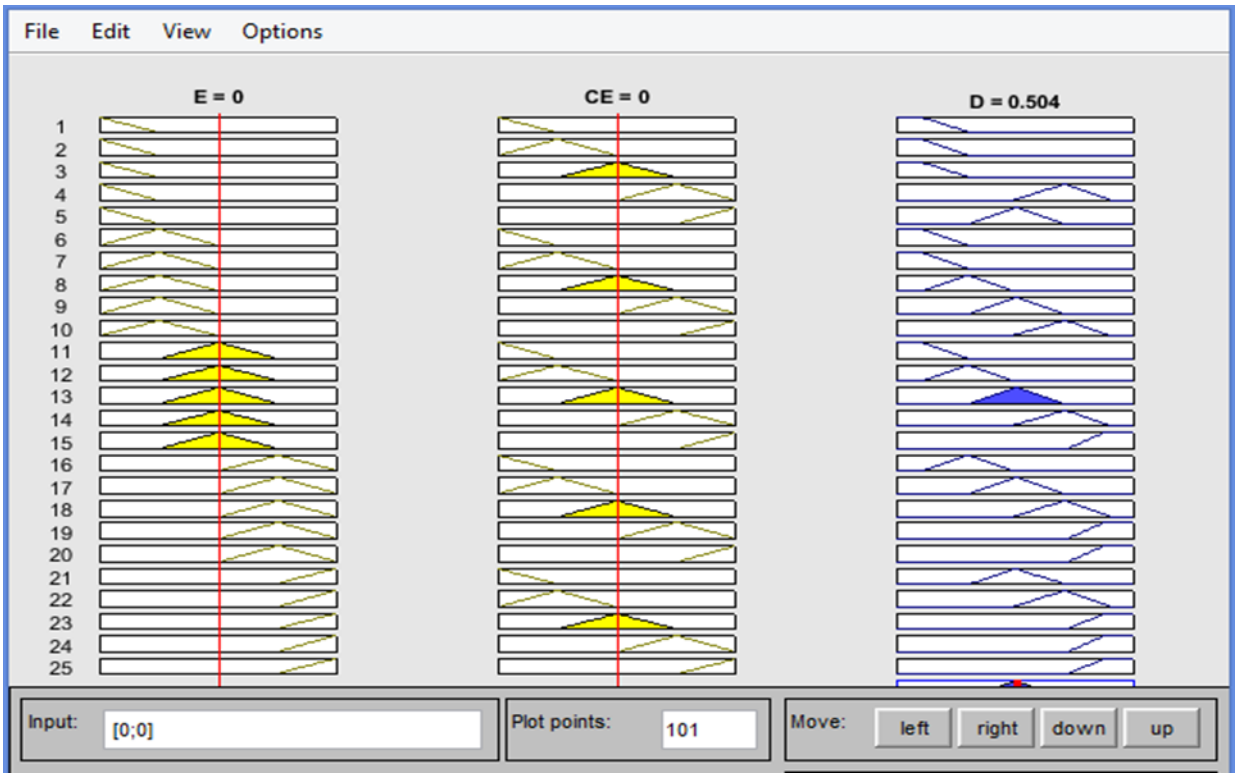

Figure 1.24. Evolution of the duty cycle with respect to the entries (E and CE)

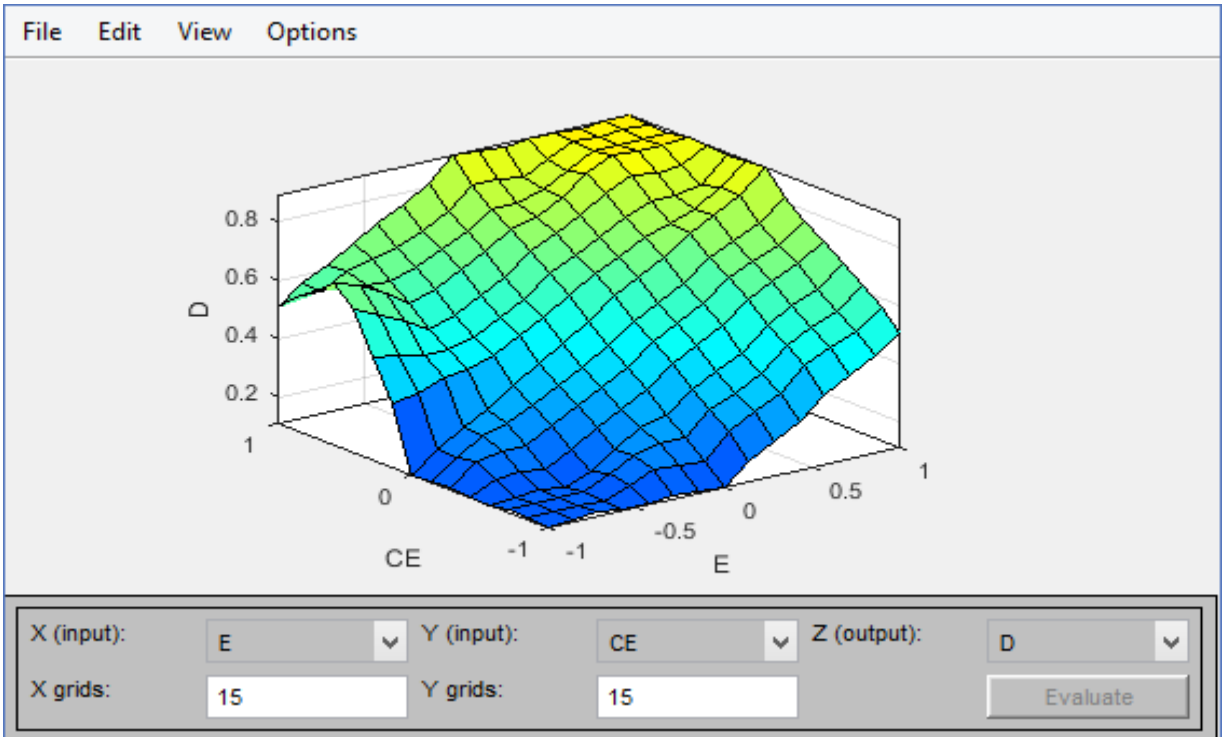

Figure 1.25. Graphical representation of the entries (E and CE) and the output D

.

The model of the fuzzy logic controller MPPT technique which has been simulated using MATLAB/Simulink, is shown in figure 1.26 consisting of a PV generator, boost converter and a signal builder block with a modified step signal showing, the variation of solar irradiation with a constant temperature is shown in figure 1.27.

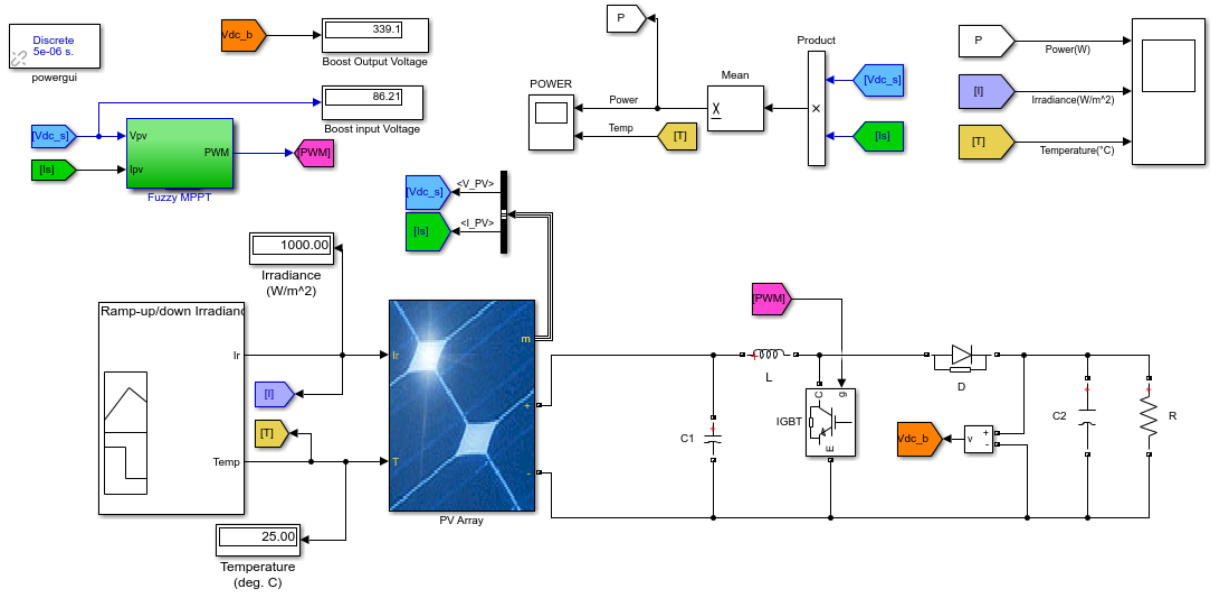

Figure 1.26. Simulation of the fuzzy logic controller MPPT on Simulink, MATLAB

1.12. Elements of the Boost Converter

Table I.3 shows the calculated values of the boost converter

Element	Value
DC Link Capacitor C1	1.5mF
Inductor L1	I mH
Capacitor C2	3.4 μF
Load resistor	82.64 Ω
Maximum PV Array Power	1.5 kW
Switching Frequency	50 kHz

The variation of solar irradiance is shown in figure 1.25 below

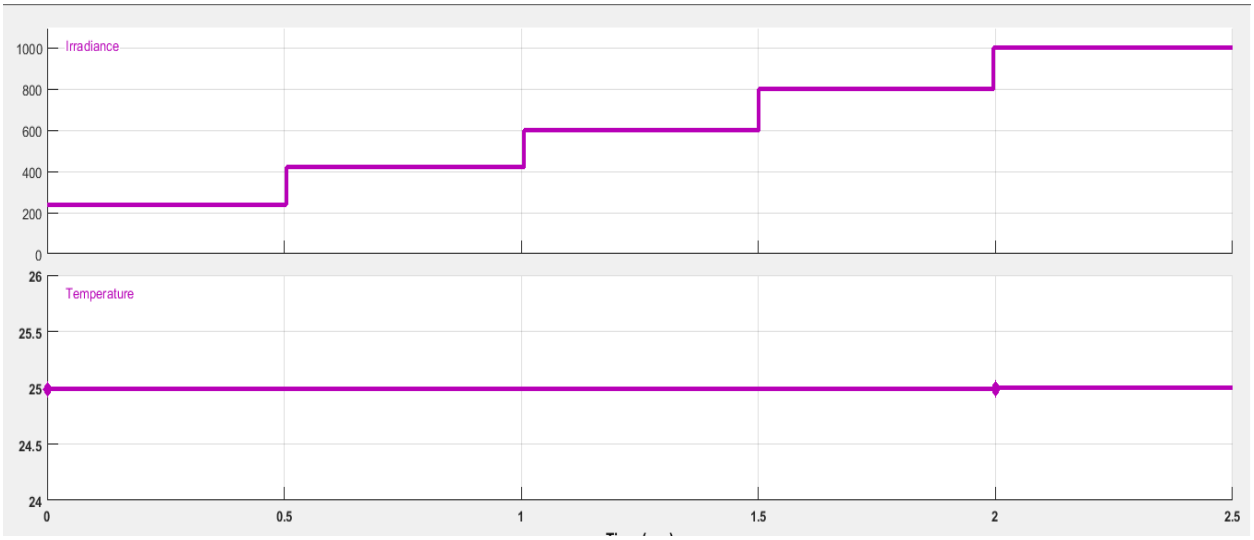

Figure 1.27. Step signal representing the variation of the solar radiation

The results of the simulation are shown in figure 1.26 below:

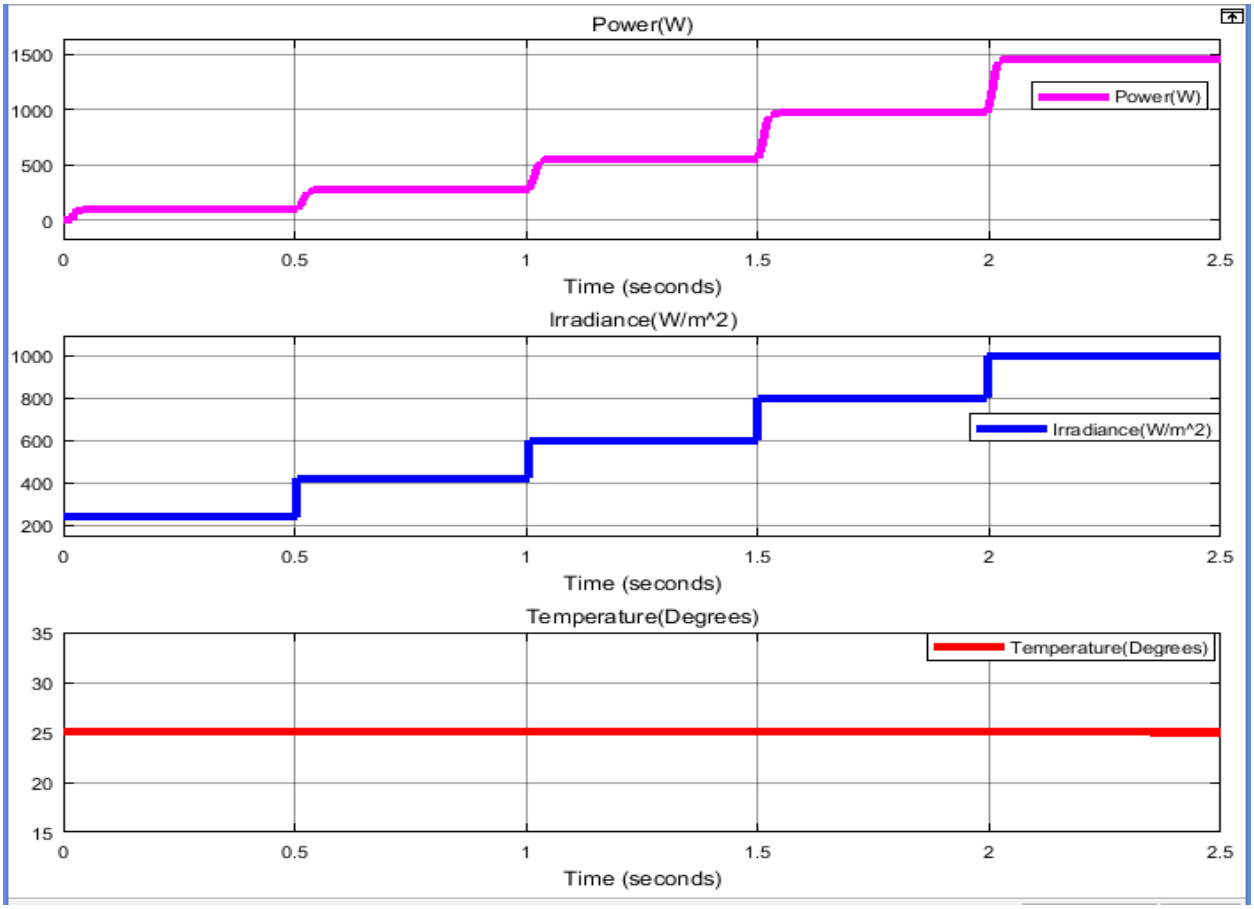

Figure 1.28. Tracking of the MPPT by fuzzy logic controller

From the simulation results, it is clearly evident that Fuzzy Logic Controller MPPT is quite efficient in tracking the maximum power point. Moreover, it limits oscillations near the maximum power which is a phenomenon experienced when other MPPT techniques such as Perturb and Observe techniques are used. The FLC MPPT technique has an advantage of being implemented without the necessity of knowing the mathematical model of the system and can perform well in nonlinear conditions.

1.13. Conclusion

In this chapter, we have discussed about the PV systems, including the influence of external factors on the performance of the PV systems. We also discussed about the power electronic devices which either steps ups or down the DC voltage or transforming DC into AC. Moreover, we discussed about the MPPT techniques which is a pivotal technique ensuring maximum extraction of power from the PV generators and the implementation of the Fuzzy Logic Controller MPPT technique which, we then simulated using MATLAB /Simulink to demonstrate the feasibility of the technique and its efficiency. The following chapter will be focusing on the SWPS. We will then discuss on several components of the pumping system including, electric motors, centrifugal pumps and sizing of SWPS.

Chapter II

An Overview of Solar Water Pumping Systems

II.1. Introduction

One of the key elements of a PV water pumping system is an electric water pump. The traditional water pumps have been designed to run at a constant speed when using a stable power source. However, the speed varies with the variation of the intensity of solar radiation and with the angle of the sunshine on the PV array. From a mechanical standpoint these pumps are divided into two categories which are centrifugal pumps and positive displacement pumps which will be discussed in this chapter. Moreover, we will discuss on types of electrical motors used, the steps taken in designing and sizing the system, and the different configurations of the solar water pumping systems.

II.2. Electrical motors classification

Electric motors used in solar water pumping systems acts as prime movers as they provide mechanical power for the operation of the pump. The choice of these electric motors depend on their performance, the operation cost and the maintenance in the long run, efficiency and power demand. There are two main types of electric motors used namely, AC and DC motors with several sub-types under their categories as shown in figure II.1.

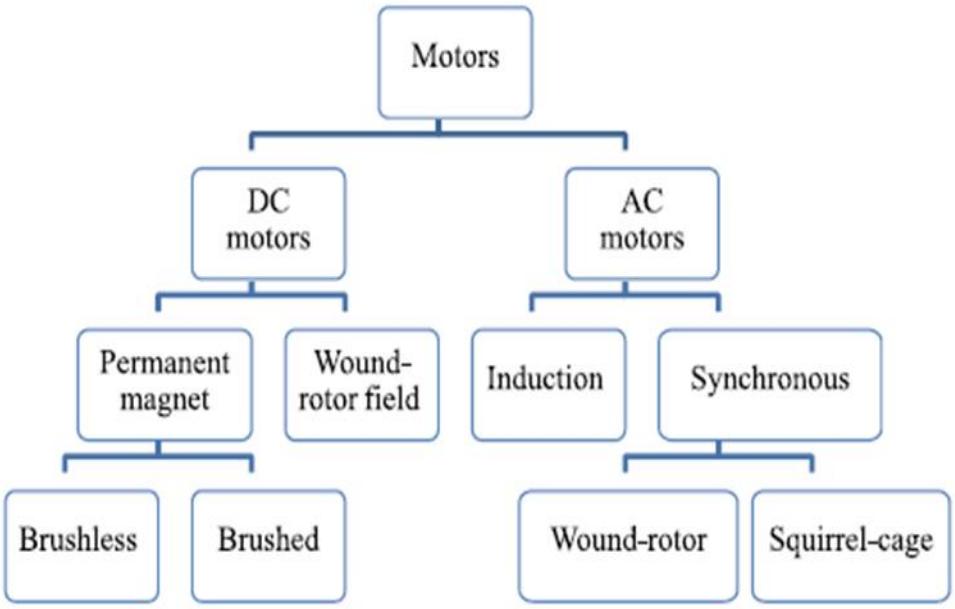

Figure II.1. Classification on electrical motors used in PV water pumping [30]

Generally, AC motors are used for high power demand and they are cost-effective while DC motors have higher efficiency than AC motors [30]. Moreover, they don't need an inverter (except for BLDC with a BLDC driver), since PV arrays generates DC voltage. However, DC motors need a periodic replacement of the mechanical moving parts

(commutators), usually after 2000h to 4000h [30]. The main types of DC motors used in solar water pumping systems are, brush-type DC motors and brushless DC motors (BLDC).

II.3. Brush-type DC motors

The brush-type DC motor is the traditional DC motor technology that has been used in DC powered applications for many decades. There are a lot of DC motors as shown in figure II.1, whereby the difference only comes on the structure of the stator and the excitation circuits. The stators of the DC motors can be made of a permanent magnet or a field winding. The brushes are small blocks of electrically conductive carbon-graphite which rubs against the spinning part of the motor (rotor) thus feeding current into it. This causes the current not to alternate (to become AC) within the motor. This simple technology has two major disadvantages which are that the brushes wear out and must be replaced periodically and the motor must be filled with air (not liquid) and must be 100% sealed against water leakage [31]. Figure II.2 shows an example of a brushed-type DC motor.

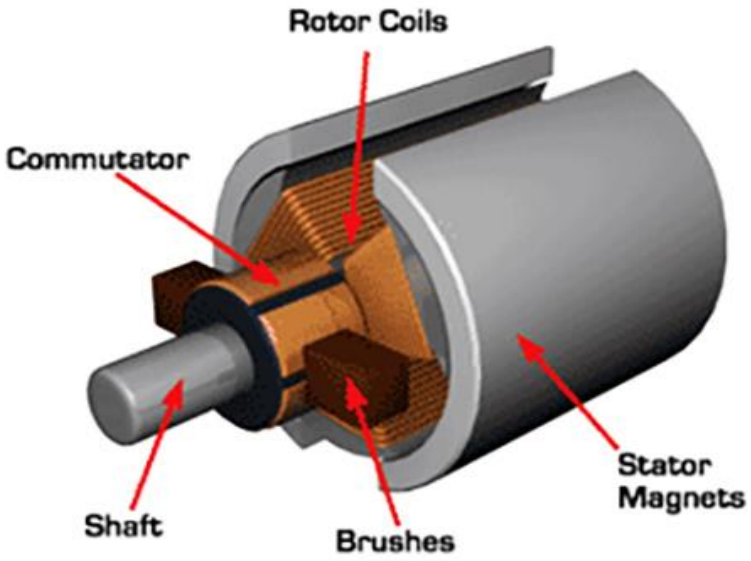

Figure II.2. An example of brushed DC motor with stator magnets [32]

DC motors offers a lot advantages including, high efficiency, wide range control and regulation of the speed and they are suitable for low-speed torque applications. The DC motor is heavy and costly as compared to brushless DC motors or AC motors.

II.4. Brushless direct current motors

BLDC motors are synchronous motors, because the speed of the motor and stator magnetic field rotate with same frequency. BLDC motors are available in single phase, two phase and three phase configurations and the three-phase configuration is commonly used. BLDC motor is constructed with a permanent magnet rotor and wire wound stator poles. The Figure II.3 shows a three-phase wire wound BLDC motor.

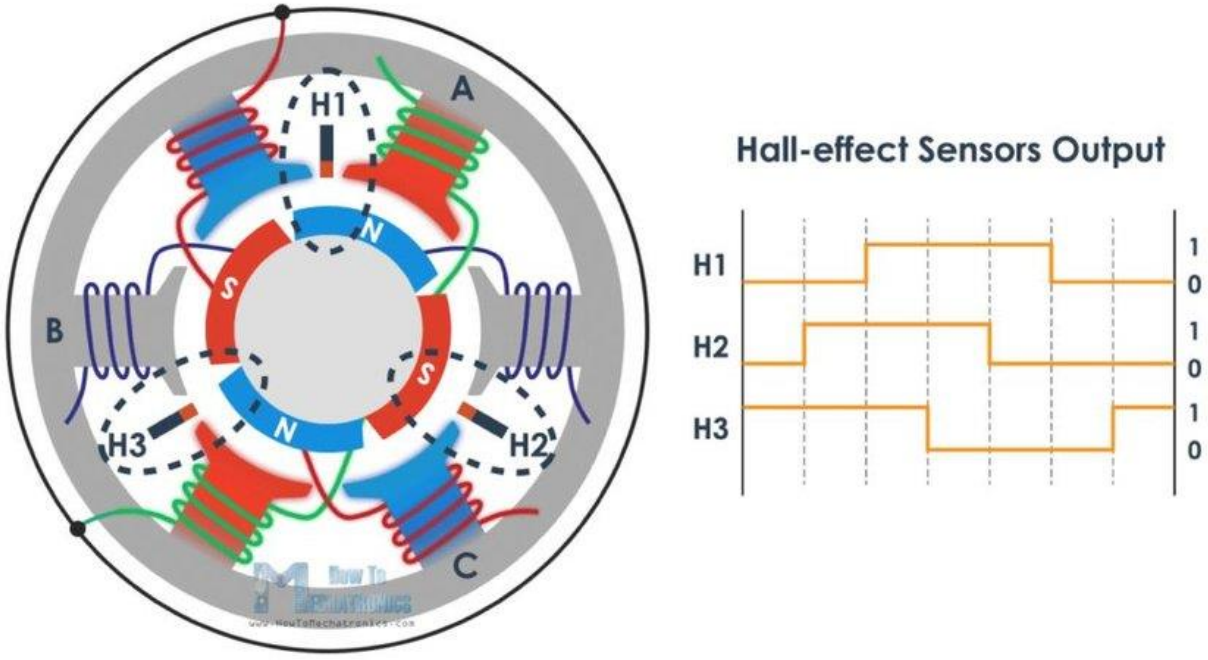

Figure II.3. Structure of the stator and rotor of a BLDC motor [33]

Due to the absence of carbon brushes or mechanical commutators this motor requires a driver (inverter) and rotor position sensors. Hall effect sensors are commonly used for sensing rotor position and these sensors are mounted on the motor shaft and most of the BLDC motors have three hall sensors. [34]

Each time the rotor magnetic poles pass near the hall sensor, they give a high or low signal, indicating the passing of the North or South Pole near the sensors. Based on the combination of the three hall sensor signals, the exact sequence of commutation can be determined and this signal is sent to the drive circuitry of the inverter circuit as shown in Figure II.4. [34]

Figure II.4 shows the driver circuit of the BLDC motor where the detection and control circuit receive signals from hall-effect sensors, and the back EMF generated when the motor is in operation.

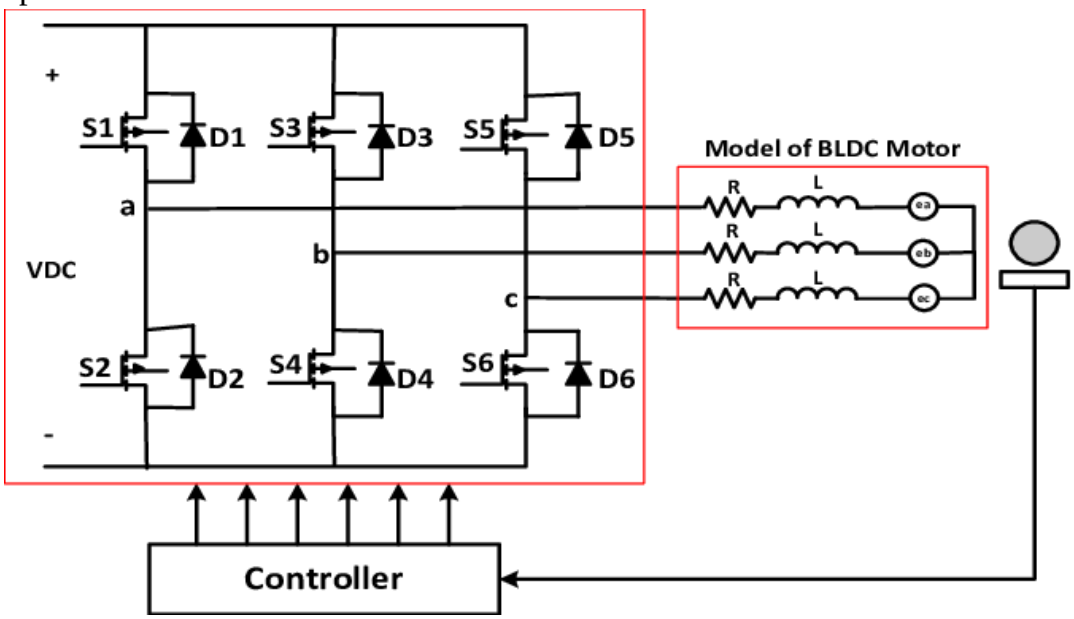

Figure II.4. Driver circuit of the BLDC motor [35]

In response to these signals, the inverter allows the flow of current to stator phase windings in a controlled sequence so that motor produces the desired torque and speed.[34]. They are various techniques of piloting a BLDC motor which are categorized as sensorless or sensor based and we chose to work with sensor based approach based on trapezoidal control as shown in Figure II.6.

II.4.1. Mathematic model of BLDC motor

The modeling of the BLDC motor is based on these assumptions:

- The motor is not saturated and should be operated with the rated current.
- The resistances of the three stator phase windings are equal.
- Self-inductance and mutual inductance are constant.
- Iron and stray losses are negligible.
- Three phases are balanced one.
- Uniform air gap.
- Hysteresis and eddy current losses are not considered.
- Semiconductor switches are ideal.

The model of the armature winding for the BLDC motor is expressed as follows:

$$V_a = Ri_a + L\frac{di_a}{dt} + e_a \quad \text{(II.1)}$$

$$V_b = Ri_b + L\frac{di_b}{dt} + e_b \quad \text{(II.2)}$$

$$V_c = Ri_C + L\frac{di_C}{dt} + e_C \quad \text{(II.3)}$$

Where;

$R_a = R_b = R_c = R$ Stator resistance per phase (Ω)

$L_a = L_b = L_c = L$ Stator inductances per phase (H)

V_a, V_b, V_c Stator phase voltages (V)

i_a, i_b, i_c Stator phase currents(A)

e_a, e_b, e, Motor Back EMFs (V)

The equivalent circuit of the BLDC windings is shown below

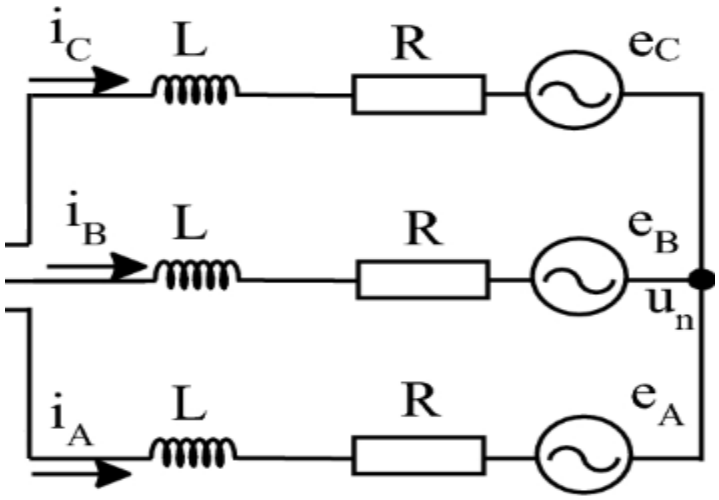

Figure II.5. The equivalent circuit of BLDC motor. [36]

When BLDC motor rotates, its windings generate an opposite voltage to the main voltage supplied to the windings according to Lenz's law. The polarity of this Back EMF is in opposite direction to the source voltage. [37]

The back EMFs generated are given by the following equations:

$$e_a = k.\omega.f(\theta) \quad \text{(II.4)}$$

$$e_b = k.\omega.f(\theta - \frac{2\pi}{3}) \quad \text{(II.5)}$$

$$e_c = k.\omega.f(\theta + \frac{2\pi}{3}) \quad \text{(II.6)}$$

where,

K is the Back EMFs constant (V/rad/s)

θ is the electrical angle

ω is the mechanical speed of the rotor (rad/s)

The Back EMFs are also related to the function of rotor position and each phase has a phase difference of 120℃. Back EMF is affected by these three main factors:

(i) Angular velocity of the rotor.

(ii) Magnetic field generated by the rotor magnets.

(iii) The number of turns in the stator windings.

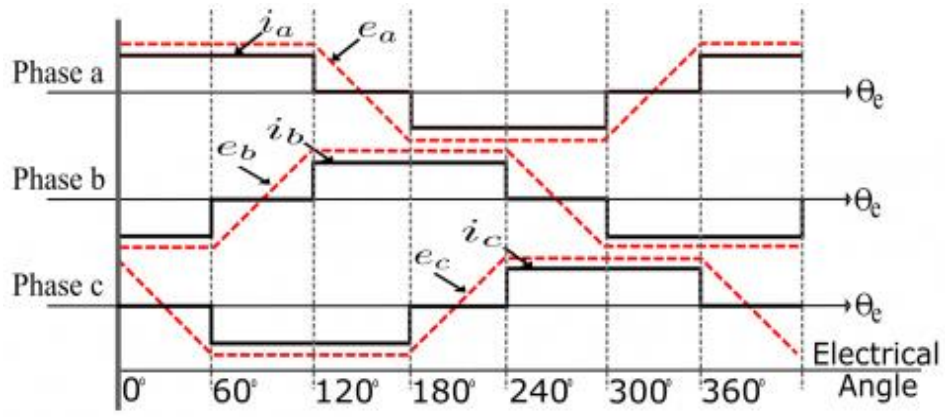

Figure II.6. Trapezoidal back EMF and phase current variation [38]

So, the total torque equation can be defined as:

$$T_e = \frac{i_a e_a + i_b e_b + i_c e_c}{\omega} = \frac{iaK.f(\theta) + ib.K.f(\theta - \frac{2\pi}{3}) + ic.K.f(\theta + \frac{2\pi}{3})}{\omega} \quad \text{(II.7)}$$

II.4.2. Operation principle of BLDC motor

A BLDC motor is piloted by voltage strokes with respect to the rotor position. These strokes have to be applied to the active phases of the three-phase winding system while keeping an angle between the stator flux and the rotor flux close to 90° so as to generate maximum torque. Therefore, there is a necessity for controller to determine the rotor's orientation/position (relative to the stator coils). The Hall-effect sensors, which are mounted in or near the machine's air gap plays that role by detecting the presence of the magnetic field of the passing rotor magnets. For a proper operation of the BLDC motor, each of the Hall-effect sensors outputs a high level for 180° of an electrical rotation, and a low level for the other 180°. These three sensors have a 60° relative offset from each other thereby dividing each rotation into six phases. Therefore, electronic commutation refers to the process of switching the current to flow through only two phases for every 60 electrical degree rotation of the rotor. The motor is supplied from a three-phase inverter (BLDC driver), and the switching actions is achieved by the use of signals from Hall-effect position sensors that are mounted at appropriate points around the stator. When mounted at 60 electrical degree intervals and aligned properly with the stator phase windings these Hall switches deliver digital pulses that can be decoded into the desired three-phase switching sequence. [39]

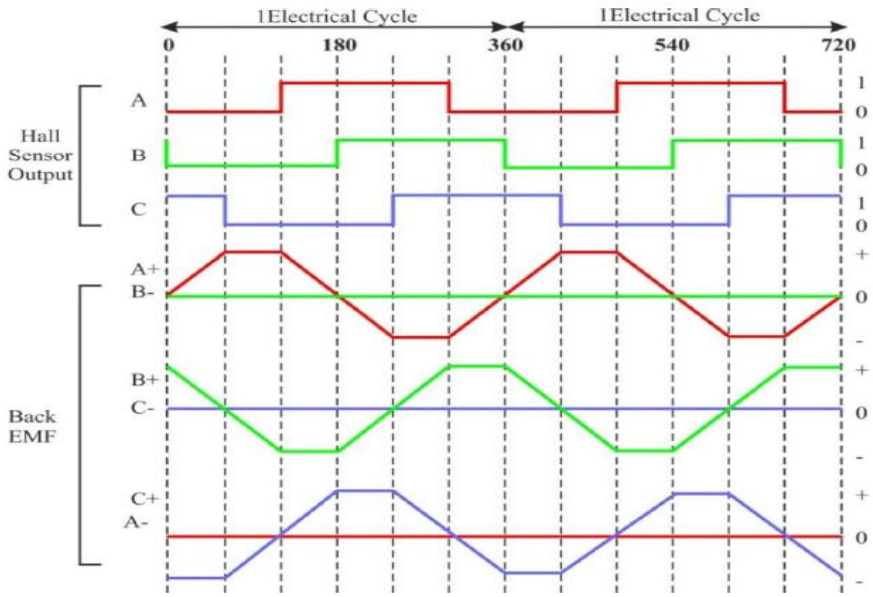

Figure II.7. Variations of back EMFs with respect to hall sensor input signals [39]

II.5. Water pumps

There are two main types of water pumps used in solar water pumping system which are centrifugal pumps and the positive displacement pumps. The choice of these pumps depend on factors like the head, the desired flow rate, the efficiency and the maintenance of these pumps.

II.5.1. Centrifugal pumps

These pumps consist of one or more impellers that spin water by subjecting it to centrifugal force. To attain high lift, a centrifugal pump may have a multitude of stages, each consisting of an impeller at each stage thus increasing the pump's lift capacity. Centrifugal pumps may use over 20 stages to attain high lifts and each stage adds pressure but also imposes friction, resulting in an efficiency loss of about 5% per stage. [40]

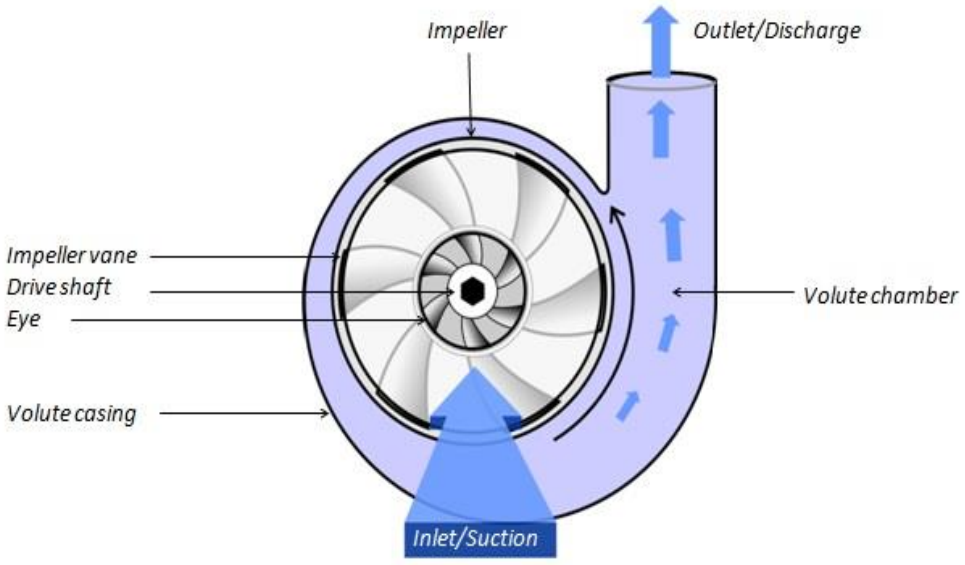

FigureII.8. Structure of a centrifugal pump [41]

The structure of the centrifugal pump mainly depends on the application, the source of the fluid to be pumped. As in this case, water is being pump from underground source, therefore, a vertical centrifugal pump is used. These pumps can be either be, single stage or multistage centrifugal pumps. Vertical centrifugal pumps are specifically designed for vertical installation and commonly for the transfer of low viscosity fluids over a range of flow rates and heads. Multi-stage centrifugal pumps consist of two more impellers mounted on the same shaft or on different shafts. For higher pressures at the outlet, impellers can be connected in series.

II.5.2. Positive displacement pumps

A positive displacement pump draws water into a sealed chamber and then force it out mechanically. This solar pump may use a diaphragm, instead of a helical rotor that traps water in cavities that progress upward as it turns. Positive displacement pumps have high lift capacity and high energy efficiency. The efficiency and lift capacity of these pumps remain high even at low rotational speeds, such as those that occur in a solar-direct pump during low-light conditions. There are several sub-types of positive displacement pumps as shown on figure II.9.

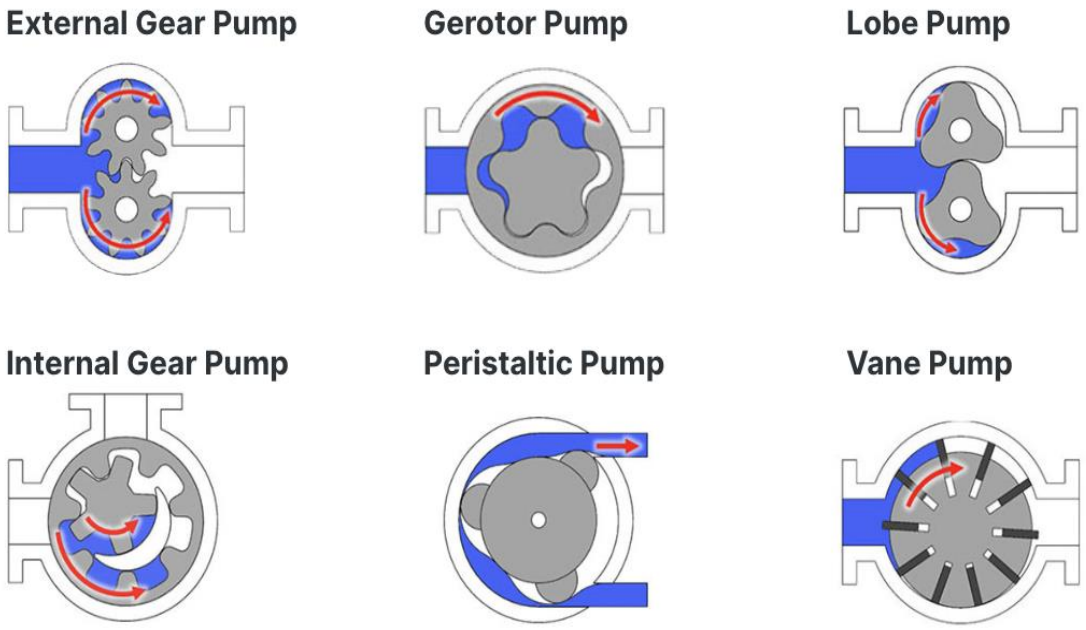

Figure II.9. Types of positive displacement pumps [42]

Positive displacement pumps, unlike centrifugal, can theoretically produce the same flow at a given speed (rpm) meaning that positive-displacement pumps are constant flow machines. However, a slight increase in internal leakage as the pressure increases prevents a truly constant flow rate.

II.6. Classification of photovoltaic water pumping systems

The type of a water pumping system used mainly depend on the head, the source of water, and these sources can be either a deep well, a dam, a river or lake. Therefore, it can be a surface water pump, submersible water pump, or a floating water pump.

II.6.1. Surface water pumps

A surface pump (Figure II.10) is installed above the water source and it naturally imposes a strict limit on the height to which water can be drawn by suction. The pump must not be more than 3 to 6 vertical meters above the water source level. Otherwise, it will extract bubbles from the water and will fail to pump. A surface pump can draw from a river, irrigation ditch, pond, or water tank, but not from a deep well. It may be less expensive than a submersible pump and more efficient for high-volume pumping as shown in figure II.10.

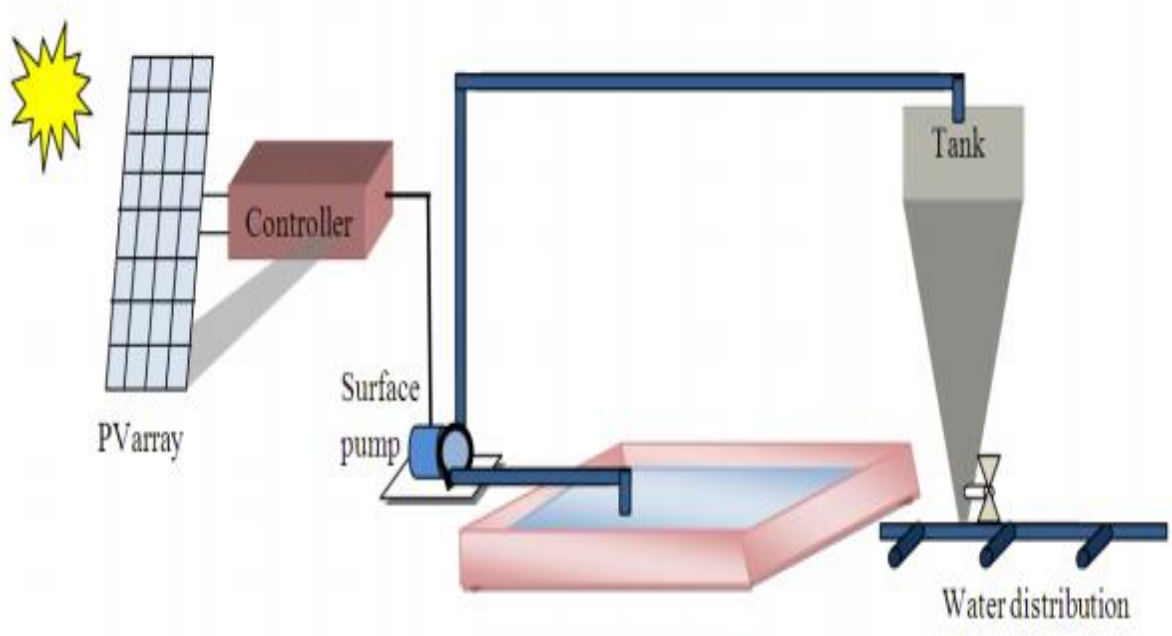

Figure II.10. Layout of a surface water pump [21]

II.6.2. Submersible pumps

A submersible pump (Figure II.11) is often simpler to install, better protected from the environment, and less likely to be damaged from running dry since through the use of water level sensors. Some solar submersible pumps use the same centrifugal mechanism as a surface pump and others use a positive displacement mechanism. Centrifugal submersible pumps are the dominant technology for deep well pumping

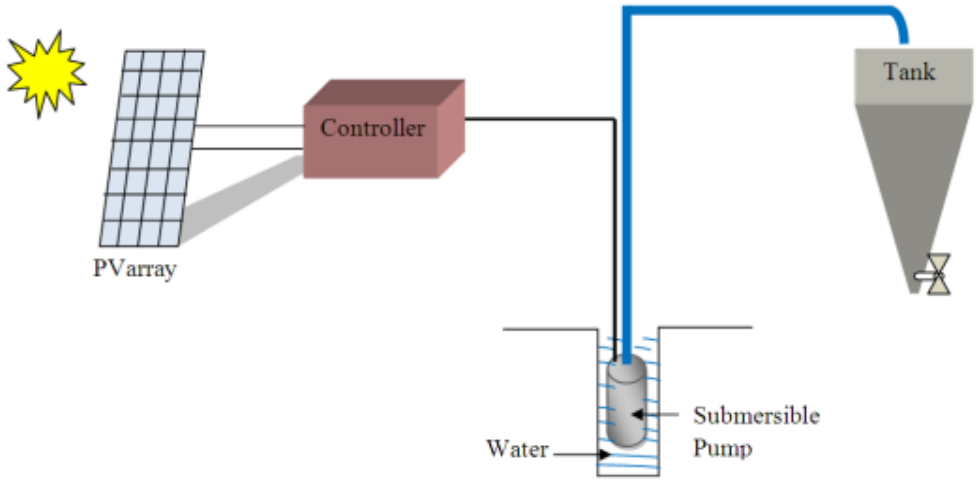

Figure II.11. Diagram of a submersible water pump [21]

II.6.3. Floating water pump

Floating pumps (Figure II.12) are semi-submersible pumps held in place and protected by a floating device. These pumps are designed for situation where an inline pump is not suitable. Floating pumps are commonly used on dams, lakes or lagoons. The floating water pumps or semi-submersible pumps can deliver up to 7,000 liters per hour. [43]

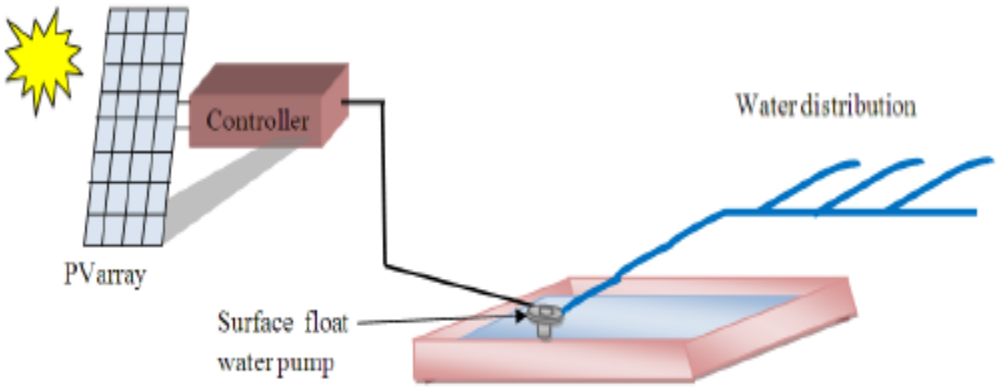

Figure II.12. Floating water pump [21]

II.6.4 Advantages and disadvantages of different solar pumps

Moreover, the process of selecting a pump is critical for a proper water pumping system. A solar pump must use energy efficiently guaranteeing a reliable water supply, having low operation and maintenance costs.

Table II.1. Advantages and disadvantages of different solar pumps. [44]

Type of solar pump	Advantages	Disadvantages
Submersible centrifugal	• Simple, one moving part • Regular mantainance not required • Efficient at high flow rates • Good tolerance at moderate amounts of sand and silt	• Poor efficiency at low volumes • Lift capacity is greatly reduced at slow speeds (during low-sun conditions)
Submersible helical rotor	• Simple, one moving part • Regular mantainance not required • Highly efficient at low to medium flow rates • Maintains full lift capacity even at low speed • Good tolerance for moderate amounts of sand and silt	
Diaphram submersible	• Low initial cost • Efficient at very low flow rates • Maintains full lift capacity even at low speed	• Requires regular preventive maintenance • Poor tolerance for sand and silt
Surface centrifugal	• Low cost • Efficient for low lift and very high flow rates • Easy to inspect and maintain due to surface location • Good tolerance for moderate amounts of sand and silt	• Suction limit is about 6 m • May be damaged by running dry if it loses prime • May be damaged by freezing in cold climates

II.7. Different configurations of water pumping systems

The configuration of a solar water pumping used mainly depend on the types of electrical motors used as this will impose the power electronic devices required for the pumping system operation. Photovoltaic water pumping system can be coupled directly to the PV generator or may contain batteries. Figure II.13 below shows PV pumping system with or without batteries.

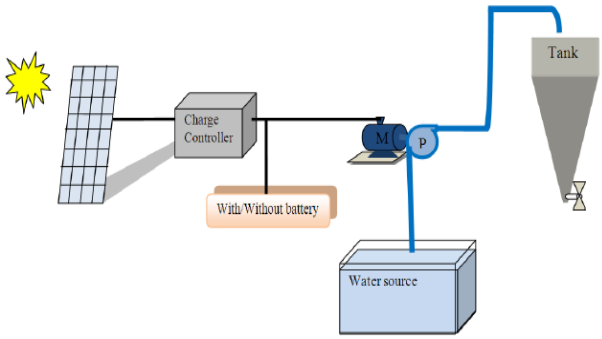

Figure II.13. Solar water pumping with/without batteries and a storage tank [21]

The battery storage in the configuration presented in fig II.13, provide backup power during the night and cloudy days. In addition, batteries are able to satisfy transient surges of current that are much higher than the instantaneous directly obtainable from a PV panel. To avoid the use of batteries, water tank storage system can be used which will reduce the cost of maintenance and replacement of batteries which might tend to be costlier in the long run. On other hand, a PV water pumping system can be coupled direct to a PV generator as shown in figure II.14 (a) and figure II.14 (b).

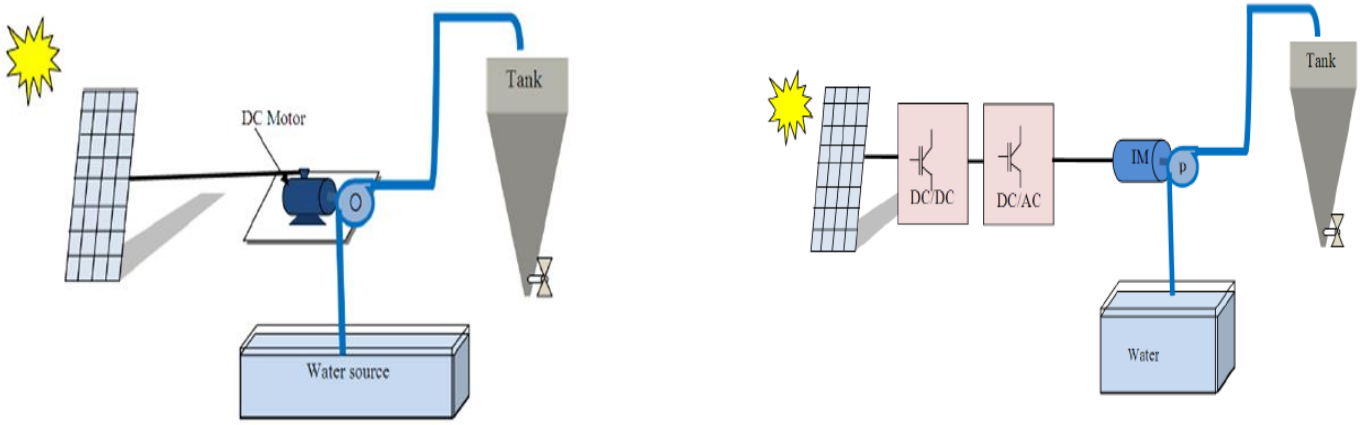

Figure II.14 (a). PV coupled to a DC motor [21] (b) PV coupled to an AC motor [21]

These common types of photovoltaic water pumping systems eliminates the use of batteries whereby, the whole system is directly coupled to the PV array. This means that, water can only be pump during the sunshine hours and that is the configuration we have chosen in this project.

II.8. System layout

There are a lot of factors taken into consideration when designing a solar water pumping system like, the water source either from a deep well, river, dam or a lake and also the static head, water drawdown and the dynamic water level as shown on figure II.15.

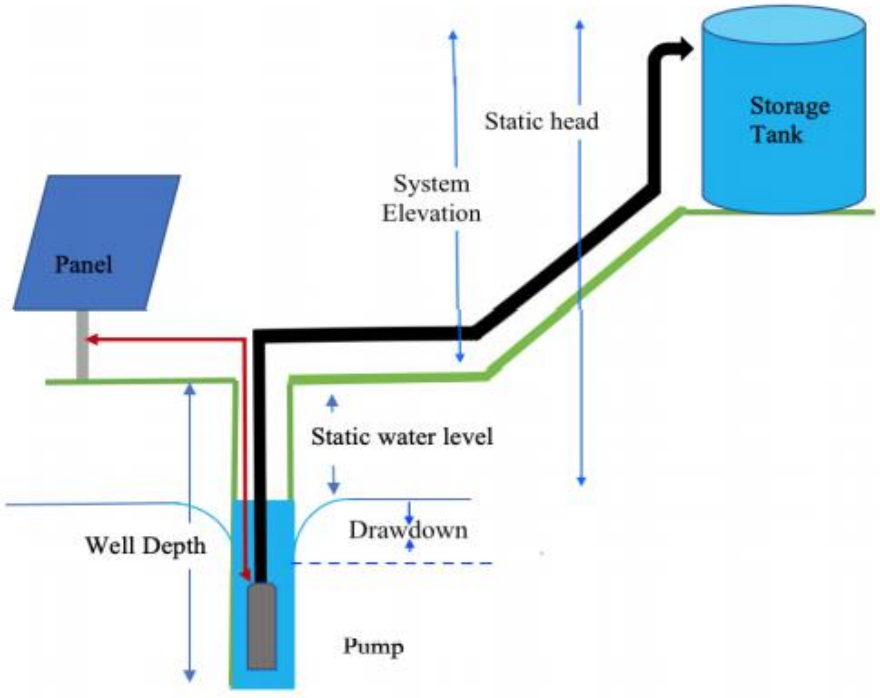

Figure II.15. Schematic diagram of the PV water pumping system layout [45]

This in turn affect the size of the water pump, the hydraulic power needed, size of inverter, characteristics of the controllers and lastly the solar power needed for such a project.

The following are the calculation necessary when designing a PV water pumping system.

II.8.1. Flow rate

The flow rate (Q in $m^3/h.$) of the pumping system is calculated as follows:

$$Q = \frac{\text{Daily water demand (in } m^3)}{\text{Sun hours (in hours)}} \quad \text{(II.8)}$$

The sunshine hours vary with the seasons whereby more sunshine hours are experienced in summer and less sunshine hours in winter. In this project, we will work with a conservative estimate of 5 sunshine hours a day**.**

II.8.2. Total dynamic head (TDH)

TDH refers to the sum total of the vertical distance that the pump needs to vertically lift water from the source to the storage facility or point of discharge. For the pump to vertically lift water from the well, it has to overcome the friction losses in the pipe and fittings. The total dynamic head is calculated by adding static head, friction head, velocity head, and the friction losses created by the fittings such as joints, couplings, and valves [45] as illustrated by the equation below:

TDH = static head + friction head of the water piping system + velocity head (II.9)

II.8.2.1. Static head

It is the vertical distance from the water level to the discharge point. In the designing of such a pumping system, the static head is calculated by adding the static water level (the vertical distance from the ground to the water level), and system elevation (vertical distance from the ground to the discharge point) as shown by the equation below:

Static Head = Static water level + drawdown level + system elevation

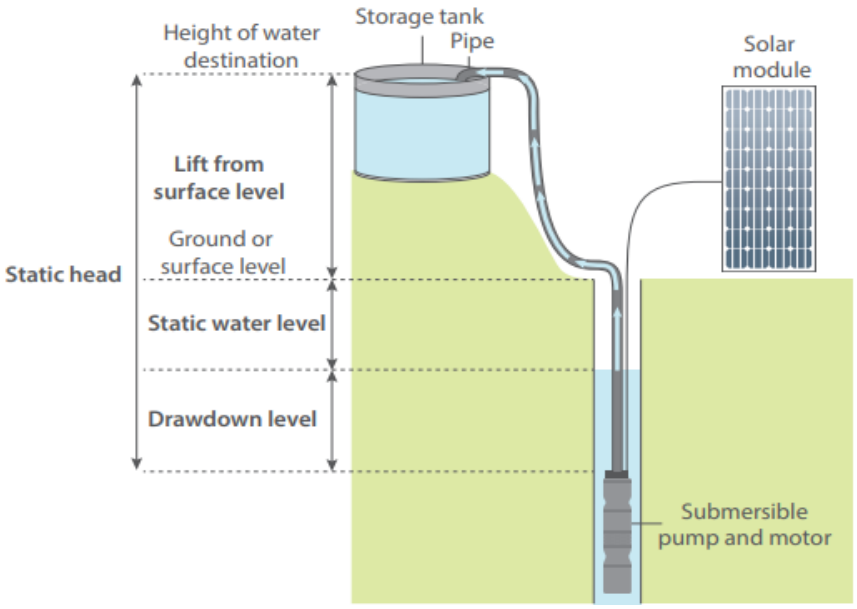

Figure II.16. Schematic diagram showing the static head [46]

II.8.2.2. Velocity head

When a fluid flow in a pipe, it also experiences various resistance to its flow. Velocity head is the head created due to the flow of water in the pipe and is a function of the velocity of the water and gravity. It can be calculated using the following equation [46].

$$\text{velocity head} = \frac{V^2}{2g} \tag{II.10}$$

where:

v: is the velocity of the water in meters per second (m/s)

g: is gravity (9.81m/s)

and v is determined as follows:

$$v = 1.273.\ \frac{Q}{d^2}\ [47] \tag{II.11}$$

where:

Q. flow rate (m^3/s)

d: Diameter(m)

II.8.2.3. Friction head

When water is transferred by the pump from the water source to the storage tank, it must travel in pipes and these pipes restrict the flow of water due to friction and therefore increase the actual head that the pump must overcome. This type of friction head depends on the type of pipe roughness, the total length of pipe, the flow rate of the fluid in the pipe, pipe diameter, and number and type of fittings and joints in the pipe. Friction head is expressed in terms of the equivalent length of pipe. Friction head can be calculated by using Hazzen–Williams formula given below

$$H_L = \frac{10.472 \times Q^{1.853}}{C^{1.852} \times D^{4.871}} \tag{II.12}$$

where:

C: Roughness coefficient variable of pipe material used as shown (Table II.2)
Q: Flow rate in m^3/s.
D: Pipe inside diameter in meters
L: Length of the pipe in meter

Table II.2. Roughness efficiencies of different piping materials [47]

Pipe Material	Hazen- William Coefficient (C)
PVC	150
Asbestos Cement	140
Welded Steel	100
Concrete	100
Copper or brass	130
Aluminum	130- 150
Corrugated Metal	60
Glass	130
Lead	130 - 140
Fiber	140

The roughness of the pipes may rise according to the rate of usage depending on the nature of the material and the fluid flowing through them. For safety reasons it is advised to change the piping system after a period after some years.

II.8.3. Hydraulic power required:

Hydraulic power required to supply water with a flow rate (Q) at a certain TDH, considering the end use of the water and/or user requirements is given by the following formula.

$$P = Q.H.\rho.g \qquad \text{(II.13)}$$

where:

Q: Flow rate (m^3/s)

H: Total Dynamic Head

ρ: water density (1000 kg/m^3);

g: gravity (9.81 m/s^2)

II.8.4. Determination of the electric power needed.

The power of an electric motor needed to operate a pump in order to fulfill the daily water requirement can be calculated as follows:

$$P_m = \frac{Q \times \rho \times g \times H_{total}}{3.6 \times 10^6 \, \eta_m} \quad \text{(II.14)}$$

where:

P_m: Pump power in kW

Q: Flow rate in m^3/h

H: Total head in m

G: Gravitation force ($9.8 m/s^2$)

$\boldsymbol{\eta}$: Motor efficiency of the pump

ρ: Density of water ($1000 kg/m^3$)

II.9. Determination of the solar output power

The total PV power output is considered as the total power input to the inverter or controller with losses inclusive, and in order to determine the array capacity of the system all losses due to temperature, soiling and cables should be considered. [48] When the maximum temperature exceeds 25°C which is the STC then the losses due to temperature will not be considered in this aspect. The following are the losses assumed during power transfer from the PV Array module to the inverter or controller:

- ✓ Module ageing,
- ✓ Solar radiation variation,
- ✓ Module soiling and dirty,
- ✓ Total cable loss,
- ✓ Manufacturing tolerance and mismatching losses.

According to the National Renewable Energy Laboratory (NREL), the standard performance ratio (PR) for a new PV system is merely 77%, and over time, the performance of the system is assumed to degrade [49]. Therefore, after taking into consideration these losses, the solar output required is calculated as follows:

$$\text{Solar output power} = \frac{\text{Power Intput of the load}}{\text{Perfomance ratio of the array system}} \quad \text{(II.15)}$$

II.9.1. Calculations of the number of solar panels

The total number of solar panels can be determined from the total solar output power required and the individual solar output power as follows:

$$\text{Number of solar panels} = \frac{\text{Total solar power output required}}{\text{individual solar power out of a chosen panel}} \quad \text{(II.16)}$$

II.9.1.1. Solar panels in parallel

The number of strings of solar panels can be calculated taking into consideration the maximum direct current input of the inverter or the load and the rated short circuit current of each solar panel as given by the equation below.

$$\text{Number of solar panel strings} = \frac{\text{Maximum rated current of the load}}{\text{Rated short circuit (Isc)of the PV panel}} \quad \text{(II.17)}$$

NB. It is crucial that the maximum direct current input of the inverter or controller has to be surpassed in order to compensate for the losses which occurs during the operation of the electric motor.

II.9.1.2. Solar panels in each string (series)

The number of solar panels in series can be calculated as follows:

$$\text{Number of panel in series} = \frac{\text{Total number of panel required}}{\text{Total number of parallel strings}} \quad \text{(II.18)}$$

II.9.1.3. Voltage in each string

The string voltage is given by the equation below:

$$\text{Voltage in each string} = \text{Npp} \times \text{Open circuit voltage} \quad \text{(II.19)}$$

II.9.1.4. Power produced

The output is calculated by the following equation:

$$\text{Ppv} = \text{Power output of each panel} \times \text{Npp} \times \text{Nps} \quad \text{(II.20)}$$

where: Ppv: Total PV power produced (W)

II.10. Conclusion

We have discussed about the electric motors used in water pumping systems and we focused mainly on brushless DC motor which has better performances when compared to other electric motors. We have also discussed about different pumps used in SWPS, their advantages and disadvantages associated with their use and operation. Moreover, we discussed about the different classifications and configurations of photovoltaic pumping systems and we ended the chapter by outlining the different steps taken in designing and sizing of a photovoltaic pumping system. The next chapter focuses on the designing and application of the steps and concepts discussed in this chapter.

Chapter III

Designing and Simulation Of the Solar Water Pumping System

III.1. Introduction

We have discussed in previous chapter, the, steps taken in designing and sizing a solar water pumping system and the various key elements of the pumping system. This chapter focuses on designing and simulation of the solar water pumping system using MATLAB/Simulink/SimPowerSystem. The configuration of the water pumping chosen is a directly coupled configuration and storage tanks have been chosen to act as a storage system. The solar water pumping systems which will design are for two case studies, that is for a small clinic with a capacity of handling about 50 people including patients and the clinic staff members and also, supplying clean and safe drinking water for a small community of about 400 people in Kazangarare, in Karoi, Zimbabwe and for small farm in Mansourah Tlemcen Algeria, growing pepper, tomatoes, strawberries, water melons covering 8 acres of land in total and rearing of 10 horses and 100 sheep.

III.2. Case Study 1: Kazangarare clinic in Karoi, Zimbabwe

The Karoi town is in Mashonaland West Province, in central northern Zimbabwe. It is located approximately 85 kilometres (by road, northwest of Chinhoyi, the nearest large town, and the location of the provincial headquarters. This location lies about 200 kilometres, northwest of Harare, Zimbabwe's capital and largest city. [50]

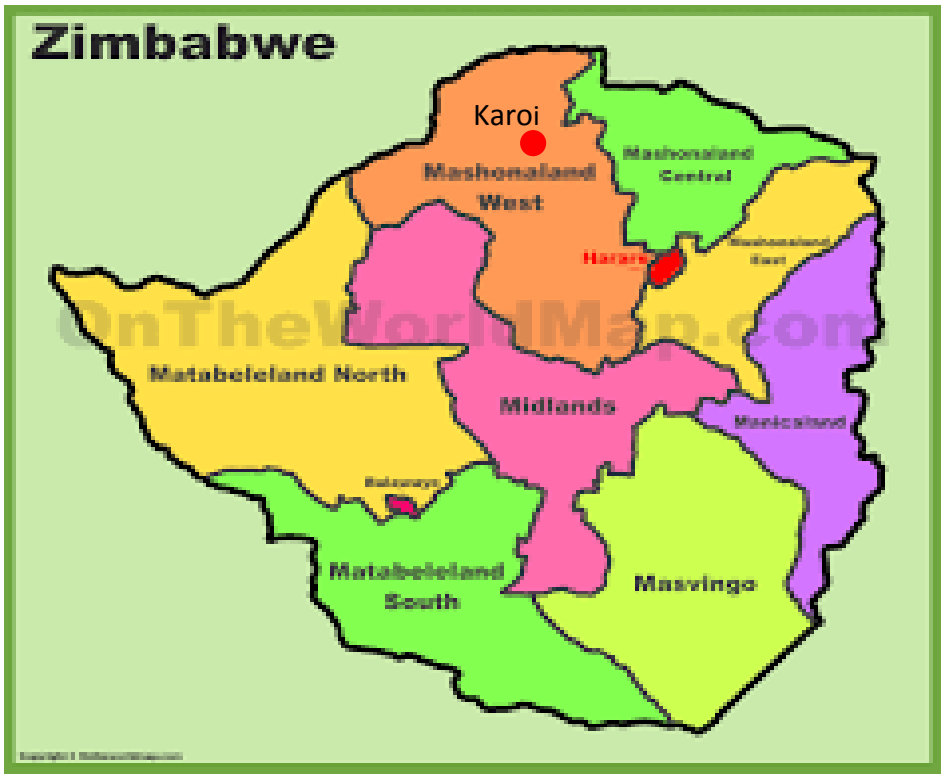

Figure III.1. Map of Zimbabwe showing the location of Karoi [51]

Karoi lies along the main road, Highway A-1, between Harare and Chirundu, at the International border with the Republic of Zambia, about 170 kilometres (110 mi), further northwest of Karoi.[35] The coordinates of Karoi are: 16° 48' 36.00"S, 29° 42' 0.00"E (Latitude:16.8100; Longitude:29.7000) [50]

III.2.1. Location of Kazangarare clinic

Kazangarare clinic is located in Kazangarare growth point that is 60 kilometers northeast of Karoi and it holds one of Zimbabwe's granaries known as Mukwichi.

Figure III.2. Location of Kazangarare clinic [52]

III.2.2 Climate conditions of the area

Since Zimbabwe has a tropical climate, Karoi experiences warm temperatures in summer and low temperatures in winter as shown in Table III.1.

Month	Jan	Feb	Mar	Apr	May	Jun	Jul	Aug	Sep	Oct	Nov	Dec	Year
Record high °C (°F)	35.8 (96.4)	33.6 (92.5)	31.7 (89.1)	33.6 (92.5)	30.9 (87.6)	28.0 (82.4)	28.1 (82.6)	31.2 (88.2)	34.7 (94.5)	35.7 (96.3)	36.5 (97.7)	33.7 (92.7)	36.5 (97.7)
Average high °C (°F)	25.8 (78.4)	25.6 (78.1)	25.8 (78.4)	25.6 (78.1)	24.1 (75.4)	22.2 (72.0)	22.2 (72.0)	24.6 (76.3)	27.8 (82.0)	29.5 (85.1)	28.0 (82.4)	26.0 (78.8)	25.6 (78.1)
Daily mean °C (°F)	20.6 (69.1)	20.3 (68.5)	20.0 (68.0)	18.9 (66.0)	16.8 (62.2)	14.7 (58.5)	14.6 (58.3)	16.6 (61.9)	20.1 (68.2)	22.2 (72.0)	21.9 (71.4)	20.7 (69.3)	18.9 (66.0)
Average low °C (°F)	16.9 (62.4)	16.8 (62.2)	15.9 (60.6)	14.0 (57.2)	11.2 (52.2)	8.7 (47.7)	8.2 (46.8)	9.9 (49.8)	13.0 (55.4)	16.0 (60.8)	16.9 (62.4)	16.9 (62.4)	13.7 (56.7)
Record low °C (°F)	13.4 (56.1)	13.0 (55.4)	10.7 (51.3)	7.3 (45.1)	4.9 (40.8)	1.9 (35.4)	2.1 (35.8)	3.6 (38.5)	5.3 (41.5)	8.1 (46.6)	10.7 (51.3)	12.2 (54.0)	1.9 (35.4)
Average rainfall mm (inches)	178.6 (7.03)	191.6 (7.54)	111.9 (4.41)	39.8 (1.57)	6.7 (0.26)	1.7 (0.07)	2.0 (0.08)	1.1 (0.04)	4.5 (0.18)	19.7 (0.78)	73.4 (2.89)	173.1 (6.81)	804.1 (31.66)
Average rainy days	17	16	11	4	2	1	0	0	1	3	9	15	79
Mean monthly sunshine hours	182.9	165.2	210.8	240.0	266.6	258.0	282.1	300.7	294.0	275.9	222.0	176.7	2,874.9
Mean daily sunshine hours	5.9	5.9	6.8	8.0	8.6	8.6	9.1	9.7	9.8	8.9	7.4	5.7	7.9

Table III.1. Climate data for Karoi (1951 – present) [50]

III.2.3. The amount of solar energy available in the area.

The monthly global horizontal irradiation received in Kazangarare is illustrated by the graph below.

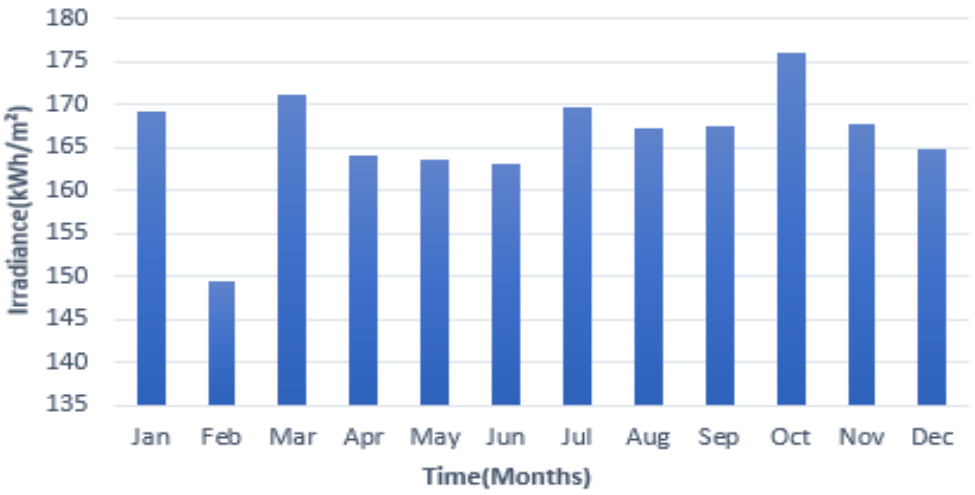

Figure III.3. Global horizontal irradiation [53]

The bar chat in figure III.3 shows that, the highest solar radiation is received in summer season with October recording the highest solar radiation while low solar radiation is usually recorded in the month of February. The average daily solar irradiance is 5kWhr/m^{2}, though it varies depending on the season. The daily sunshine hours are shown in figure III.4 and they also vary with the season and atmospheric conditions.

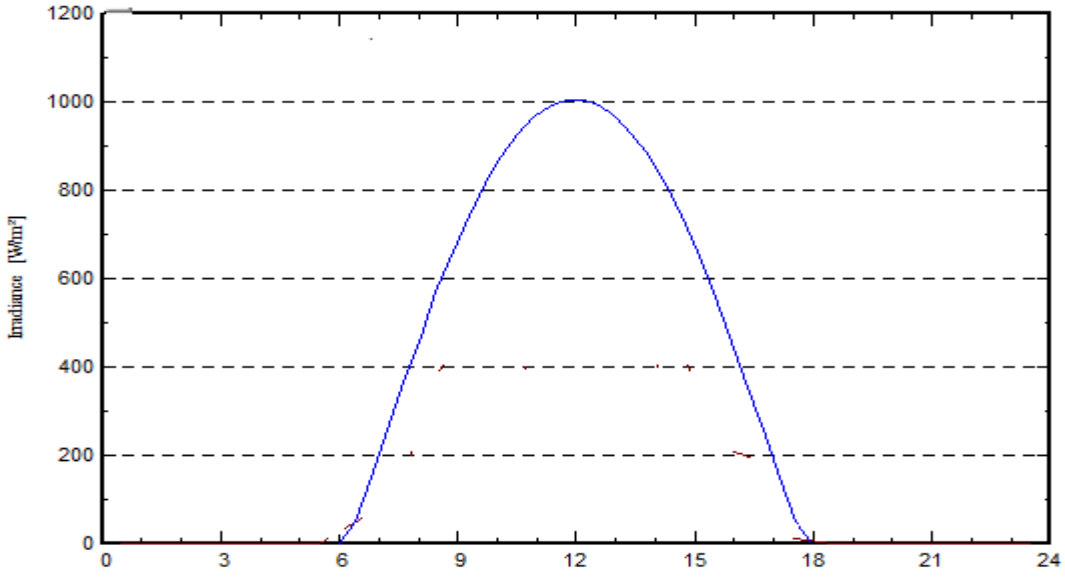

Figure III.4. Daily sunshine hours of the area [53]

III.2.4. Water availability

Overally, all the hydrogeological units in Zimbabwe are suitable for the development of small, single point primary water supplies, either by means of dug wells or by boreholes.

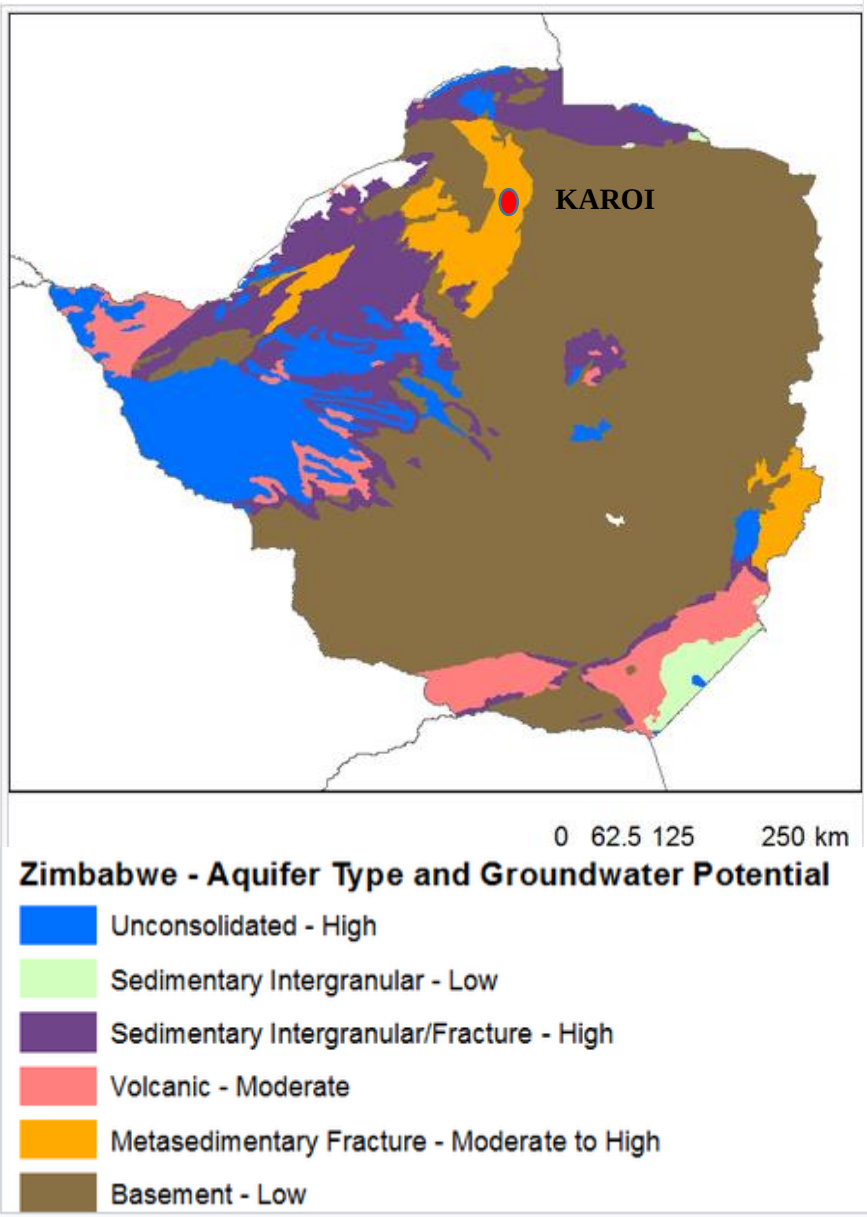

Groundwater development potential

In the National Master Plan for Rural Supply, Interconsult (1986) classed aquifers in Zimbabwe by their groundwater development potential, as follows:

- High: Suitable for primary supply, piped supplies, and small and large-scale irrigation schemes
- Moderate: Suitable for primary supplies, small piped schemes and small-scale irrigation schemes
- Low: Suitable for primary supplied from boreholes.

These groundwater development potential rankings are reflected in the hydrogeology map above, with a description of the aquifer type (hydrogeological environment) of each aquifer.[54]

Figure III.5. Classification of underground water aquifers in Zimbabwe [54]

The area in our cases study is located on Cretaceous sedimentary aquifer with water tables which are typically less than 15 m deep, and boreholes are usually drilled to a depth of 70 – 100 m. [54]

III.2.5. Water requirements

Table III.2. WHO Guidelines on water quantity used in healthcare [55]

Area	Quantity
Outpatients	5 litres /consultation
In patience	40 – 60 litres /patient/ day
Dry supplementary feeding centres	0.5 – 5 litres / consultation
Wet supplementary feeding centres	15 litres / consultation
Inpatient feeding centres	30 litres / consultation
Cholera treatment centres	60 litres /patient/day
Operating Theatre (OT) or midwife Obstetric unit (MOU)	100 litres / intervention
Viral Hemorrhagic Fever isolation	300-400 litres / isolation

Table III.3. Recommended basic water requirements for human needs [56]

Purpose	Recommended minimum (litres per person per day)
Drinking water	5
Sanitation services	20
Bathing	15
Cooking and Kitchen	10
Total basic water requirement	**50**

Currently, the existing pumping system has a storage tank with a capacity of 5 000 litres.. We are proposing a pumping system, that will add another 5000 litres for the health institution and, 20 000 litres to supply the community. The motivation of adding 5000 litres for the institution is to cater of the unforeseeable events like pandemics and other diseases outbreak that might occur thereby exerting pressure on the water supply system as much water will be required. So, in total, the SWPS we are proposing is to provide **30 000** litres of water daily.

The old diesel pumping system was recently replaced by an electric pumping system, but because of power cuts and load shedding which are happening in Zimbabwe as a result of drought which has crippled the hydropower electricity generation capacity, a SPWS would be a better alternative since the country receives considerable amount of solar radiation. The depth of the well is **58 m** and the pump is **56 m** below the ground.

III.3. Calculations of the hydraulic power needed

The following calculation are for the determination of the hydraulic power for the SWPS.

III.3.1 Flow rate

The flow rate (Q in m^3/h) of the pumping system is:

$$Q = \frac{\text{Daily water demand}}{\text{Sun hours}} \qquad \text{(III.1)}$$

$$Q = \frac{30}{5} = \mathbf{6m^3\ /h}$$

III.3.2. Total dynamic head (TDH)

The total dynamic head for this project is determined below:
THD = Static head + friction head of the complete water piping system + velocity head.

III.3.2.1. Static head

The static head of the proposed system is calculated below

Static Head = Static water level + Drawdown level + System elevation (III.2)

Static Head = **20 m + 34m + 3m = 57 m**

III.3.2.2. Velocity head

For a flow rate of 0.00167 m^3/s using PVC pipes with internal diameter of 2 inches (5.08cm)

$$\text{Velocity of the water} = 1.273.\frac{Q}{d^2} = 1.273\times\frac{0.00167}{0.0508^2} = \mathbf{0.82\ m/s} \qquad \text{(III.3)}$$

$$\text{Velocity Head} = \frac{V^2}{2g} = \frac{0.82^2}{2*9.81} = \mathbf{0.04\ m}$$

II.3.2.3. Friction head

The roughness coefficient of a PVC pipes is 150 as shown in table II.2, therefore:

$$H_L = \frac{10.472 \times Q^{1.853}}{C^{1.852} \times D^{4.871}} = \frac{10.472 \times 0.00167^{1.853}}{C^{1.852} \times 0.0508^{4.871}} = \mathbf{0.014\ m} \quad \text{(III.4)}$$

TDH = 57m + 0.04m + 0.014m =57.054m

Since piping system has 3 elbows which reduces the pressure of the water, we will use a TDH of 58 **m.**

III.3.3. Hydraulic power required

We have calculated: **Q = 0.00167m^3/s**, **TDH = 58 m**, $\boldsymbol{\rho}$ **= 1000 kg/ m^3**, **g =9.81 m/s^2**

$$P = Q.H.\rho.g \quad \text{(III.5)}$$

$$P = 0.00167 \times 58 \times 1000 \times 9.81 = \mathbf{950\ W}$$

III.4. Size of the electric motor required

The size of the electric motor needed is calculated below using equation II.14:

$$P_m = \frac{Q \times \rho \times g \times H_{total}}{3.6 \times 10^6\ \eta_m} = \frac{6 \times 1000 \times 9.81 \times 58}{3.6 \times 10^6 \times 0.85} = \mathbf{1.1\ kW} \quad \text{(III.6)}$$

$$Ppv = \frac{Pm}{PR} = \frac{1100}{0.77} = \mathbf{1429\ W} \quad \text{(III.7)}$$

We will choose a **1.1kW** centrifugal pump for this project but however, we do recommend **1.5kW** pump and this voluntary overestimation is due to the fact that, the water demand may increase with time, as result of either extension of the facility so to increase its capacity or some other factors.

III.5. PV system sizing

For this project we have chosen a monocrystalline, **SUNTECH POWER STP250S-20-Wd** solar panel included in the MATLAB /Simulink library for the simulation and its parameters are shown below:

Table III.4. Electrical Characteristics of the module (STC, 1000W/m^2, 25°C, AM = 1.5)

Parameters (STC)	**Values**
Maximum Power	250W
Optimum operating voltage	30.7 V
Optimum Operating Current	8.15 A
Open Circuit voltage	37.4 V
Short Circuit current	8.63 A
Module Efficiency	15.4 %
Operating temperature	-40° C to +85°C
Maximum Voltage	1000 V
Maximum Series Fuse rating	20 A
Power Tolerance	0/ +5W
Number of cells	72 cells

The following curves shows the, power, voltage and current output of the chosen PV module simulated using MATLAB. The condition used are the same as STC which we have mentioned in chapter and in table III.2

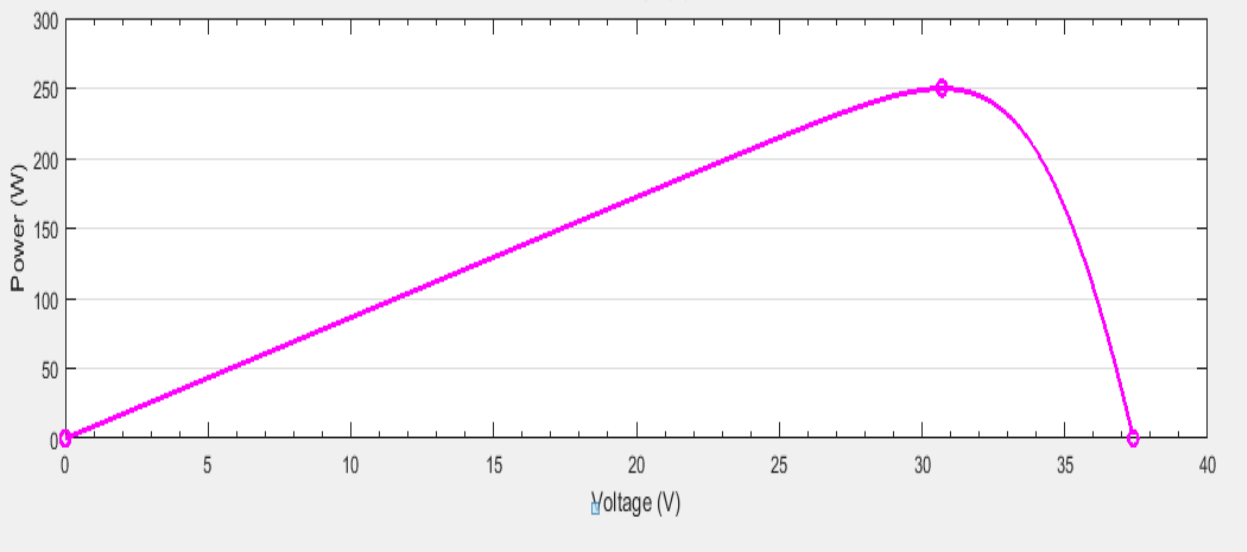

Figure III.6. P-V characteristics of the module

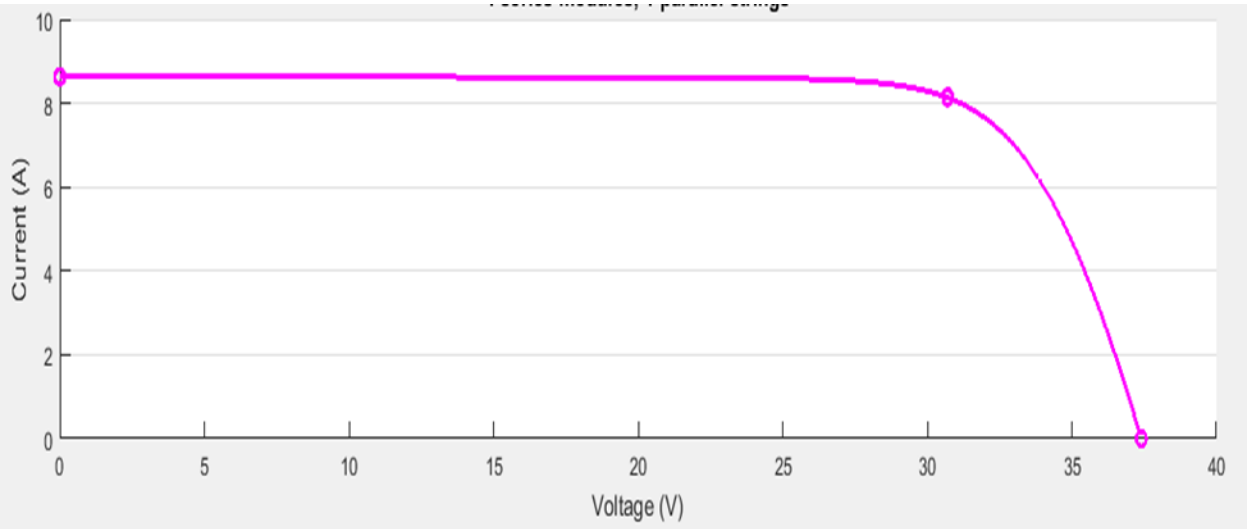

Figure III.7. I-V Characteristics of the module

For this project, we have decided to power the SWPS by a total PV power output of 1.5kW using 250 W PV modules. The oversizing PV array is to compensate for the power losses due to, atmospheric condition, wiring cables and other power losses during the operation of the pump system.

III.5.1. Calculations of the number of solar panels

From equation II.15, the number of solar panels are determined below:

$$\text{Number of solar panels (Np)} = \frac{\text{Total solar power output required}}{\text{individual solar power out of a chosen panel type}} \quad \text{(III.8)}$$

$$\text{Np} = \frac{1500\ \text{W}}{250\text{W}} = 6\ \textbf{modules}$$

III.5.2. Parallel and series connection of the solar panels

The number of PV panels in series and parallel are determined below:

III.5.2.1. Solar panels in parallel

From equation II.17, the PV panels in parallel are calculated below:

$$\text{Number of solar panels in parallel (Npp)} = \frac{\text{Maximum rated direct current for BLDC}}{\text{Rated short circuit solar outpout current (Isc)}} \quad \text{(III.9)}$$

$$\text{Npp} = \frac{13.7}{8.63} = 1.58 \approx 2 \text{ string of solar panels}$$

III.5.2.2. Solar panels in each string (series)

From equation II.18, the PV panels in each string are calculated below:

$$\text{Number of panels in series (Nps)} = \frac{\text{Total number of panel required}}{\text{Total number of parallel strings}} \quad \text{(III.10)}$$

$$\text{Nps} = \frac{6}{2} = \mathbf{3\ panels}$$

III.5.3. Voltage in each string

From equation II.19, the total voltage output of each panel is determined below

Voltage in each string = Total number of panels × Open circuit voltage

(11)

$$= 3 \times 37.4\ \text{V} = \mathbf{112.2\ Volts}$$

III.5.4. PV power produced

From equation II.20, the total power output of the PV array is calculated below

$$\text{Ppv} = \text{Power output of each panel} \times \text{Npp} \times \text{Nps} \quad \text{(III.12)}$$

$$\text{Ppv} = 250 \times 2 \times 3 = \mathbf{1.5\ kW}$$

III.6. Calculation of the boost parameters

The parameter of the boost converter is determined as follows:

II1.6.1. Duty Cycle

The boost converter for this SWPS has the following input voltage and output voltage, V_{in} = 112.2V and V_{out} = 400V respectively, therefore, the value of the duty cycle:

$$D = \frac{400-112.2}{400} = \mathbf{0.7195} \quad \text{(III.13)}$$

III.6.2. Determination of the size of the Inductor

Using a switching frequency of 20 kHz and ripple current equivalent to 30% of the input current

$$L = D\frac{V_{in}}{f\,\Delta I_L} = 0.7195 \times \frac{112.2}{20000 \times 0.3 \times 17.26} = \mathbf{0.78\ mH} \quad \text{(III.14)}$$

1II.6.2. Determination of the size of the capacitor

With a switching frequency of 20 kHz and ripple voltage equivalent to 1% of the output voltage.

$$C_2 = \frac{D\ I_0}{f\,\Delta V_0} = 0.7195 \times \frac{(1-0.7195)(17.26)}{20000\times 0.01(400)} = \mathbf{43.5\ \mu F} \qquad \text{(III.15)}$$

III.6.3. Model of the boost converter

The model of the boost converter simulated using MATLAB is shown below

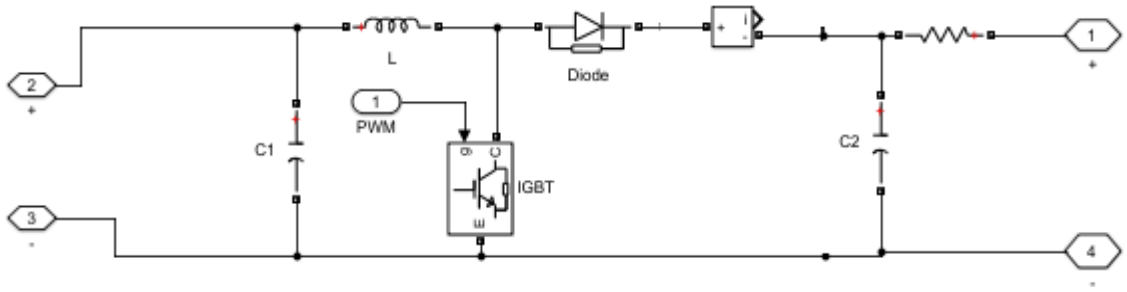

Figure III.8. Structure of the boost converter

III.7. Model of the BLDC motor

The submersible centrifugal pump for this project is driven by BLDC motor shown below. The speed controller regulates the speed of the motor hence the desired maximum flow rate.

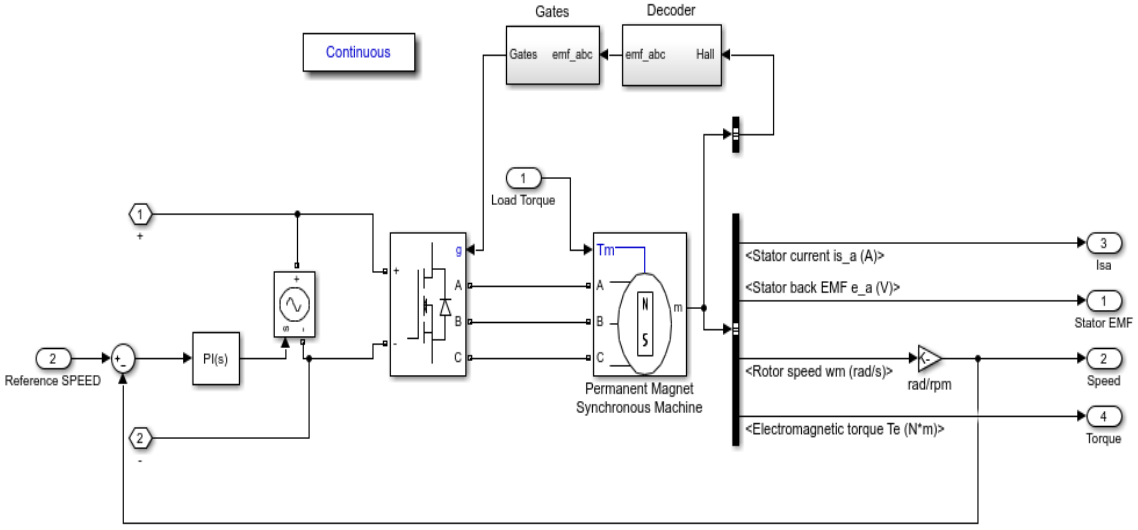

Figure III.9. Model of the BLDC motor

III.8. Model of the submersible centrifugal pump

The diagram below shows a simulated model of a submersible centrifugal pump driven by a brushless DC motor shown in figure III.9. The piping system consist of 3 elbows as shown below.

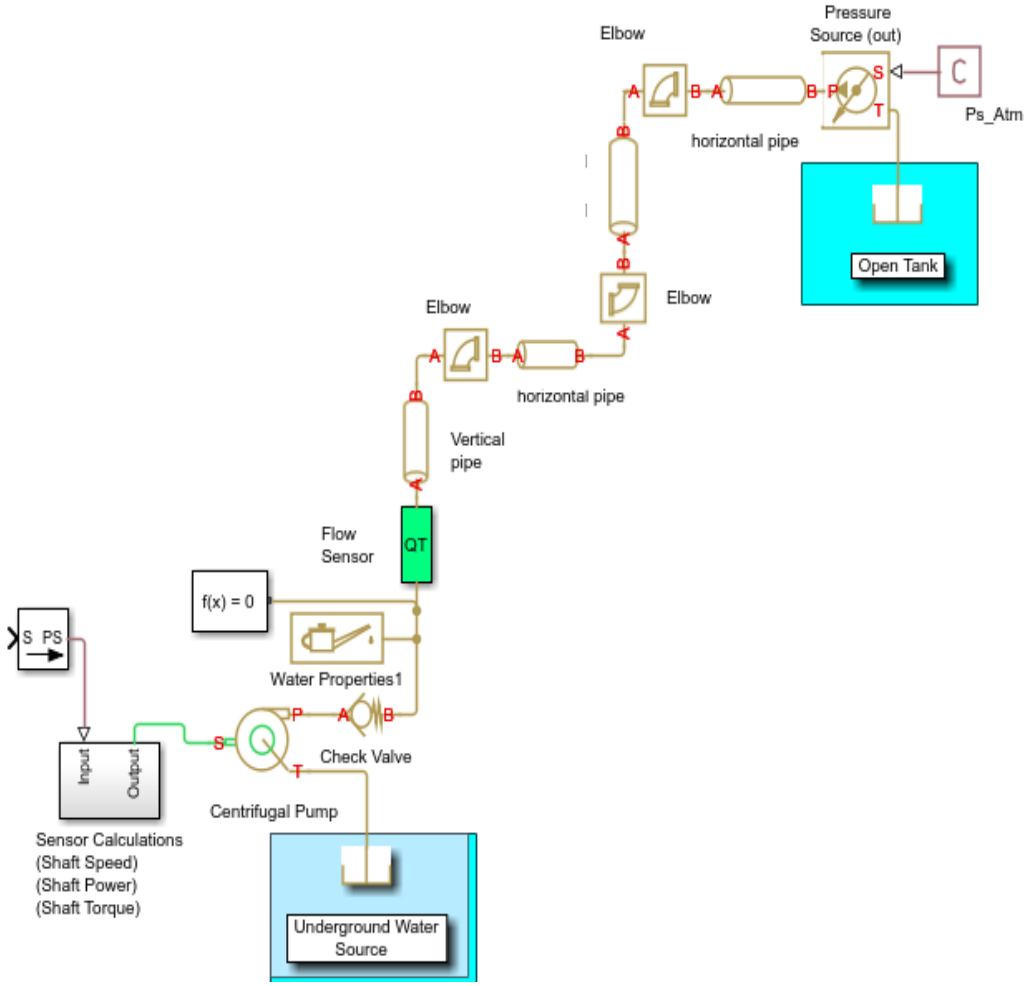

Figure III.10. Model of a submersible centrifugal pump

III.9. Characteristics of the motor – pump group

For this project, we have selected a centrifugal pump shown in table III.5 below [57]
The system has been voluntarily oversized and this makes it possible to increase the daily water supply in case the water demand increases.

Table III.5. Characteristics of the centrifugal pump selected

103	HD-3SC6-85-110-1100-A/D	110V-240V	80V-400V	1100W	6m³/h	85m	1.25"	2m
104	HD-3SC6-125-110-1500-A/D	110V-240V	80V-400V	1500W	6m³/h	125m	1.25"	2m
105	HD-3SC7-46-72-750-A/D	110V-240V	80V-400V	750W	7m³/h	46m	1.25"/1.5"	2m
106	HD-3SC8-62-110-1100-A/D	110V-240V	80V-400V	1100W	8m³/h	62m	1.25"/1.5"	2m
107	HD-3SC8-78-110-1500-A/D	110V-240V	80V-400V	1500W	8m³/h	78m	1.25"/1.5"	2m

III.10. Specifications of the motor-pump group.

We have selected a hybrid BLDC motor that can be power by both AC and DC voltages. This is advantageous since both sources of power will allow the daily water requirement to be met. The specifications of the selected motor pump group are shown in Table III.6.

Table III.6. Specification of the selected motor pump group. [57]

Brand Name	Handuro
Model Number	HD-3SC8-62-110-11000-A/D
Voltage	AC 110-240 V; DC 80V-400 V
Power	1100 W
Outlet Size	1.25 inch
Cable Length	2 m
Structure	Multistage Pump
Impeller	Plastic
Product Name	Deep well solar water pump
Material	Brass Inlet & Outlet
Pressure	High Pressure

III.11. Charge controller

The characteristics of the selected charge controller for this SWPS are shown below.

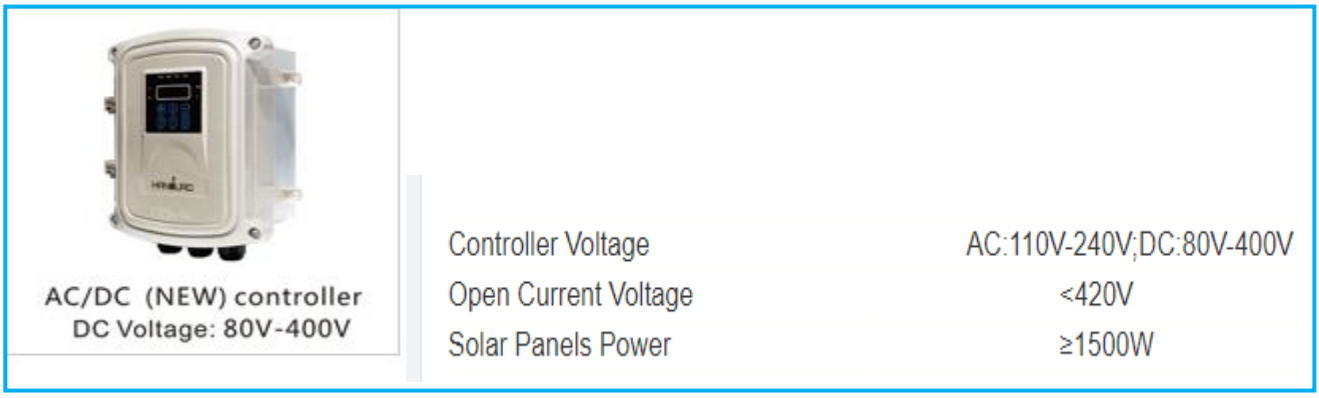

Figure III.11 Specifications of the charge controller. [57]

The parameters of the boost converter have been calculated in such way that; the maximum output voltage of the boost converter should not exceed 420V.

III.12. Performance curve of the pump

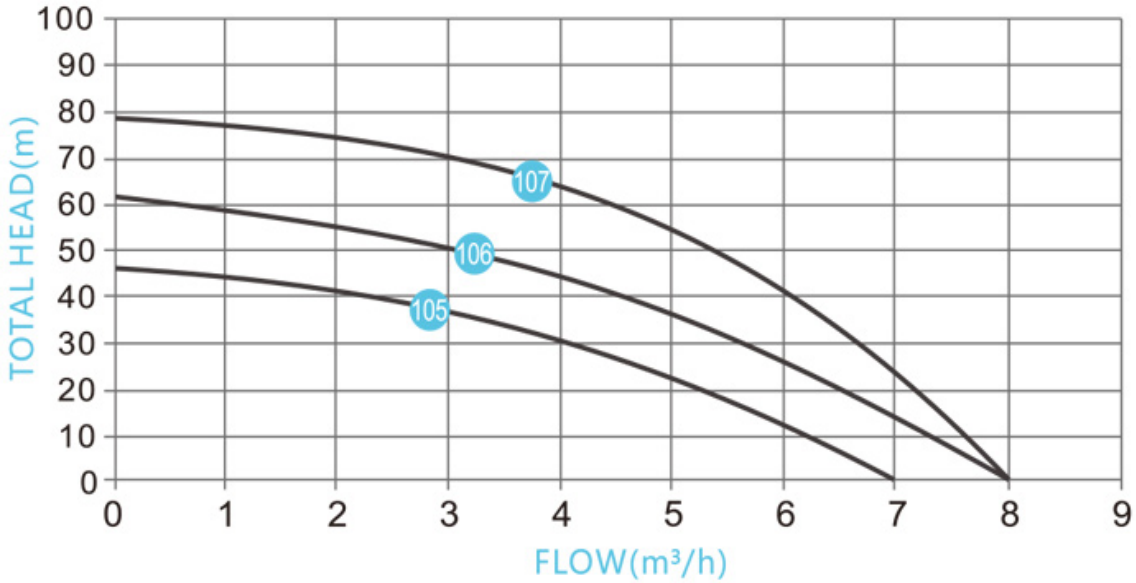

Figure III.12. Pump curves [57]

The selected centrifugal pump is represented by the curve labelled **106** capable of supplying a maximum of $8m^3/h$ for a maximum head of 62m as shown in figure III.12 above.

The complete SPWS is shown in the figure below

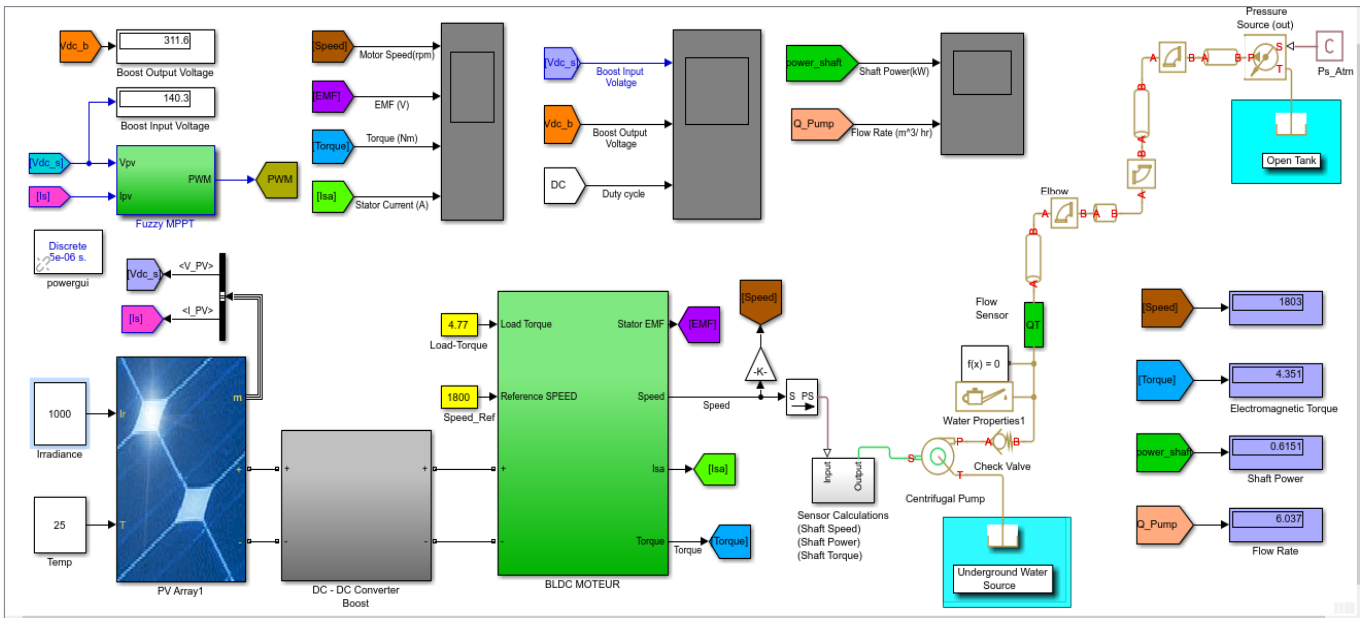

Figure III.13. The complete SWPS model simulated using MATLAB/Simulink

III.13. Speed regulation of the BLDC motor

The rate of discharge of the pump is directly proportional to the speed of the pump. A classic PI regulator has been used in order to stabilize the discharge rate by maintaining the speed of the motor according to the requirement of the operator. The parameters of the regulator are shown in figure III.14 below.

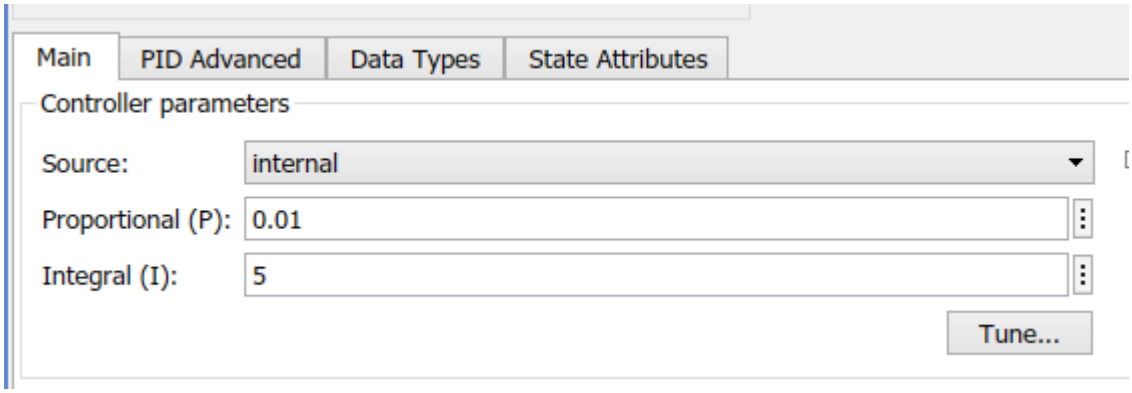

Figure III.14. Parameters of the PI regulator

III.14. Results of the simulation

The following figures shows the results of the simulation.

Figure.III.15. Duty cycle

The calculated duty cycle of **0.7195** for the boost converter is shown in figure III.15

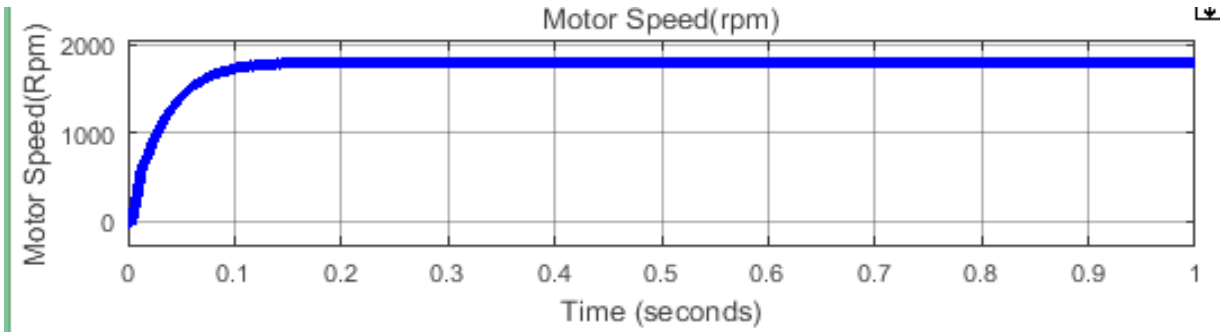

Figure III.16. Rotation speed of the motor

The rotation speed of the motor for a maximum flow rate of 6 m^3 is 1800 rpm as shown in figure III.16.

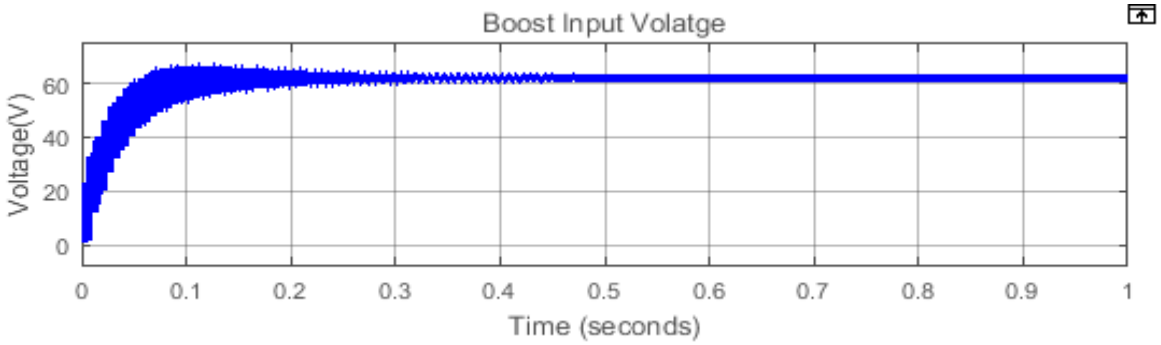

Figure III.17. Boost input voltage

The input voltage supplied by the PV array which is then fed to the boost converter is shown in figure III.17.

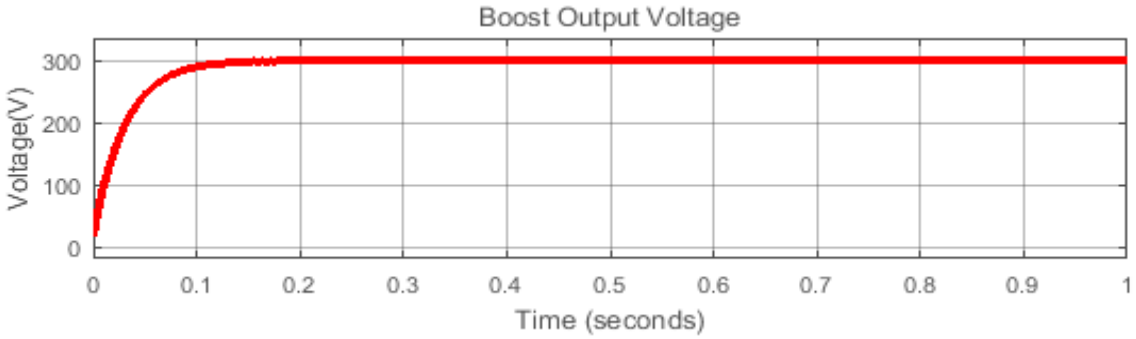

Figure III.18. Boost output voltage

The stepped-up, boost output voltage of 300V which is then fed to the controller is shown by the graph in figure III.18

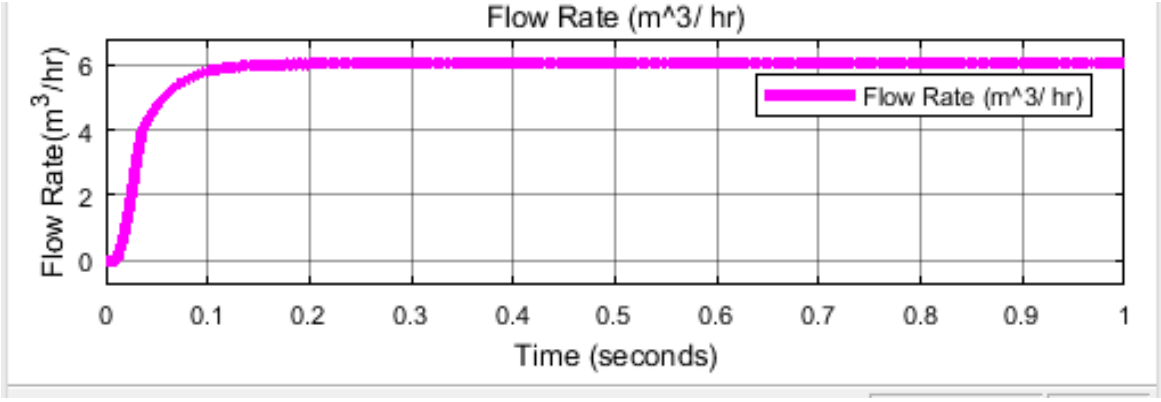

Figure III.19. Flow rate

The flow rate is directly proportional to the speed of the motor. Therefore, to fulfill the daily requirement of 30m^3 of water pumped in 5 sunshine hours, the water pump has to run at a speed of 1800rpm.In case the daily water requirement increases, only the speed of the motor has to varied but only within the limits of the designed system.

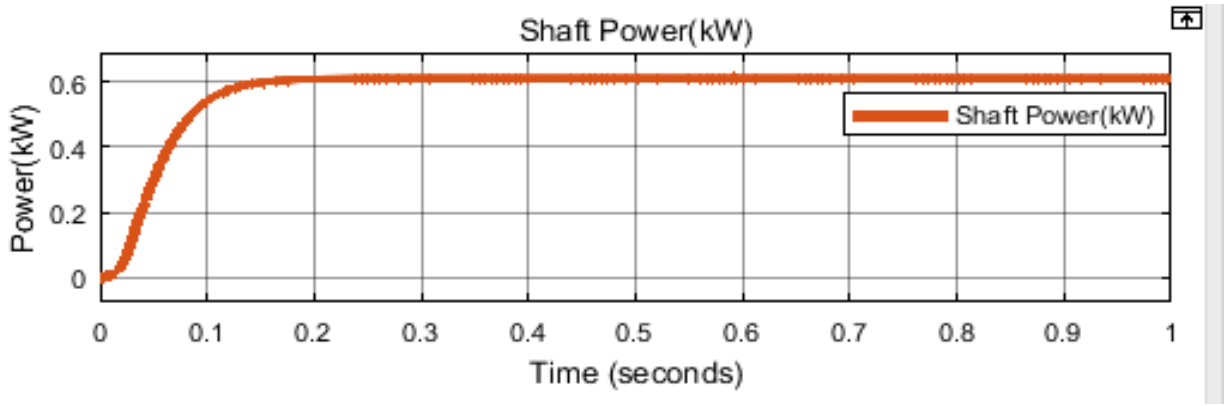

Figure III.20. Shaft power

The mechanical power deliverd to the centrifugal pump by the BLDC motor is shown in figure 11.20. This shaft power influences the maixum flow rate of the pump.

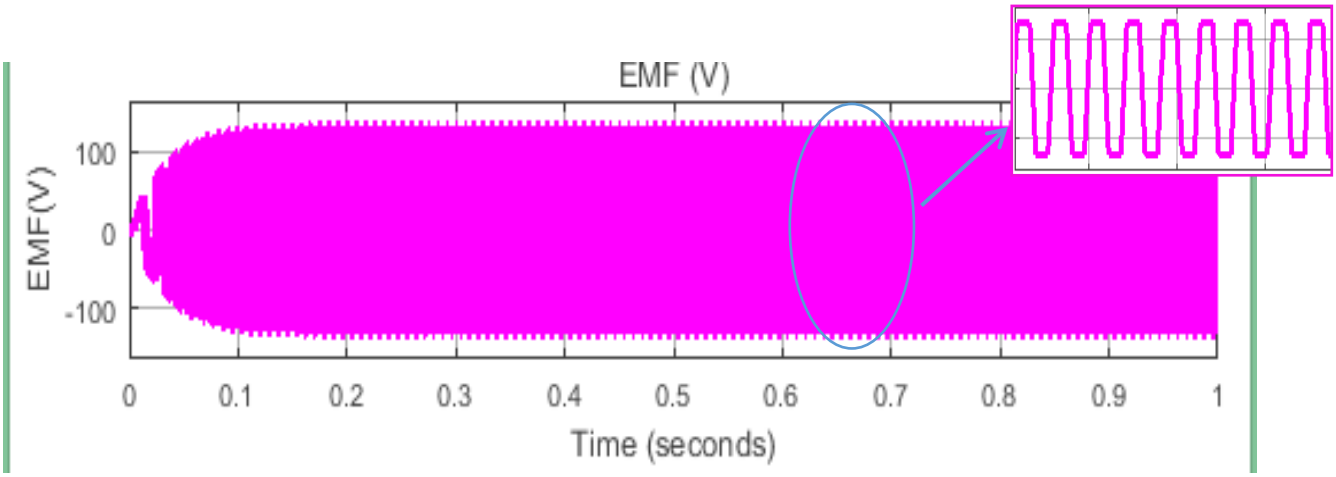

Figure III.21. Back EMF

The back EMF generated during the operation of the motor- pump group is shown in figure III.21 which is in a trapezoidal form. The variation of the back EMF is directly proportional to the speed of rotation of the BLDC motor.

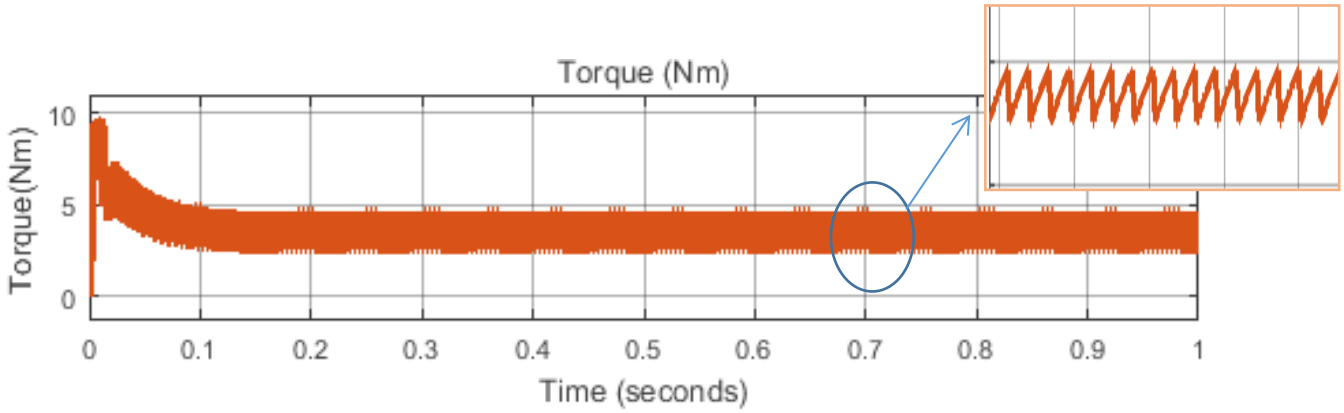

Figure III.22. Electromagnetic torque

The electromagnetic torque developed by the BLDC during the operation of the submersible centrifugal pumps is shown in figure III.22. The torque produced contains ripples due the types of electronic commutation chosen which is based on Hall sensors.

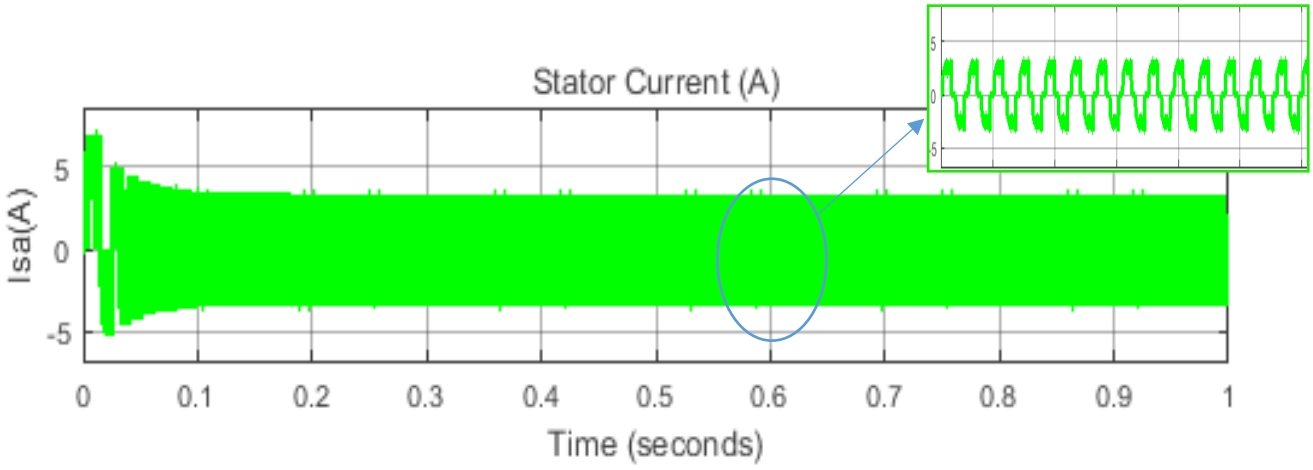

Figure III.23. Stator current

The inrush current during starting period of the motor is high reaching 7A while the steady current is approximately equal to 3.87A shown in figure III.23

From the results of the simulation, we can conclude that, the maximum flow rate is directly proportional to the rotation speed of the motor and the input voltage is used to vary the speed of electrical motors while the stator current reflects an image of the torque.

III.15. Case study II. Agriculture Mansourah Tlemcen, Algeria

Tlemcen is a city located northern west Algeria as shown in figure III. 23. It consists of 20 districts and 50 communities [58]

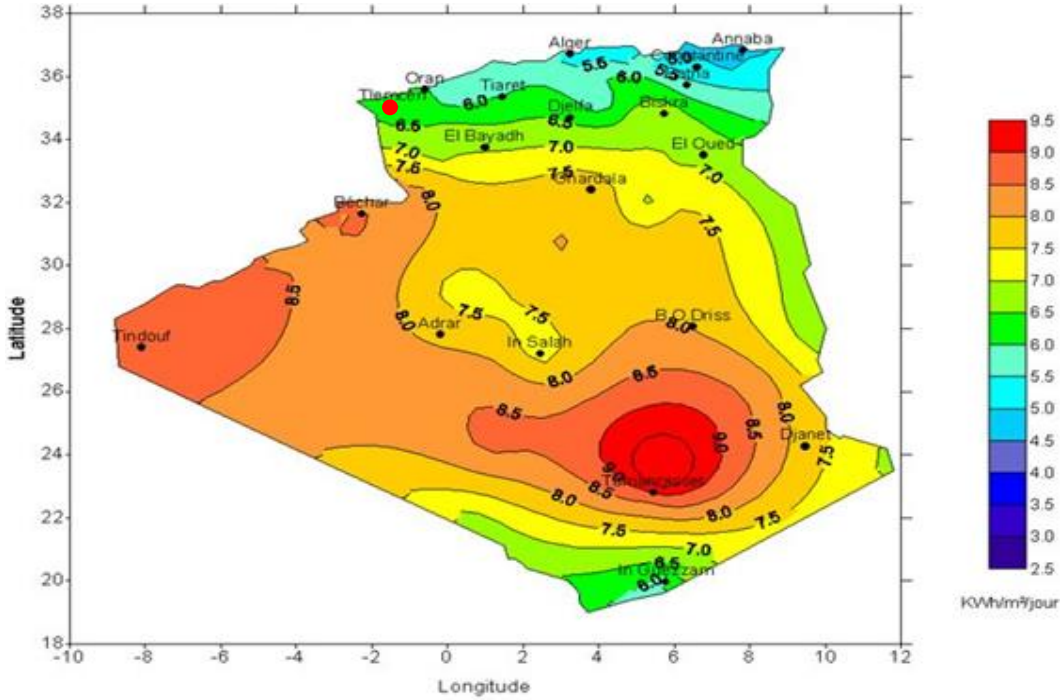

Figure III.24. Map of Algeria [10]

III.15.1. Location of Mansourah in Tlemcen

Mansourah is a town and commune in Tlemcen province in northwestern Algeria. The town is the seat of Mansourah District. The commune of Mansourah is composed of 8 localities which are, Mansourah, Imama, Béni Boublène, Wone Ouest, ZHUN Champ de tir, Kifan Sud-Ouest, Attar, Ouali Mustapha (Riat El Kébir). [59]

Figure III.25. Location of Mansourah commune [60]

III.15.2. Climatic condition of the area.

This region has hot, dry summers and cold wet winters. The highest temperatures are experienced around June to August while lowest temperatures are experienced around December to February as shown in Table III.7

	January	February	March	April	May	June	July	August	Septem-ber	October	November	December
Avg. Temperature °C (°F)	7.1 °C (44.8) °F	7.9 °C (46.2) °F	10.6 °C (51.1) °F	13.2 °C (55.8) °F	16.8 °C (62.3) °F	21.5 °C (70.7) °F	25.2 °C (77.4) °F	25.3 °C (77.5) °F	21 °C (69.7) °F	17.1 °C (62.7) °F	11 °C (51.7) °F	8.2 °C (46.8) °F
Min. Temperature °C (°F)	2.5 °C (36.5) °F	2.9 °C (37.3) °F	5.2 °C (41.3) °F	7.4 °C (45.3) °F	10.6 °C (51.2) °F	14.8 °C (58.6) °F	18.3 °C (64.9) °F	18.7 °C (65.6) °F	15.2 °C (59.4) °F	11.7 °C (53) °F	6.5 °C (43.6) °F	3.9 °C (38.9) °F
Max. Temperature °C (°F)	13 °C (55.3) °F	13.7 °C (56.7) °F	16.8 °C (62.2) °F	19.5 °C (67.1) °F	23.2 °C (73.7) °F	28.1 °C (82.6) °F	32.2 °C (89.9) °F	32.3 °C (90.1) °F	27.5 °C (81.6) °F	23.5 °C (74.3) °F	16.5 °C (61.8) °F	13.9 °C (57) °F
Precipitation / Rainfall mm (in)	62 (2.4)	52 (2)	59 (2.3)	55 (2.2)	38 (1.5)	11 (0.4)	2 (0.1)	5 (0.2)	23 (0.9)	41 (1.6)	61 (2.4)	45 (1.8)
Humidity(%)	69%	69%	67%	65%	61%	55%	48%	50%	59%	63%	67%	70%
Rainy days (d)	7	6	5	6	4	1	0	1	3	5	6	6
avg. Sun hours (hours)	7.0	7.6	8.5	9.5	10.6	11.9	12.3	11.5	10.0	9.0	7.4	7.0

Table III.7. Climatic conditions of the region [61]

III.15.3 The amount of solar irradiation received in the area

The graph below shows the monthly global horizontal radiation received in the area. The highest amount of insolation is received around May to August that is during the summer season as shown in figure III.26.

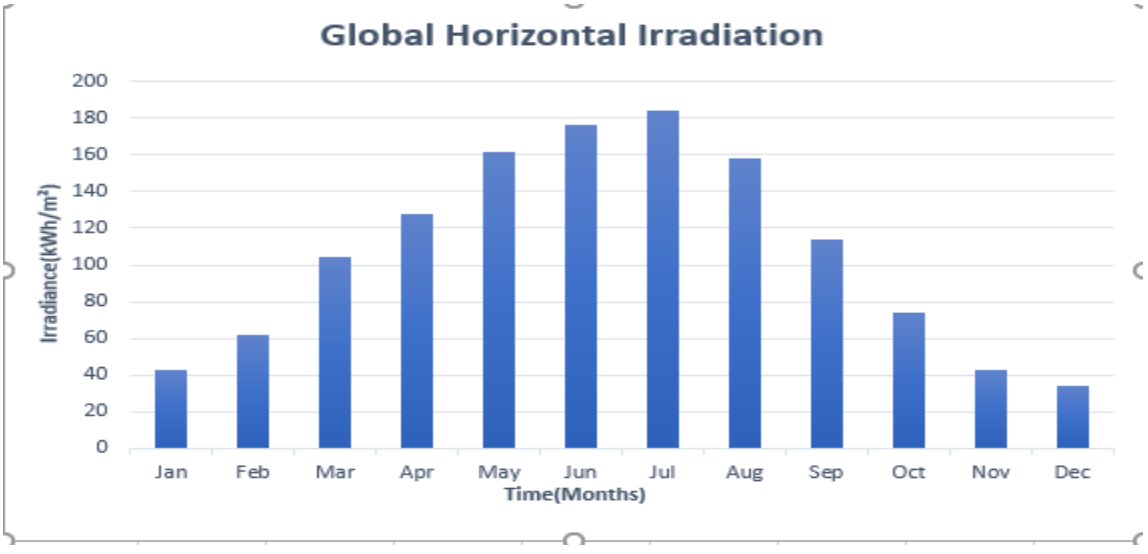

Figure III.26. Monthly global irradiation [53]

III.15.4. Daily sunshine hours

The variation of the daily sunshine hours, on a monthly basis is illustrated in figure III.26 where long sunshine hours are experienced around June – August (summer season)

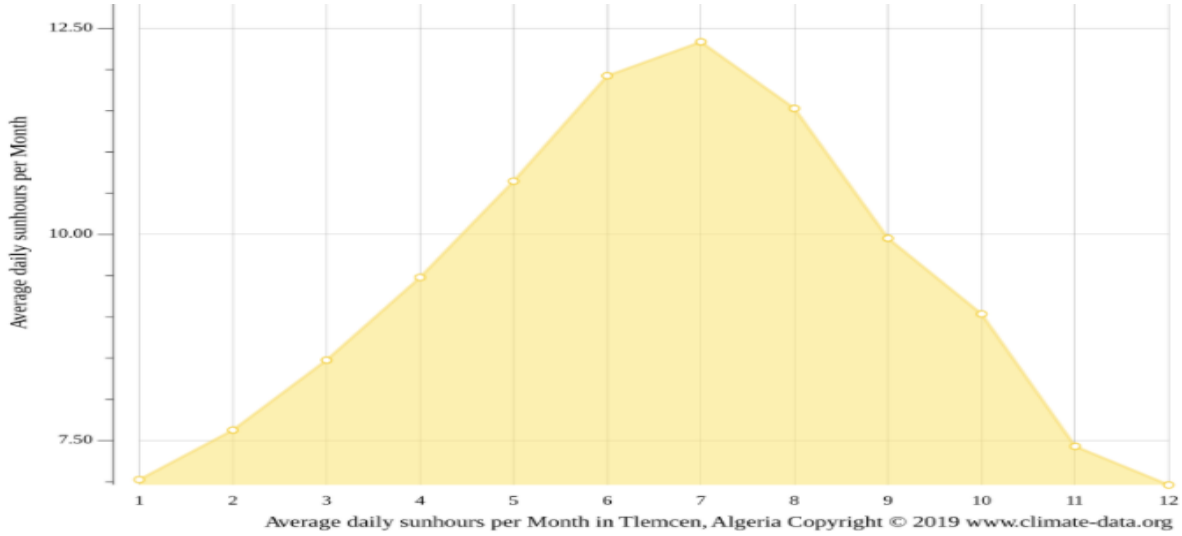

Figure III.26. Average daily sunshine hour [61]

III.15.5. Water availability

The karst aquifers of the Tlemcen Mountains are the region's main groundwater resource. More than 270 boreholes have been drilled in this region and have a total production capacity of 40 million m^3/year. However, the numerous boreholes drilled in the region showed that the carbonate reservoirs are well karstified (and this to a depth of more than 500 m). [62]

III.15.6. Water requirements

According to the irrigation water policies of Algeria, the descriptive statistics are shown in the table below:

Table III.8. Descriptive statistics of irrigation water policy in Algeria [63]

Crop	Amount of water required (m^3/hectare)
Tomato (OF)	2760
Tomato (GH)	3540
Watermelon (OF)	3400
Strawberry (GH)	4920
Pepper (GH)	3340

OF: open field, GH: greenhouse

The daily water requirements for domesticated animals are shown in Table III.9 and these requirements are influenced by the diet and seasonal changes. [64]

Table III.9. Daily water requirement for domesticated animals

Stock Type	**Consumption per head per day(L)**
Sheep (Weaners)	3 - 4
Adult dry sheep Grassland Saltbush	 2 -6 4 -12
Ewes with lambs	4 -10
Cattle Lactating cows - grassland - saltbush	 40 -100 70 -140
Young Stock	25 - 50
Dry Stock (400kg)	35 -80
Horses	40 -50

III.15.7. Calculation of the total daily water requirement

- Water melons: 7.5 m^3 for two acres
- Pepper: 7.5 m^3 for two acres
- Tomatoes: 6 m^3 for two acres
- Strawberry: 10 m^3
- 100 sheep: 1.2 m^3
- 10 Horses: 0.5 m^3

Therefore, the total quantity of water required is:

Quantity of water = 7.5 +7.5 + 6 + 10 + 1.2 + 0.5 (III.16)

= 32.7 **m^3**

The daily water requirement varies with seasonal changes and feed consumption of the domesticated animals. Therefore, an amount of 35 m^3 pumped during an average of 5 sunshine hours is a reasonable estimate for this project and such an oversizing of the system will help to cover water losses that occurs due to evapotranspiration.

III.15.8. Calculations of the hydraulic power needed

The following calculation are for the determination of the hydraulic power for the SWPS.

III.15.8.1. Flow rate

Using equation II.8:

The flow rate (Q in m^3/h) of the pumping system is: (III.17)

$$Q = \frac{\text{Daily water demand}}{\text{Sun hours}}$$

$$Q = \frac{35}{5} = 7m^3/h$$

III.15.8.2. Total dynamic head (TDH)

The total dynamic head is calculated below:
THD = Static head + friction head of the complete water piping system + velocity head.

III.15.8.2.1. Static head

The static head of the proposed system is calculated below

Static Head = Static water level + Drawdown level + System elevation (III.18)

Static Head = 50m + 85m + 1m **= 136m**

III.15.8.2.2. Velocity head

For a flow rate of 0.00194 m^3/s using PVC pipes with internal diameter of 2 inches (5.08cm)

$$\text{Velocity of the water} = 1.273\times \frac{Q}{d^2} = 1.723\times \frac{0.00194}{0.0508^2} = \mathbf{0.957\ m/s} \quad \text{(III.19)}$$

$$\text{Velocity Head} = \frac{V^2}{2g} = \frac{0.957^2}{2*9.81} = \mathbf{0.047\ m} \quad \text{(III.20)}$$

III.15.8.2.3. Friction head

The roughness coefficient for a PVC pipes is 150 as shown in table II.2, therefore:

$$H_L = \frac{10.472 \times Q^{1.853}}{C^{1.852} \times D^{4.871}} = \frac{10.472 \times 0.00194^{1.853}}{C^{1.852} \times 0.0508^{4.871}} = \mathbf{1.32m} \quad \text{(III.21)}$$

Therefore:

TDH = 136m + 0.047m + 1.324m =137.371 m

Since the piping system has **3** elbows which reduces the pressure of the water, we will use a TDH of **140 m.**

III.15.8.3. Hydraulic power required

We have calculated: **Q = 0.00194m^3/s**, **TDH = 140 m**, ρ **= 1000 kg/ m^3**, **g =9.81 m/s^2**

$$P = Q.H.\rho.g \quad \text{(III.22)}$$

$$P = 0.00194 \times 140 \times 1000 \times 9.81 = \mathbf{2.7\ kW}$$

III.15.8.4. Size of the electric motor required

The size of the electric motor needed is calculated below using equation II.14:

$$P_m = \frac{Q \times \rho \times g \times H_{total}}{3.6 \times 10^6\ \eta_m} = \frac{7 \times 1000 \times 9.81 \times 140}{3.6 \times 10^6 \times 0.85} = \mathbf{3.4\ kW} \quad \text{(III.23)}$$

$$Ppv = \frac{Pm}{PR} = \frac{3400}{0.77} = \mathbf{4\ kW} \quad \text{(III.24)}$$

We will choose a **4 kW** centrifugal pump for this project but however, we do recommend a pump **5.5kW**. This voluntary overestimation is due to the fact that, the water demand may increase with time, as result of either extension of the farm.

III.16. PV system sizing

For this project we have chosen a monocrystalline, **SUNTECH POWER STP250S-20-Wd** solar panel included in the MATLAB/ Simulink library and its parameters are shown below.

Table III.10. Electrical Characteristics of the module (STC, 1000W/m^2, 25°C, AM = 1.5)

Parameters (STC)	**Values**
Maximum Power	250W
Optimum operating voltage	30.7 V
Optimum Operating Current	8.15 A
Open Circuit voltage	37.4 V
Short Circuit current	8.63 A
Module Efficiency	15.4 %
Operating temperature	-40° C to +85°C
Maximum Voltage	1000 V
Maximum Series Fuse rating	20 A
Power Tolerance	0/ +5W
Number of cells	60cells

The following curves show the power, voltage and current output of the chosen PV module simulated using MATLAB under the standard test conditions

Figure III.27. P-V characteristics of the module

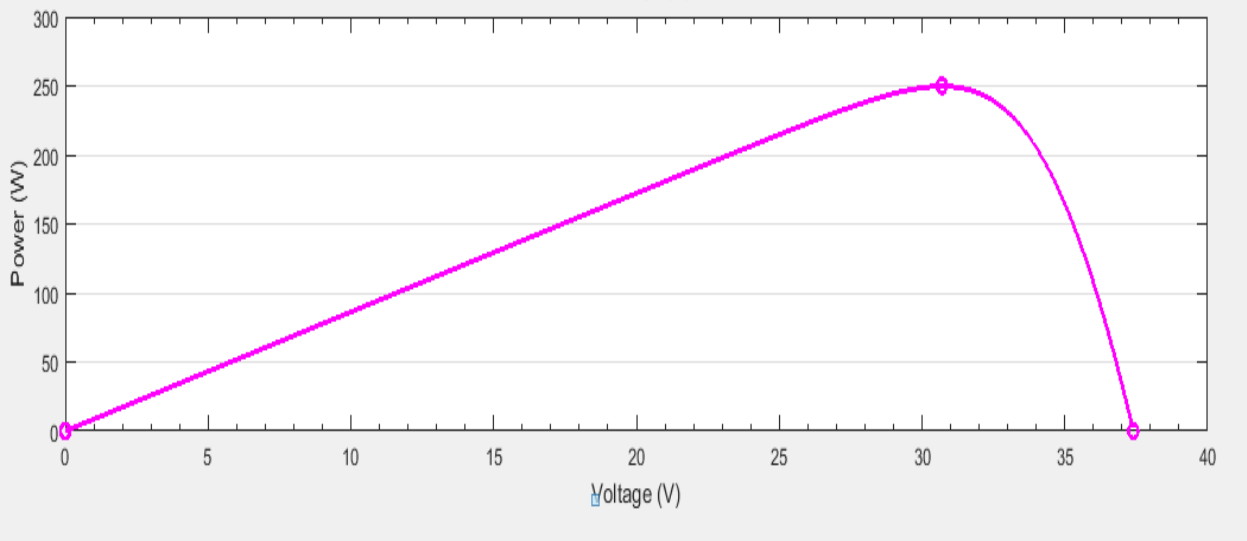

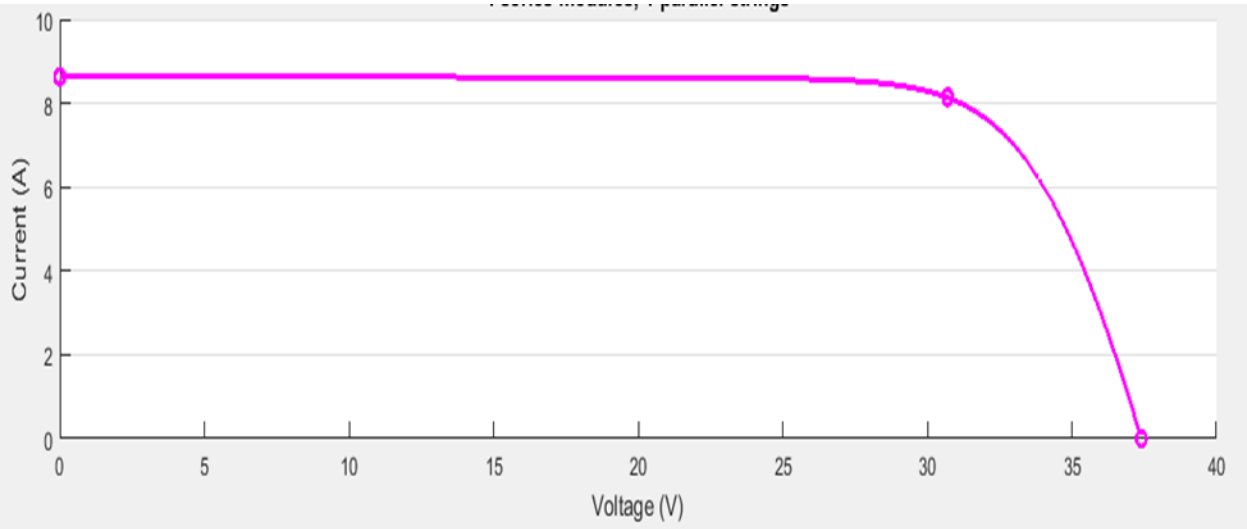

Figure III.28. I-V Characteristics of the module

For this project, we have decided to power the SWPS by a total PV power output of 4000W using 250 W PV modules. The oversizing PV array is to compensate for the power losses due to, atmospheric condition, wiring cables and other power losses during the operation of the pump system.

III.16.1. Calculations of the number of solar panels

From equation II.15, the number of solar panels are determined below:

$$\text{Number of solar panels } (N_p) = \frac{\text{Total solar power output required}}{\text{individual solar power out of a chosen panel type}} \quad \text{(III.25)}$$

$$N_p = \frac{4000\ W}{250W} = 16 \textbf{ modules}$$

III.16.2. Parallel and series connection of the solar panels

The number of PV panels in series and parallel are determined below:

III.16.2.1. Solar panels in parallel

From equation II.17, the PV panels in parallel are calculated below:

$$\text{Number of panels in parallel } (N_{pp}) = \frac{\text{Maximum rated direct current for BLDC}}{\text{Rated short circuit solar outpout current (Isc)}} \quad \text{(III.26)}$$

$$N_{pp} = \frac{13.7}{8.63} = 1.58 \approx 2 \text{ string of solar panels}$$

III.16.2.2. Solar panels in each string (series)

From equation II.18, the PV panels in each string are calculated below:

$$\text{Number of panels in series } (N_{ps}) = \frac{\text{Total number of panel required}}{\text{Total number of parallel strings}} \quad \text{(III.27)}$$

$$N_{ps} = \frac{16}{2} = \textbf{8 panels}$$

III.16.3. Voltage in each string

From equation II.19, the total voltage output of each panel is determined below

$$\text{Voltage in each string} = \text{Total number of panels} \times \text{Open circuit voltage} \quad \text{(III 28)}$$

$$= 8 \times 37.4\ V = \textbf{299.2 Volts}$$

III.16.4. PV power produced

From equation II.20, the total power output of the PV array is calculated below

$$Ppv = \text{Power output of each panel} \times N_{pp} \times N_{ps} \quad \text{(III.29)}$$

$$Ppv = 250 \times 8 \times = \textbf{4 kW}$$

III.17. Calculation of the boost converter parameters

The parameters of the boost converter is determined as follows:

II1.17.1. Duty cycle

The boost converter for this SWPS has the following input voltage and output voltage, V_{in} = 299.2V and V_{out} = 750V respectively, therefore the value of the duty cycle is:

$$D = \frac{750-299.2}{750} = \mathbf{0.6} \qquad \text{(III.30)}$$

III.17.2. Determination of the size of the Inductor

Using a switching frequency of 40 kHz and ripple current equivalent to 30% of the input current

$$L = D\,\frac{V_{in}}{f\,\Delta I_L} = 0.6\times\frac{299.2}{40000\times0.3\times17.26} = \mathbf{0.867\ mH} \qquad \text{(III.31)}$$

1II.17.3. Determination of the size of the capacitor

With a switching frequency of 40 kHz and ripple voltage equivalent to 1% of the output voltage.

$$C_2 = \frac{D\,I_0}{f\,\Delta V_0} = 0.6\times\frac{(1-0.6)(17.26)}{40000\times0.01(750)} = \mathbf{13.8\ \mu F} \qquad \text{(III.32)}$$

III.18. Selection of the pump

The characteristics of the selected pumps are shown in Table III.11 below.

Table III.11. Pump selection

ITEM	Voltage	Best DC Voltage	Power	Max. Flow	Max. Head	Outlet	Cable	Solar panel	
								open voltage	Power
HD-4SSC5-67-220/300-750-A/D	AC220/DC300V	300V-400V	750W	5.0m³/h	67m	1.25"	2m	<450V	≥1800w
HD-4SSC4.5-203-220/300-1500-A/D	AC220/DC300V	300V-400V	1500W	4.5m³/h	203m	1.25"	2m	<450V	≥2000w
HD-4SSC5-101-220/300-1100-A/D	AC220/DC300V	300V-400V	1100W	5.0m³/h	101m	1.25"	2m	<450V	≥1800w
HD-4SSC5-146-220/300-1500-A/D	AC220/DC300V	300V-400V	1500W	5.0m³/h	146m	1.25"	2m	<450V	≥2000w
HD-4SSC5-255-220/300-2200-A/D	AC220/DC300V	300V-400V	2200W	5.0m³/h	255m	1.25"	2m	<450V	≥3000w
HD-4SSC5-255-380/550-2200-A/D	AC380/DC550V	480V-750V	2200W	5.0m³/h	255m	1.25"	2m	<800V	≥3000w
HD-4SSC5-300-380/550-3000-A/D	AC380/DC550V	480V-750V	3000W	5.0m³/h	300m	1.25"	2m	<800V	≥4000w
HD-4SSC7-80-220/300-1300-A/D	AC220/DC300V	300V-400V	1300W	7.0m³/h	80m	1.25"	2m	<450V	≥1800w
HD-4SSC7-100-220/300-1500-A/D	AC220/DC300V	300V-400V	1500W	7.0m³/h	100m	1.25"	2m	<450V	≥2000w
HD-4SSC7-150-220/300-2200-A/D	AC220/DC300V	300V-400V	2200W	7.0m³/h	150m	1.25"	2m	<450V	≥3000w
HD-4SSC7-150-380/550-2200-A/D	AC380/DC550V	480V-750V	2200W	7.0m³/h	150m	1.25"	2m	<800V	≥3000w
HD-4SSC7-210-380/550-3000-A/D	AC380/DC550V	480V-750V	3000W	7.0m³/h	210m	1.25"	2m	<800V	≥4000w
HD-4SSC7-265-380/550-4000-A/D	AC380/DC550V	480V-750V	4000W	7.0m³/h	265m	1.25"	2m	<800V	≥5000w

III.19. Pump performance curves

The motor –pump group we have chosen is shown in figure III.29 denoted by number "91" with maximum flow rate of 7m^3 for a head of 210m. [65]

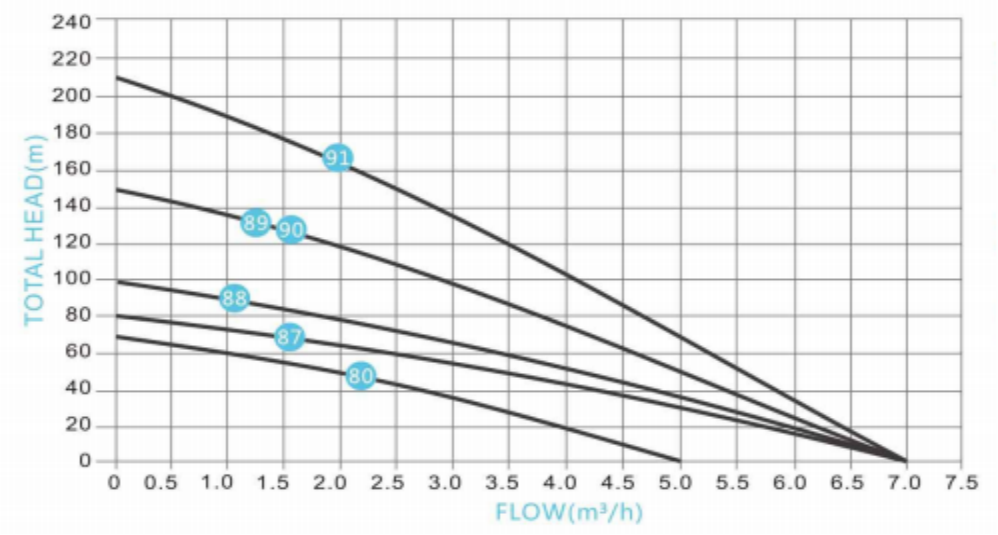

Figure III.29. Performance curve of the pump [66]

III.20. Specification of the pump.

The specification of the pump selected for this project are shown in Table III.12. The selected pump is a hybrid pump powered **by** both AC and DC voltages**.**

Table III.12. Specification of the pump [65]

Brand Name	Handuro
Model Number	HD-4SSC7-210-380/550-3000-A/D
Power	3000 W
Voltage	AC380 V /DC 550 V
Max Flow rate	7 m^3
Max Head	210 m
Motor Type	Permanent Magnet DC Brushless motor
Impeller	Stainless steel
Structure	Multistage
Motor Body	Stainless steel
Outlet	1.25''
Pump Head	Iron

The Simulink model of the boost converter, BLDC motor and the centrifugal pumps are the same shown in figure III.9, figure III.10 and figure III.13 respectively.

III.21. Results of the simulation

The results of the simulated will be illustrated with the following figures. The calculated torque for the pumping system is 17.5Nm.

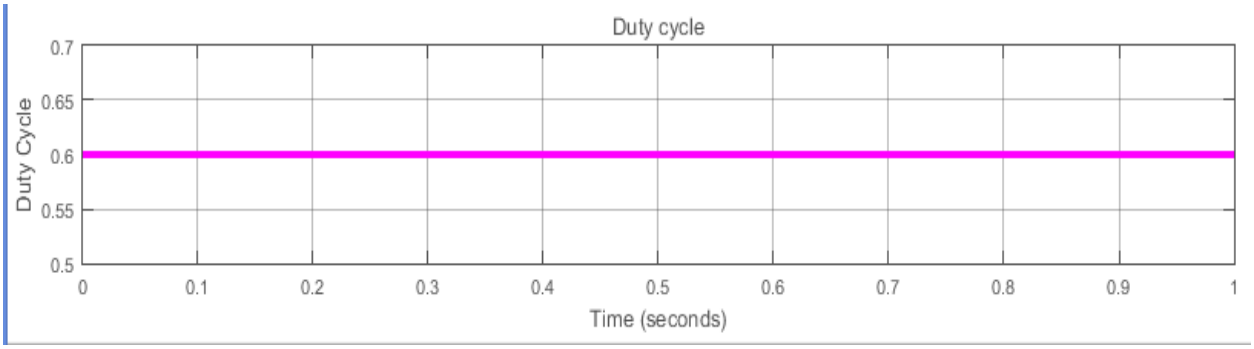

Figure III.30. Duty cycle

The calculated duty cycle of **0.6** for the boost converter used in this case study is shown on the graph in figure III.30

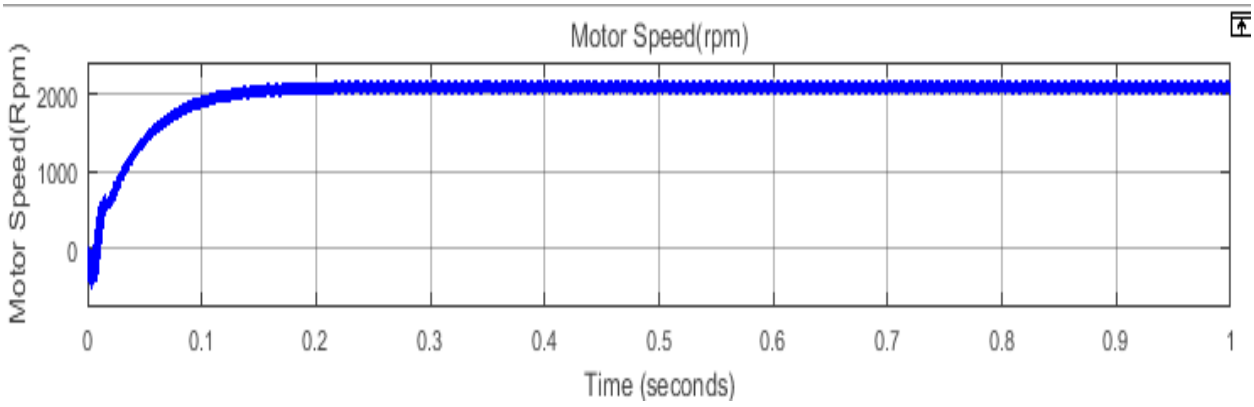

Figure III.31. Motor rotation speed

For a discharge of 7 m^3/ h the motor has to run on a speed of 2100 rpm

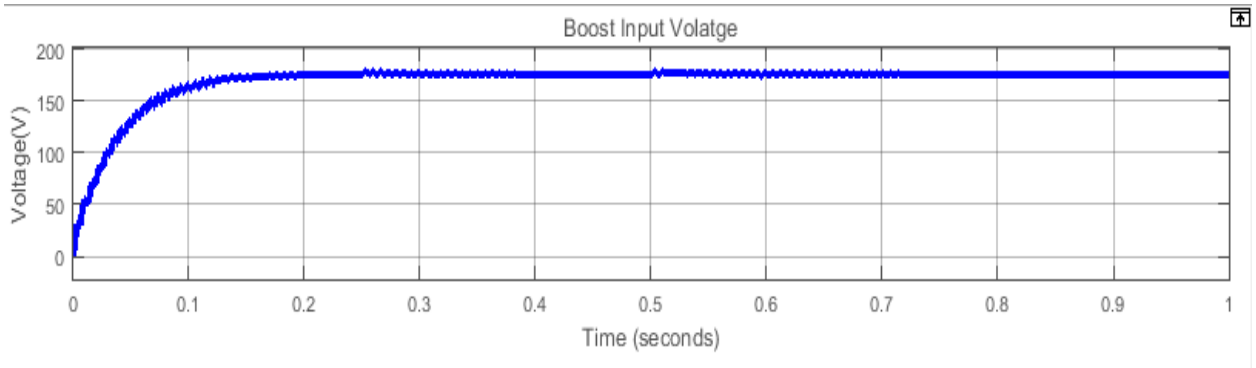

Figure III.32. Boost input voltage

As previously mention in figure III.17, the rotation speed of the BLDC motor is directly proportional to the input voltage. For this project, the input voltage stabilized at 175.8 V

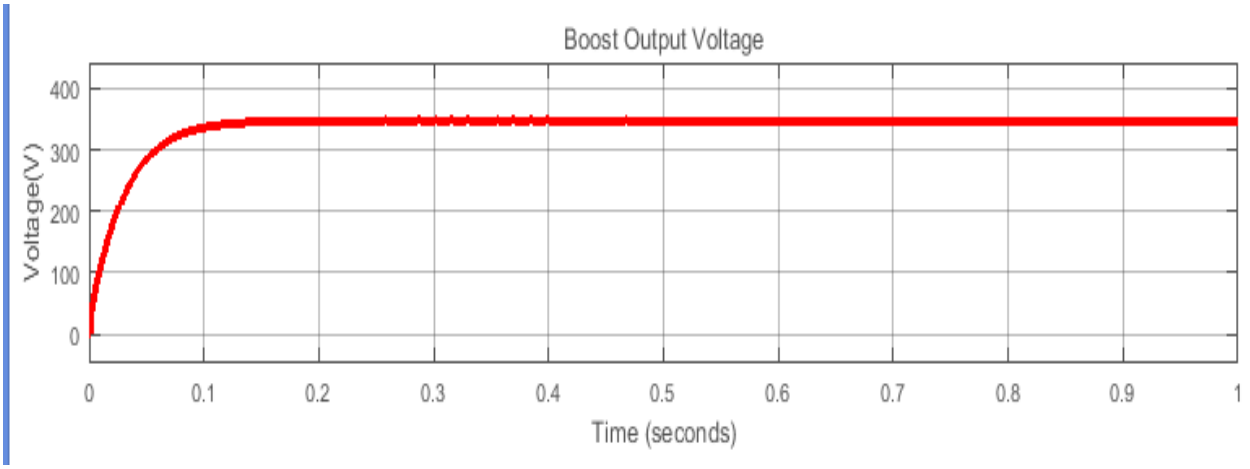

Figure III.33. Boost output voltage

The output voltage of the boost converter stabilized at 483V for an input voltage of 175.8 and a duty cycle of 0.6.

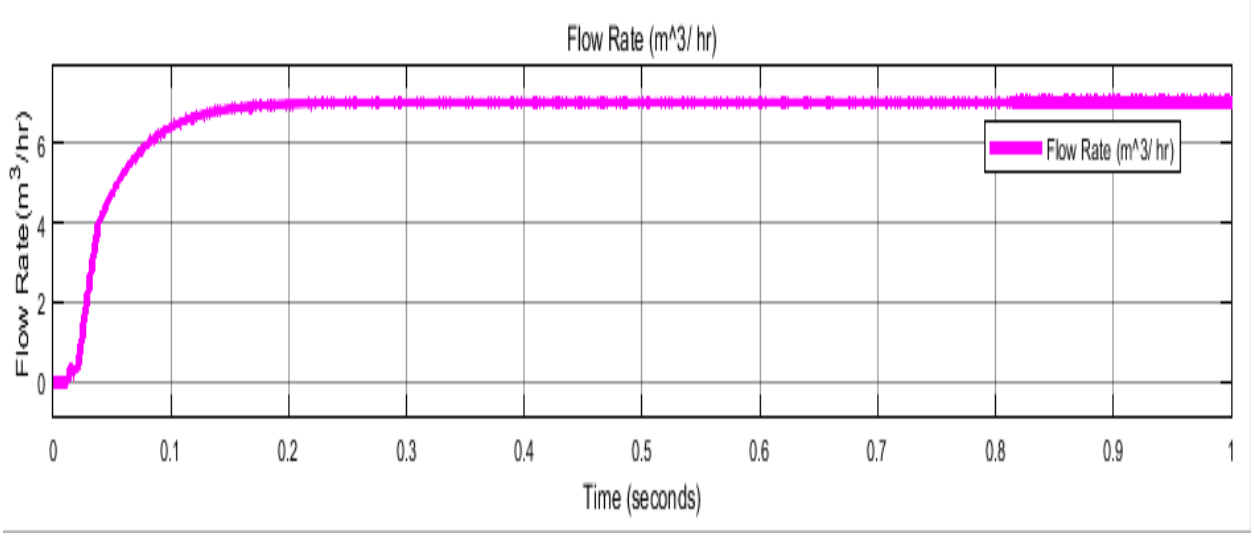

Figure III.34. Flow rate

To fulfill the daily water requirement of 35 m^3, the pump has to discharge an amount of 7 m^3 daily as shown in figure III.34. The flow rate corresponds to the motor speed of 2100rpm.

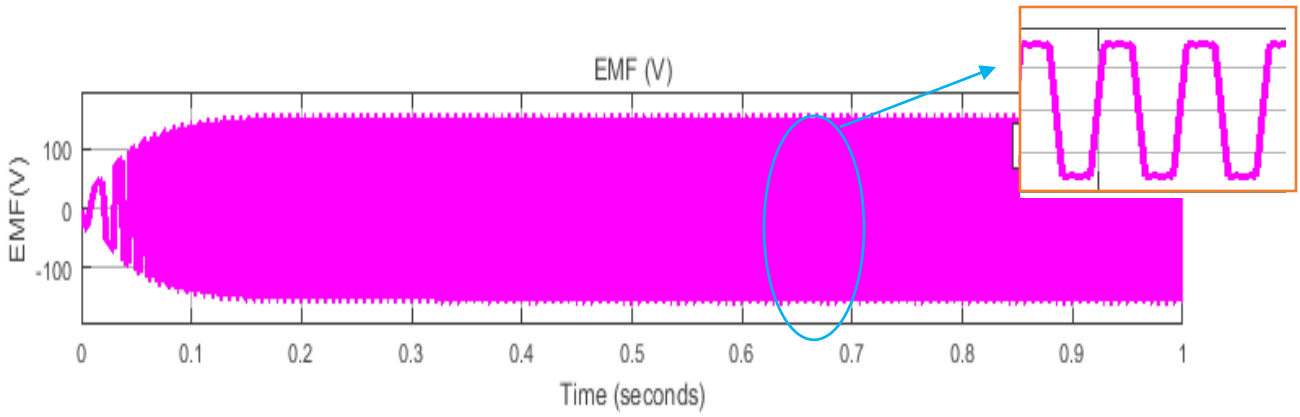

Figure III.34. Back EMF

The back EMF generated during the operation of the BLDC motor is shown in figure III.34 and it is in a trapezoidal form due to the technique of control chosen for this project.

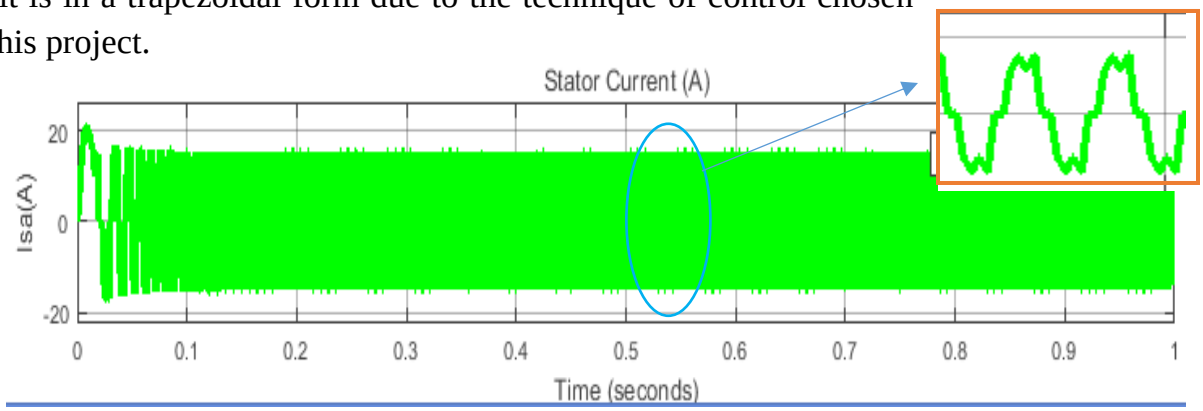

Figure III.35. Stator current

There is high inrush current which stabilized at approximately 15A, and the current has some ripples due to the effect of electronic switches and the trapezoidal technique of controlling the BLDC motor. These ripples exist also in the electromagnetic torque as shown in figure III.36.

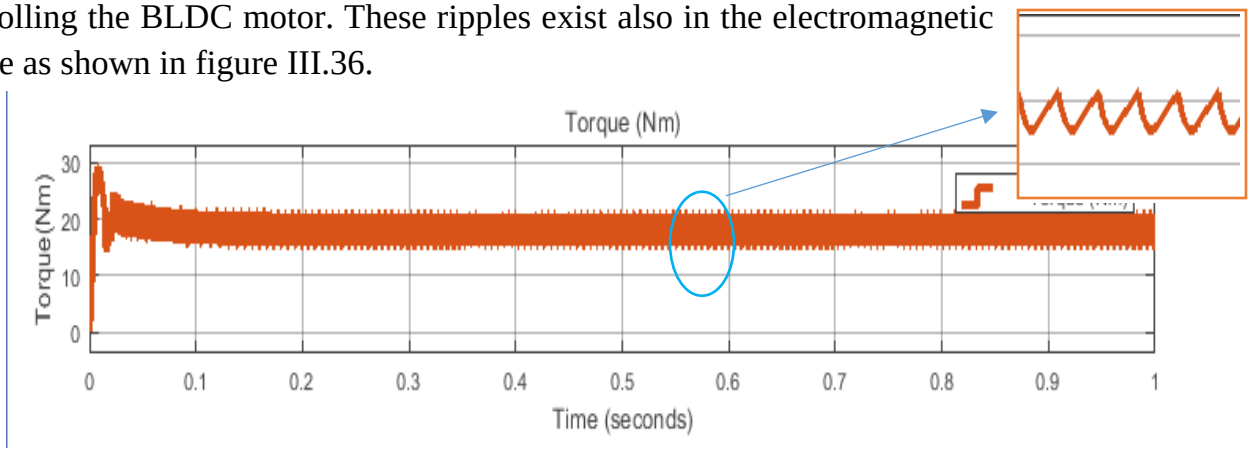

Figure III.36. Torque

III.21. Conclusion

We have designed two solar water pumping systems, firstly for a small clinic and also for a small community of 400 people which supplies an amount of 30m^3 daily in Kazangarare in Zimbabwe and secondly for a small farm in Mansourah in Tlemcen, Algeria which supplies an amount of 37 m^3. We also discussed about the climatic conditions of the areas and solar radiation received in these areas. We have simulated a Hall sensor-based BLDC motor with trapezoidal control and a speed regulator which drives vertical, submersible, multistage centrifugal pump. The proposed solar water pumping system includes a boost converter to step up the input voltage and also for the maximum power point tracking. The chapter concludes with a discussion on the results of the simulation

General Conclusion

The use of solar energy in remote areas for various applications such as water pumping is of great interest. However, photovoltaic generators have some disadvantages which are low efficiency and a high initial cost, and also these systems can be affected by climatic conditions like temperature, humidity and solar irradiation variation as we have discussed in chapter I. This means that during cloudy days, the daily water requirement may not be fulfilled. Therefore, there is need for a backup system by either storing water in tanks or storing energy in batteries.
This research work started with a presentation of the photovoltaic systems, including a study on the influence of external factors on their performance. Moreover, we discussed about the MPPT techniques and a Fuzzy logic MPPT technique was applied in this research work. This technique has proved to be efficient in tracking the maximum power point with less oscillations at the MPP.

In addition, the evolution of power electronics which plays a pivotal role in transforming voltage and current from either DC-DC or DC-AC has allowed a widespread application of the electric motors. Moreover, the use of DC speed controller for DC motor or AC speed controller for AC motor drivers has improved the control of speed and torque of these motor with precision Thus improving the overall performance of the systems driven by electrical motors.

Permanent magnet brushless DC machines provide an interesting solution for the realization of photovoltaic pumping systems. These machines have several advantages compared to synchronous or DC machines with brushes, such as a long service life, high efficiency, low maintenance, etc. The BLDC driver pilot the motor by providing electronic commutation using signal from Hall sensors.

The designing of solar water pumping systems depend on water sources which are either deep wells, rivers, dams or lakes. This in turn affected the types of the water pumping systems used and these include, surface water pumps, submersible or floating water pumps. The SPWS can be coupled directly to a photovoltaic array or may contain a bank of batteries. Moreover, the water pumps chosen depends on factors like, the total dynamic head, and the flow rate.

References

[1] World Vision, Web 19 June 2021
https://www.worldvision.org/clean-water-news-stories

[2] UN Sustainable Development Goals, Web 19 June 2021
https://www.un.org/sustainabledevelopment/water-and-sanitation/

[3] Vivint solar, Web 19 June 2021
https://www.vivintsolar.com/learning-center/history-of-solar-energy

[4] How big is our solar system, NASA, Web 19 June 2021
https://www.nasa.gov/sites/default/files/files/YOSS_Act1.pdf

[5] Energygov, Web 19 June 2021
https://www.energy.gov/eere/solar/solar-radiation-basics

[6] Christiana Honsberg and Stuart Bowden, Web 19 June 2021
https://www.pveducation.org/pvcdrom/properties-of-sunlight/air-mass

[7] Laser focus world, Web 19 June 2021

https://www.laserfocusworld.com/lasers-sources/article/16566681/photovoltaics-measuring-the-sun

[8] VisionLearning, Web 19 June 2021

https://www.visionlearning.com/en/library/Earth-Science/6/Factors-that-Control-Earths-Temperature/234

[9] Martin Schlecht, Richard Meyer, in Concentrating Solar Power Technology (Second Edition) , Web 19 June 2021

[10] Amine Boudghene Stambouli,, Algerian renewable energy assessment: The challenge of sustainability, Energy Policy, Volume 39, Issue 8,2011
https://doi.org/10.1016/j.enpol.2010.10.005.

[11] Renewable Energy Development in Algeria, Web 19 June 2021

http://www.new.anasr.org/2013/08/16/feature-renewable-energy-development-in-algeria/

[12] Solargis, Web 19 June 2021

https://solargis.com/maps-and-gis-data/download/zimbabwe

[13] Greenmatch, Web 19 June 2021

https://www.greenmatch.co.uk/blog/2015/09/types-of-solar-panels

[14] National Encyclopedia, Web 19 June 2021

https://www.nationsencyclopedia.com/Africa/AlgeriaCLIMATE

[15] Climate of Matebeleland North, Zimbabwe –Worddata.info, Web 19 June 2021

https://www.worlddata.info/africa/zimbabwe/climate-matabeleland-north.php

[16] Clean energy review, Web 19 June 2021

https://www.cleanenergyreviews.info/blog/solar-panel-components-construction

[17] Bessam-Abdelghani, Modélisation et Simulation d'un pompage photovoltaïque, Mémoire de magister, Badji Mokhtar- ANNABA University 2018

[18] Afghan, Syeda Adila & Abdul Kareem, Hassam & Hussy, Gaza. (2017). Simulating the electrical characteristics of a photovoltaic cell based on a single-diode equivalent circuit model.

[19] Alternative Energy Tutorials, Web 19 June 2021

https://www.alternative-energy-tutorials.com/photovoltaics/bypass-diode.html

[20] Electronic tutorial, Web 19 June 2021

https://www.electronics-tutorials.ws/diode/bypass-diodes.html

[21] DJERIOU Salim, Performance Improvement of photovoltaic pumping system, PhD Dissertation, University M'Hamed BOUGARA – Boumerdes 2018, Page 27

[22] Components 101, Web 19 June 2021

https://components101.com/asset/sites/default/files/components/Boost-Converter.png

[23] Learn about electronics, Web 19 June 2021

https://learnabout-electronics.org/PSU/psu32.php

[24] S. K. Sahoo, A. Ramulu, S. Batta and S. Duggal, "Performance analysis and simulation of three phase voltage source inverter using basic PWM techniques," IET Chennai 3rd International on Sustainable Energy and Intelligent Systems (Seiscon 2012), 2012, pp. 1-7, doi: 10.1049/cp.2012.2223.

[25] Md. Rabiul Islam, Faz Rahman, Wei Xu, Advances in Solar Photovoltaic Power Plants. Green Technology, 2016 DOI 10.1007/978-3-662-50521-2

[26] Tchouani Njomo, A.F., Sonfack, L.L., Douanla, R.M. et al. Nonlinear Neuro-Adaptive Control for MPPT Applied to Photovoltaic Systems. J Control Autom Electr Syst 32, 693–702 (2021). https://doi.org/10.1007/s40313-021-00691-3

[27] Md. Rabiul Islam, Faz Rahman, Wei Xu, Advances in Solar Photovoltaic Power Plants. Green Technology, 2016 DOI 10.1007/978-3-662-50521-2

[28] Bendib, B., Krim, F., Belmili, H., Almi, M. F., & Boulouma, S. (2014). Advanced fuzzy MPPT controller for a stand-alone PV system. In Energy Procedia (Vol. 50, pp. 383–392). Elsevier Ltd. https://doi.org/10.1016/j.egypro.2014.06.046

[29] Alamir, Nehmedo & Ismeil, Mohamed & Orabi, Mohamed. New MPPT technique using phase-shift modulation for LLC resonant micro-inverter. (2017) 10.1109/MEPCON.2017.8301376.

[30] Tamer Khatib, Dhiaa Halbot Muhsen, Photovoltaic Water Pumping Systems Concept, Design, and Methods of Optimization,

[31] Robert Foster, James Witcher, Vaughn Nelson, Majid Ghassemi, Luz Elena Mimbela, Abbas Ghassemi,, Solar Energy Renewable Energy and the Environment 2010, Page 216.

[32] Linear Motion Tips, Web 19 June 2021

https://www.linearmotiontips.com/are-brushed-motors-suitable-for-industrial-applications/

[33] Randriakotonjanahary, Tolotra Samuel. (2019). A low-cost, small scale Unmanned Aerial Vehicle capable of a real-time onboard deep learning-based object detection system. 10.13140/RG.2.2.36225.40806.

[34] Gamazo-Real, J.C.; Vázquez-Sánchez, E.; Gómez-Gil, J. Position and Speed Control of Brushless DC Motors Using Sensorless Techniques and Application Trends. Sensors **2010**, 10, 6901-6947. https://doi.org/10.3390/s100706901

[35] Obed, Adel & L. Saleh, Ameer. (2014). Speed Control of BLDC Motor Based on Recurrent Wavelet Neural Network. DCIraq J. Electrical and Electronic Engineering. 10. 118-129. 10.33762/eeej.2014.95599.

[36] Rajesh Kanna, G.R., Sasiraja, R.M. & Prince Winston, D. Design and development of Truncated Angle Variant controller for multi-source-fed BLDC motor drive. Electrical Eng **102,** 1931–1946 (2020). https://doi.org/10.1007/s00202-020-01004-8

[37] S. Mondal, A. Mitra and M. Chattopadhyay, "Mathematical modeling and simulation of Brushless DC motor with ideal Back EMF for a precision speed control," 2015 IEEE International Conference on Electrical, Computer and Communication Technologies (ICECCT), 2015, pp. 1-5, doi: 10.1109/ICECCT.2015.7225944.

[38] Dahbi, M., Doubabi, S., Rachid, A. (2020). Real time implementation for a low-cost control for BLDC motor current ripple minimization. European Journal of Electrical Engineering, Vol. 22, No. 1, pp. 63-69. https://doi.org/10.18280/ejee.220108

[39] Gamazo-Real JC, Vázquez-Sánchez E, Gómez-Gil J. Position and speed control of brushless DC motors using sensorless techniques and application trends. Sensors (Basel). 2010;10(7):6901-6947. doi:10.3390/s100706901

[40] Foster, Majid Ghassemi, Alma Cota, Solar Energy: Renewable Energy and the Environment, Page 213

[41] Michael Smith Engineers Ltd, Web 19 June 2021

https://www.michael-smith-engineers.co.uk/resources/useful-info/centrifugal-pumps

[42] DIENER Precision Pumps, Web 19 June 2021

https://dienerprecisionpumps.com/positive-displacement-pumps/

[43] Rainbow Power Company, Web 19 June 2021

https://www.rpc.com.au/solar-systems/solar-pump-systems/floating-pumps.html

[44] Foster, Majid Ghassemi, Alma Cota, Solar Energy: Renewable Energy and the Environment

[45] Girma, Misrak & Assefa, Abebayehu & Molinas, Marta. (2015). Feasibility study of a solar photovoltaic water pumping system for rural Ethiopia. AIMS Journal. 2. 697-717. 10.3934/environsci.2015.3.697.

[46] Solar water pumping system, Design, Selection and Installation guidelines V1,

[47] The Engineering Toolbox, Web 19 June 2021

https://www.engineeringtoolbox.com/hazen-williams-coefficients-d_798.html

[48] Frank Prosperous, Solar water pumping systems for rural water supply and small-scale irrigation, Master Dissertation, Pan- African University Institute for Water and Energy Sciences, 2019

[49] Andy Walker, Jal Desal, Donna Heimiller, Performance of Photovoltaic Systems Recorded by Open Solar Performance and Reliability Clearinghouse (oSPARC°NREL,2020

[50] Location of Karoi, Web 19 June 2021

https://en.wikipedia.org/wiki/Karoi

[51] Map of Zimbabwe, Web 19 June 2021

https://ontheworldmap.com/zimbabwe/administrative-divisions-map-of-zimbabwe.html

[52] Location of Kazangarare Clinic, Web 19 June 2021

https://www.google.com/maps?q=kazangarare+clinic&um=1&ie=UTF-8&sa=X&ved=2ahUKEwi6pvuJ1ZzxAhUIjaQKHTIRAZsQ_AUoAnoECAIQBA

[53] Pv-Syst NASA-SSE

[54) Earthwise, British Geological Survey, Web 19 June 2021

http://earthwise.bgs.ac.uk/index.php/Hydrogeology_of_Zimbabwe

[55] World health organization-how much water is needed in emergencies page 3

[56] Peter H. Gleick M IWRA, Basic Water Requirements for Human Activities: Meeting Basic Needs, Pacific Institute for Studies in Development, Environment, and Security 1204 Preservation Park Way, 1996

[57] Handuro Water Pumps, Web 19 June 2021

https://handuro.en.alibaba.com/product/62415197002-814984971/HD_3SC8_62_110_1100_A_D_3inch_deep_well_solar_power_centrifugal_water_pump.html

[58] Location of Tlemcen, Web 19 June 2021

https://en.wikipedia.org/wiki/Tlemcen_Province

[59] Mansourah Tlemcen, Web 19 June 2021

https://en.wikipedia.org/wiki/Mansoura,_Tlemcen

[60] Location of Mansourah, Web 19 June 2021

https://www.google.com/maps/place/Mansourah/@34.8663643,-1.3610357,15z/data=!4m5!3m4!1s0xd78c872578de5d1:0x57392e401cc5e7e8!8m2!3d34.8789634!4d-1.3486934

[61] Climate-data.org, Web 19 June 2021

https://en.climate-data.org/africa/algeria/tlemcen/tlemcen-990323/

[62] Abdelazim M. Negm, Abdelkader Bouderbala, Haroun Chenchouni, Damià Barceló, Water Resources in Algeria - Part I: Assessment of Surface and Groundwater Resources

[63] Oulmane, Amine & Frija, Aymen & Brabez, Fatima. (2019), Modelling farmers' responses to irrigation water policies in Algeria: An economic assessment of volumetric irrigation prices and quotas in the Jijel-Taher irrigated perimeter. Irrigation and Drainage. 68. 10.1002/ird.2327.

[64] NSW Department of primary Industries, July 2014, Water requirement for sheet and cattle

[65] Handuro water pumps, Web 19 June 2021

https://www.handuro.com/product/detail/id/666